

Effects of Age Related Degeneration on Cervical Spine Mechanics

by

James Christopher Boak

B.A.Sc., The University of British Columbia, 2006

A THESIS SUBMITTED IN PARTIAL FULFILLMENT OF
THE REQUIREMENTS FOR THE DEGREE OF
MASTER OF APPLIED SCIENCE

in

The Faculty of Graduate Studies

(Mechanical Engineering)

THE UNIVERSITY OF BRITISH COLUMBIA
(Vancouver)

September 2012

© James Christopher Boak 2012

Abstract

The average age of people suffering spinal cord injuries (SCIs) is shifting toward an older population, frequently occurring in the spondylotic (degenerated) cervical spine, due to low energy impacts. Since canal stenosis (narrowing) is a common feature of a spondylotic cervical spine, flexion or extension of such a spine can compress the spinal cord. This thesis involves two studies investigating the effects of spondylosis on the kinematics of the cervical spine and on compression of the spinal cord during spine motion.

The first study developed and evaluated an image analysis technique that measures a new combination of degenerative and kinematic continuous, quantitative variables in cervical spine sagittal plane flexion-extension image pairs. This technique, evaluated using plane X-ray, effectively quantified angular range of motion, anterior-posterior (AP) translation, intervertebral disc height, pincer spinal canal diameter, and osteophyte length. The angular accuracy and linear precision were found to be $\pm 1.3^\circ$ and approximately $\pm 0.6\text{mm}$, respectively. This compared well to previous studies and is adequate for potential clinical applications.

The second study quantified the effect of increasing anterior canal stenosis on spinal cord compression during spine motion. This study used a whole porcine cadaveric cervical spine, a radio-opaque surrogate spinal cord, and an artificial osteophyte. The spine was imaged by sagittal plane X-ray during quasistatic pure moment flexion-extension bending. This study demonstrated that the cadaveric model could simulate the typical spondylotic SCI mechanisms in both flexion (bowstring stretching) and extension (pincer). Spinal cord AP diameter could be measured accurately within $\pm 0.25\text{mm}$ and cord diameter differences could be measured within $\pm 0.5\text{mm}$. Cord compression due to the artificial osteophyte increased with increased canal stenosis, but never exceeded 1mm.

The image analysis techniques developed in the first study and results of future studies based on these techniques may be used to improve cadaveric modelling of SCI due to low energy impacts in the presence of age-related spine degeneration. Improved understanding of injury mechanisms may aid clinical intervention to both prevent and treat SCI in the presence of age-related spine degeneration.

Preface

Portions of the work described in this thesis were presented at numerous conferences. The work was the result of collaboration between all the co-authors, as described.

While in progress, work related to the content of Chapter 2 was presented at the following conferences. The same analysis techniques were used, but a data set of clinical X-rays was analyzed to address research questions relating to cervical spine range of motion.

- *Investigation Of Cervical Spondylosis And Range Of Motion: Methodology And Preliminary Results* J.C. Boak, D. Popovic, E. Itshayek, L. Koenig, M. Dvorak, P.A. Crompton **Northwest Biomechanics Symposium (NWBS)**. 2007. Eugene, Oregon, USA
- *Range Of Motion In The Elderly Is Related To Cervical Spondylosis: Preliminary Results Of A Clinical X-Ray Investigation* J.C. Boak, D. Popovic, E. Itshayek, L. Koenig, M. Dvorak, P.A. Crompton **International Collaboration On Repair Discoveries (ICORD)**. 2007. Bern, Switzerland
- *Range Of Motion In The Elderly Is Related To Cervical Spondylosis: Preliminary Results Of A Clinical X-Ray Investigation* J.C. Boak, D. Popovic, E. Itshayek, L. Koenig, M. Dvorak, P.A. Crompton **Cervical Spine Research Society (CSRS)**. 2007. San Francisco, California, USA
- *Range Of Motion In The Elderly Is Related To Cervical Spondylosis: Preliminary Results Of A Clinical X-Ray Investigation* James C. Boak, Dina Popovic, Eyal Itshayek, Lyne Koenig, Marcel F. Dvorak, Peter A. Crompton **AO World**. 2008. Kyoto, Japan
- *X-Ray Analysis Shows Disc Height Is Related To Range Of Motion In The Cervical Spine Of Elderly Subjects* J.C. Boak, D. Popovic, E. Itshayek, L. Koenig, M. Dvorak, P.A. Crompton **Spine Week**. 2008. Geneva, Switzerland
- *X-Ray Analysis Shows Degeneration is Related to Range of Motion in the Cervical Spine of Geriatric Subjects* J.C. Boak, D. Popovic, E. Itshayek, L. Koenig, M. Dvorak, P.A. Crompton **European Society of Biomechanics (ESB)**. 2008.

Luzern, Switzerland

- *Clinical X-ray Analysis Shows Degeneration Accompanies a Reduction in Range of Motion in the Cervical Spine of Geriatric Subjects* J.C. Boak, D. Popovic, E. Itshayek, L. Koenig, M. Dvorak, P.A. Crompton **International Collaboration On Repair Discoveries (ICORD) Annual Research Meeting. 2009.** Vancouver, BC, Canada

Dr Dina Popovic was an orthopaedic surgery medical resident from Vancouver General Hospital (VGH). Dr Eyal Itshayek was a spine surgery fellow from VGH. Dr Marcel Dvorak is Professor and Head of the Academic Division of Spine, Department of Orthopaedics, at UBC and the Medical Director of the Combined Neurosurgical and Orthopaedic Spine Program at VGH. They provided guidance and feedback at all stages of the project in particular with issues related to identification and digitization of cervical spine landmarks. Dina Popovic provided the clinical X-ray image pairs that were used in the study. She marked up the images with dots identifying the landmarks to be digitized. Eyal also marked up a subset of the images for validation of the methods.

Lyne Koenig was an engineering co-op student at Synaptic Analysis Consulting Group (Vancouver, Canada). She provided assistance developing an early version of the MATLAB scripts used to analyze the X-ray images.

Dr. Peter Crompton is a professor of mechanical engineering at UBC, and the Co-director of the Orthopaedic and Injury Biomechanics Laboratory. Peter is my master's thesis supervisor. He guided all aspects of my work.

While in progress, the work described in Chapter 3 was presented at the following conferences.

- *At What Point Does Cervical Spinal Canal Stenosis Endanger The Spinal Cord? A new cadaveric model* James Boak, Philippe Gédet, Marcel F. Dvorak, Stephen Ferguson, Peter A. Crompton **Pre-IRCOBI Workshop on Experimental Methods (International Research Council on Biomechanics of Injury). 2008.** Bern, Switzerland.
- *Cervical Spinal Motion That Would Otherwise Be Safe, Can Cause Spinal Cord Compression in a Stenotic Spine* James Boak, Philippe Gédet, Marcel F. Dvorak, Stephen Ferguson, Peter A. Crompton **Canadian Orthopaedic Research Society, 2009.** Whistler, BC, Canada
- *Cervical Spine Stenosis Experimentally Observed To Cause Spinal Cord Compression During Spine Motion That Would Otherwise Be Safe* James Boak, Philippe Gédet, Marcel F. Dvorak, Stephen Ferguson, Peter A. Crompton **Ohio**

Injury Biomechanics Symposium. 2009. Columbus, Ohio, USA

Mr Philippe Gédet was the lab engineer at the ARTORG Center (Bern, Switzerland) where the cadaveric experiments were conducted. Philippe reviewed and advised all aspects of the cadaveric work. This included the experimental design and my design of a new reusable mould for the surrogate spinal cord. Philippe assisted with some of the cadaver preparation and all of the experiments as they required two people to operate all of the different equipment simultaneously.

Dr Stephen Ferguson is a professor of Biomechanics at the Department of Mechanical and Process Engineering (D-MAVT) at ETH Zurich. During my time working at the ARTORG Center, Stephen was a private lecturer at the University of Bern and the Co-Director of the ARTORG Spine Research Center. He was my “supervisor away from home” in Switzerland and provided guidance over all my work while in Switzerland.

Table of Contents

Abstract	ii
Preface	iii
Table of Contents	vi
List of Tables	viii
List of Figures	ix
List of Terms and Acronyms	xi
Acknowledgements	xiii
Dedication	xv
1 Introduction	1
1.1 Cervical Spine Anatomy	3
1.1.1 Normal Anatomy	5
1.1.2 Degenerated Anatomy	11
1.2 Cervical Spine and Spinal Cord Biomechanics	15
1.2.1 Normal Biomechanics	15
1.2.2 Degenerated Biomechanics	20
1.3 Study Objectives	24
2 X-ray Predictors of Cervical Spinal Canal Diameter Change	25
2.1 Introduction	25
2.2 Materials and Methods	26
2.2.1 Intra-reader Repeatability Assessment	31
2.2.2 X-ray Image Analysis Accuracy and Precision Assessment	32
2.3 Results	35
2.3.1 X-ray Image Analysis Accuracy and Precision Assessment	35

Table of Contents

2.3.2	Kinematic and Degenerative Variables Sample Results and Repeatability	36
2.4	Discussion	38
2.4.1	Accuracy, Precision, Repeatability and Sources of Error	40
2.4.2	Comparisons to Previous Studies	42
2.4.3	Future Considerations	44
2.5	Conclusions	47
3	Effect of Canal Stenosis on Surrogate Cord Compression During Cervical Spine Motion	48
3.1	Introduction	48
3.2	Materials and Methods	50
3.2.1	Cadaver Specimens and Preparation	50
3.2.2	Quasi-static Flexion-extension Tests with a Follower Load	52
3.2.3	X-ray Imaging and Analysis	56
3.2.4	Image Analysis Accuracy and Distortion Quantification	59
3.3	Results	61
3.3.1	Image Analysis Accuracy and Distortion Quantification	61
3.3.2	Surrogate Cord Compression	62
3.3.3	Range of Motion	73
3.4	Discussion	75
3.4.1	Comparisons to Previous Studies	76
3.4.2	Limitations	79
3.4.3	Future Work	82
3.5	Conclusions	83
4	Integrated Discussion	84
4.1	Comparisons to Previous Studies	85
4.2	Strengths and Limitations	86
4.3	Future Work	87
4.4	Conclusions	88
	Bibliography	90

List of Tables

2.1	Results of the in-plane angular accuracy study.	35
2.2	Results of the out-of-plane angular accuracy study.	36
2.3	Static canal diameter difference between flexion and extension views.	36
2.4	First sample results for kinematic and degenerative variables.	37
2.5	Second sample results for kinematic and degenerative variables.	37
2.6	Difference between sample results for kinematic and degenerative variables.	38
2.7	Vertebral landmark intra-reader digitization repeatability.	38
3.1	Static moments due to the follower loads.	54
3.2	Specimen sagittal canal diameters.	54
3.3	Test conditions carried out on each specimen.	55
3.4	X-ray image analysis technique accuracy.	62

List of Figures

1.1	The anatomical planes and directions.	4
1.2	The anatomical orthogonal rotations.	5
1.3	The cervical spine and spinal column.	6
1.4	Illustrations of the atlas and axis.	7
1.5	Typical cervical vertebra.	7
1.6	Healthy cervical intervertebral disc.	8
1.7	A typical cervical functional spinal unit.	9
1.8	Spinal cord anatomy.	10
1.9	Contrast a healthy and a degenerated cervical vertebra.	11
1.10	Magnetic resonance images of intervertebral disc degeneration grades.	12
1.11	Large anterior osteophytes.	14
1.12	Posterior osteophyte reduces spinal canal pincer diameter.	14
1.13	Continuous pure-moment bending test range of motion and neutral zone.	17
1.14	Average vertebral centre of rotation.	18
1.15	Pincer canal diameter.	18
1.16	Spinal cord bowstring stretching.	23
2.1	Sample flexion-extension image pair.	27
2.2	Landmarks used for image analysis.	28
2.3	Mid-lines used to calculate vertebral angle.	29
2.4	Dorso-ventral displacement.	29
2.5	Posterior and anterior disc height.	30
2.6	Pincer canal diameter.	31
2.7	Osteophyte length.	31
2.8	Intra-reader repeatability.	32
2.9	Angular accuracy assessment apparatus.	33
2.10	Angular accuracy assessment X-ray image.	33
2.11	Static canal diameter.	35
3.1	Illustration of artificial osteophyte.	51
3.2	A typical spine specimen before and after preparation.	52
3.3	ARTORG Research Center spine machine.	53

List of Figures

3.4	Specimen canal diameter measurement.	55
3.5	C-arm in position around spine machine.	56
3.6	X-ray imaging timing compared to flexion-extension loading sequence.	57
3.7	X-ray image segmentation.	58
3.8	Surrogate cord minimum diameters.	59
3.9	Accuracy assessment set-up.	60
3.10	X-ray image of the micrometer compressing the surrogate cord.	60
3.11	Calibration grid X-ray image used for this study.	61
3.12	Perimeter where pincushion distortion was detected.	62
3.13	Quantitative cord results 0% occlusion, 2.5Nm moment.	63
3.14	Quantitative cord results 25% occlusion, 2.5Nm moment.	64
3.15	Quantitative cord results 50% occlusion, 2.5Nm moment.	65
3.16	Specimens C and D full flexion X-ray images.	66
3.17	Specimen A maximum canal occlusion X-ray images.	67
3.18	Specimen C maximum canal occlusion X-ray images.	68
3.19	Specimen F maximum canal occlusion X-ray images.	69
3.20	Specimen B maximum canal occlusion X-ray images.	70
3.21	Specimen D maximum canal occlusion X-ray images.	71
3.22	Quantitative cord results maximum occlusion, 2.5Nm moment.	72
3.23	Quantitative cord results 25% occlusion, 3.75Nm moment.	74
3.24	Specimen range of motion results.	75
3.25	Range of motion compared to previous studies.	79
3.26	Human versus porcine cervical vertebra.	80

List of Terms and Acronyms

AP	Anterior-Posterior
Central Cord Syndrome	An incomplete spinal cord injury that disproportionately impairs motor function of the upper limbs, while function below the lesion is relatively preserved
CNS	Central Nervous System
COR	Centre Of Rotation
CSF	Cerebrospinal Fluid
CT	Computed Tomography
FSU	Functional Spinal Unit (composed of two adjacent vertebrae and the connecting disc and ligaments)
Ischemia	Inadequate blood supply
Hypertrophy	Enlargement of an organ such as a joint
JOA	Japanese Orthopaedic Association
LF	Ligamentum Flavum
MRI	Magnetic Resonance Imaging
Myelogram	An X-ray image (plane or CT) with contrast enhancing dye injected into the spinal canal making the spinal cord visible
Myelopathy	Mechanical compression of the spinal cord resulting in neurologic dysfunction
NZ	Neutral Zone
OLF	Ossification of the Ligamentum Flavum
OPLL	Ossification of the Posterior Longitudinal Ligament
Osteophyte	A bone spur from the margin of a vertebral body adjacent to the intervertebral disc
PLL	Posterior Longitudinal Ligament
PMMA	Polymethylmethacrylate
PNS	Peripheral Nervous System
Radiculopathy	Mechanical compression of nerve roots resulting in neurologic dysfunction
ROM	Range Of Motion
SCI(s)	Spinal Cord Injury (or Injuries)
SCIWORA	Spinal Cord Injury Without Radiographic Anomaly

List of Terms and Acronyms

SCIWORET	Spinal Cord Injury Without Radiographic Evidence of Trauma
Spondylosis	A generic term for spine degeneration
Stenosis	Narrowing of a tubular organ or structure such as the spinal canal

Acknowledgements

Thanks go my supervisor, Peter Cripton, for giving me this amazing opportunity and the pivotal roll he's played in my education. Peter's encouragement and support made it possible for me to work at the AO Research Institute for my last co-op work-term during my bachelor degree and then to go back to Switzerland to do my master's thesis cadaver experiments in collaboration with the ARTORG Center. The experiences and people I have had the privilege to know and work with as a result of Peter's faith in me have left an indelible mark on me.

Thanks to everyone at the ARTORG Center. Stephen Ferguson for being my "supervisor away from home" and for welcoming all us wayward Canadians to Bern. Paul Thistlethwaite for showing me what real Matlab programming looks like. Philippe Gédet for all the time spent with me in and out of the testing lab. The little I know about conducting spine cadaver tests, I learned from Philippe. Also, thanks to Urs Rohrer for his feedback and enthusiasm in the design and manufacture of the reusable surrogate cord mould.

Thanks to everyone at the OIBG, especially Robyn, Claire, Colin, Tim, Seth, and Qingan. You were all so generous with your time. You taught me so much and helped me to work through countless problems over the years. I must give special thanks to two people in particular, who over this last year took it upon themselves to help me when they saw I needed it most. Our weekly "thesis support group" meetings helped me to turn a corner with writing my thesis. For all the good advice, engineering expertise, writing guidance, and emotional support, Carolyn and Hannah, I thank you.

Thanks to all my clinical collaborators from Vancouver General Hospital. Marcel and Dina and Eyal, your insight helped shape this research. Thanks also to everybody at the radiology department and Hongbin for his expert statistics advice.

Thanks to Jenn for helping me get to the emergency room when I first hurt my back. Thanks to Dr Bishop and Dr Lloyd-Smith, whose medical expertise started me on the long road to recovery from my low back injury. Thanks to Meena Sran and Janice LeBlond for guiding me through the most difficult parts of my rehabilitation.

Acknowledgements

I would like to acknowledge my funding sources: Natural Sciences and Engineering Research Council of Canada (NSERC), The AO Foundation, International Collaboration on Repair Discoveries (ICORD), Synaptic Consulting, Vancouver Coastal Health Research Institute, and The University of British Columbia.

Finally, I would like to thank my family and friends for supporting me in so many ways, encouraging me to persevere, and helping me to keep perspective throughout my studies. Mom and Dad, you've been so patient and now you can see what I've been working on for all these years! Thanks for believing in me.

Dedication

For everyone who believed in me

Chapter 1

Introduction

Despite a low incidence rate, often reported between 25 to 52 per million people per year, [30, 36, 120, 170, 193, 206] spinal cord injuries (SCIs) take a great toll on society both personally and financially. In North America, in 2001-2002, 1,173 per million people were estimated to be suffering from temporary or permanent neurologic impairment due to SCI, [30] which ranges from complete motor and sensory loss, to dysfunction such as pain, bladder and bowel complications, and weakness of the extremities. [1] The estimated life-time health care costs of a 50-year old SCI patient in the USA is approximately \$500,000 if the injury is incomplete in the lower spine and over \$1,800,000 for high tetraplegia. [193] The annual economic burden of traumatic SCI in Canada is approximately \$3.6 billion but only half of that figure is due to direct health care costs. [1] This is roughly a 0.2% drain on the Canadian economy, if the size of the economy is estimated to be \$1.8 trillion, based on the 2011 GDP. [2]

SCI incidence in developed countries has a bimodal age distribution. [36, 120, 170, 206] SCIs are most common among young adult males (usually defined as 15 to 29 years). [30, 36, 120, 167, 170, 194, 206] SCI incidence is next highest for elderly people (usually defined as 65 years or greater). [30, 36, 120, 170, 206] When the incidences of SCI in Canada and Finland are age-adjusted, (a statistical correction for the size difference of the population groups) the incidences for elderly people exceed those of the rest of the adult population. [100, 170] Traumatic SCI incidence among elderly people is increasing in all countries with an aging population, including Canada. In most cases, this increase is proportional to the shift in demographics. [92, 101, 120, 170, 190, 193, 206]

Although SCIs suffered by elderly patients are typically not as severe as those suffered by younger patients, and they have similar neurological recovery, older patients typically exhibit less functional recovery due to other comorbidities. [33, 34, 53, 54, 86, 92, 193, 194] Elderly SCI patients have a higher mortality rate [33, 34, 55, 92, 120, 123, 170, 193, 194] and do not tolerate surgery as well as younger patients. [204] SCIs suffered by the elderly are frequently incomplete compression-related central cord injuries in the cervical spine. [33, 69, 92, 120, 170, 193] Due to their greater tendency to suffer injury to the cervical spine, the proportion of tetraplegics to paraplegics

increases with age. [24, 33, 69, 120]

The leading cause of SCI depends on the age demographic. Most SCIs suffered by young adults are due to a high-energy traumatic event; most commonly a motor vehicle accident (38% to 49%). [24, 36, 120, 170, 193, 206] This is also the leading overall cause of SCI (35% to 57%). [24, 30, 36, 120, 170, 172, 206] Falls are the leading cause of SCI for the elderly population (57% to 84%). [24, 69, 100, 120, 170, 193, 206] Falls are also the second leading cause of SCI for the entire population (19% to 45%). [24, 30, 36, 120, 170, 172, 206]

Epidemiological data about fall-related injuries often lack detail and when details are reported, the nature of the falls that cause the most injuries differ between studies. Most studies report the majority of falls causing injury to elderly people are low energy (such as a level fall from standing) [24, 92, 100, 120, 125, 167, 170, 193, 194] but some suggest that higher energy falls (such as a fall from a height greater than 1m) are more common. [33, 69, 201] Studies of geriatric spinal cord injury without radiographic anomaly (SCIWORA) or spinal cord injury without radiologic evidence of trauma (SCIWORET) suggest that many of the fall related injuries are due to low energy impacts (consistent with falls from standing height), since they do not cause osseous or ligamentous injury. [39, 68, 75, 79, 103, 112, 113, 176, 187, 201]

In cases of geriatric SCI due to a low energy traumatic event, such as a level fall from standing height, that same impact would likely be trivial to a younger adult. [24, 92, 100, 103, 120, 125, 167, 170, 193, 194] Spondylosis (a generic term for spine degeneration) may change the mechanical characteristics of the cervical spine that make it and the spinal cord more vulnerable to injury. [29, 32, 33, 39, 40, 69, 92, 103, 112, 113, 125, 176, 188, 193, 194]

Spondylosis may also result in myelopathy or radiculopathy (mechanical compression of the spinal cord or nerve roots, respectively, resulting in neurologic dysfunction). Common symptoms of myelopathy and radiculopathy are reduced balance, reaction speed, coordination, and upper body strength which increase the frequency and severity of impact of level falls. [77, 92, 186]

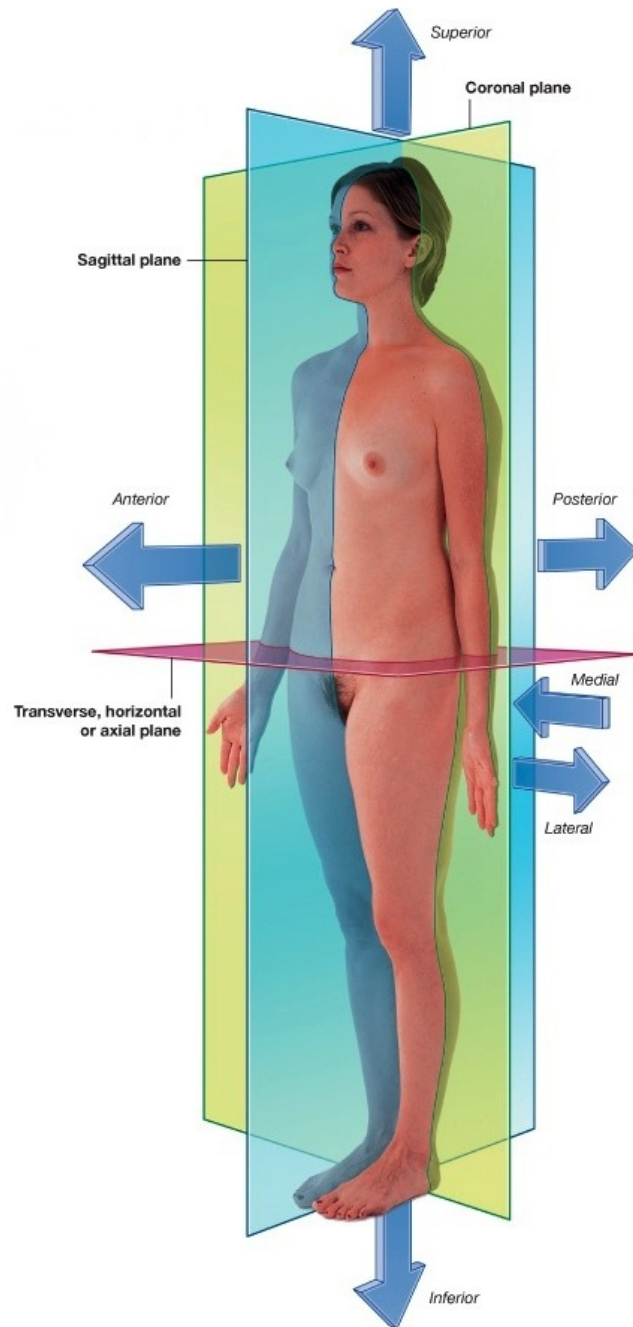
The degenerative process is complex and it may begin in humans as young as 25 years. [29, 121, 191] It affects 90% of men and women by the age of 50 and 60 respectively. [92] Degeneration can affect many aspects of spine anatomy but this thesis is most concerned with degeneration relating to the cervical spinal canal that may directly interact with the spinal cord during spine motion.

1.1 Cervical Spine Anatomy

The cervical spine is a complicated system comprised of bones called vertebrae, intervertebral discs, a spinal cord, nerves, ligaments, muscles, tendons, and vasculature. Its primary functions are supporting the many structures of the head and neck, and housing and protecting the spinal cord, while retaining incredible flexibility.

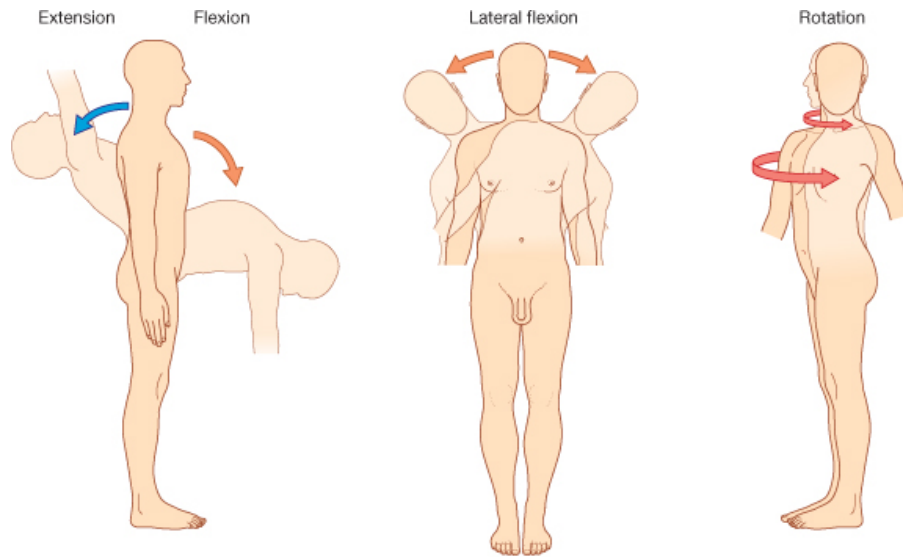
Common terminology makes description of the relative location and direction of anatomical features clear and precise. When discussing the common anatomical planes and directions, the human body is assumed to be in the conventional anatomical pose (Figure 1.1). Images of the human body are regularly presented relative to the three orthogonal anatomical planes: coronal, sagittal, and transverse. The superior-inferior (sometimes referred to as cranial-caudal) directions run along the intersection of the coronal and sagittal planes. The anterior-posterior (AP, sometimes referred to as ventral-dorsal) directions run along the intersection of the sagittal and transverse planes. The medial-lateral directions run along the intersection of the coronal and transverse planes and are unique because they describe position relative to the body's midline. The closer a feature is to the midline (from either side) the more medial, the further the more lateral (Figure 1.1). Since all large movements of the human body are rotations about a joint, these rotations are generally grouped into three orthogonal directions: flexion-extension, lateral flexion (or lateral bending), and axial rotation (Figure 1.2). [35]

1.1. Cervical Spine Anatomy



© Elsevier Ltd. Drake et al: Gray's Anatomy for Students www.studentconsult.com

Figure 1.1: The anatomical planes and directions. Adapted from Drake et al., 2005 [35] with permission from Elsevier.



© Elsevier Ltd. Drake et al: Gray's Anatomy for Students www.studentconsult.com

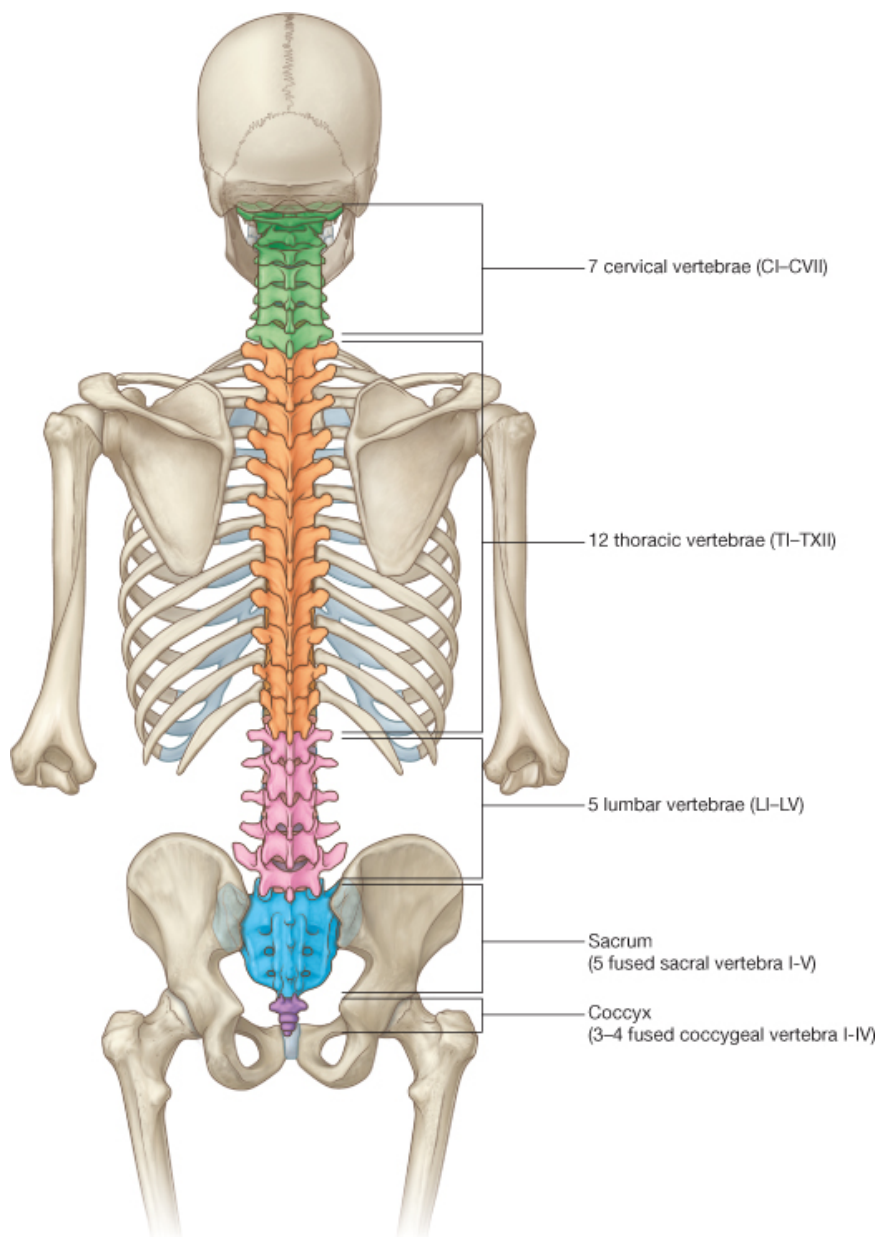
Figure 1.2: The anatomical orthogonal rotations. Reprinted from Drake et al., 2005 [35] with permission from Elsevier.

1.1.1 Normal Anatomy

The human cervical spine is composed of the seven most superior vertebrae (Figure 1.3). The atlas (C1) and axis (C2) are special vertebrae (Figure 1.4) and feature many unique characteristics. The atlas can be characterized as a ring with two superior and two inferior facets on the lateral masses. The axis interfaces with the atlas via two synovial joints and the dens (or odontoid): a bony projection extending cranially from the vertebral body of the axis. The sub-axial cervical vertebrae (C3-C7) all share common features and they more closely resemble vertebrae from the rest of the spine (Figure 1.5). [35, 121]

The sub-axial cervical vertebrae all have two pairs of superior and inferior synovial joints. A pair of superior and inferior facet joints (sometimes called apophyseal joints, or zygapophyseal joints) are located lateral and posterior to the vertebral body. A pair of superior and inferior uncovertebral joints (sometimes called joints of Luschka) are located on each vertebral body where the uncinat process extends superiorly around the disc to meet the adjacent vertebra. The uncinat process can provide lateral stability to the cervical spine. [121, 153] The primary purpose of the facet joints is to limit axial rotation and share the load with the vertebral body (Figure 1.5). [35, 121, 153, 155]

1.1. Cervical Spine Anatomy



© Elsevier Ltd. Drake et al: Gray's Anatomy for Students www.studentconsult.com

Figure 1.3: The cervical spine and spinal column. Reprinted from Drake et al., 2005 [35] with permission from Elsevier.

1.1. Cervical Spine Anatomy

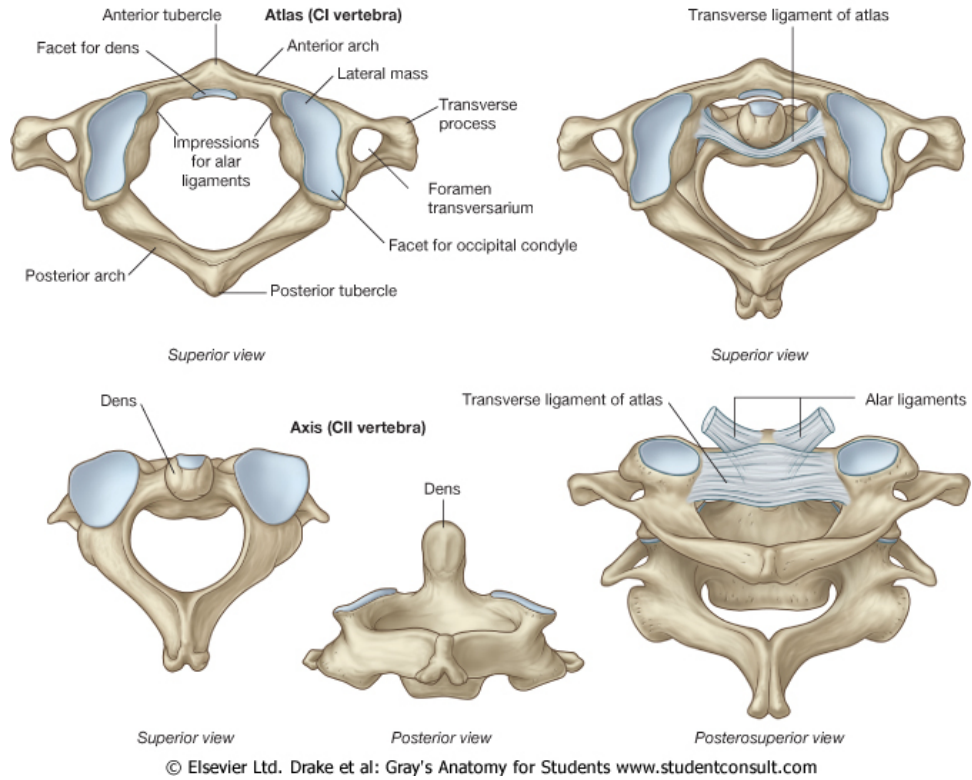


Figure 1.4: Illustrations of the atlas and axis. Reprinted from Drake et al., 2005 [35] with permission from Elsevier.

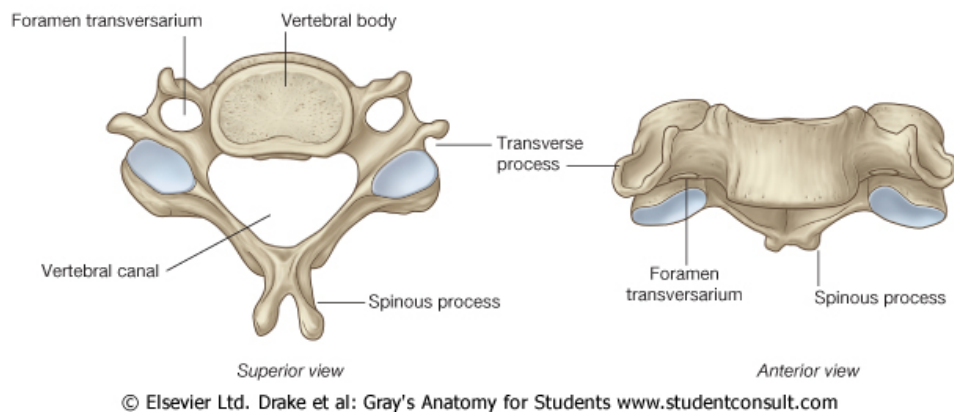


Figure 1.5: Typical cervical vertebra. Reprinted from Drake et al., 2005 [35] with permission from Elsevier.

1.1. Cervical Spine Anatomy

Intervertebral discs are located between each vertebral body of the sub-axial cervical spine. The intervertebral disc is an avascular organ, composed of an outer annulus fibrosis that surrounds a fibrocartilaginous nucleus pulposus with high water content. The annulus fibrosis is a series of highly organized concentric lamellae of fibrocartilaginous tissue that are thick in the anterior but thinner in the posterior and unciniate region. The fibres are oriented in alternating directions in each successive layer. This construction allows the disc to transmit the majority of the load carried by the spine evenly, by hydrostatic pressure, while allowing the vertebrae to move relative to each other. (Figure 1.6). [35, 121, 130, 173]

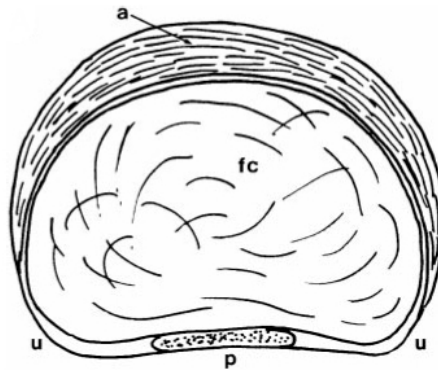


Figure 1.6: Sketch of a healthy cervical intervertebral disc illustrates a thick anterior annulus (a) that becomes more narrow in the posterior (p) and unciniate region (u). The annulus surrounds a fibrocartilaginous nucleus pulposus (fc). Reprinted from Mercer and Bogduk, 1999. [130] with permission from Wolters Kluwer Health.

By examining a functional spinal unit (FSU), composed of two adjacent vertebrae and a disc, important features can be visualized. Each vertebra is a ring of bone and together this ring creates the spinal canal. The spinal canal runs the entire length of the spine and houses the spinal cord. The intervertebral foramen on each lateral side, between the vertebral body and posterior elements, is the space that allows nerves to exit the spinal canal. Each typical vertebra articulates with its adjacent vertebra by four synovial joints (two facet and two uncovertebral joints) and an intervertebral disc (Figure 1.7). [35]

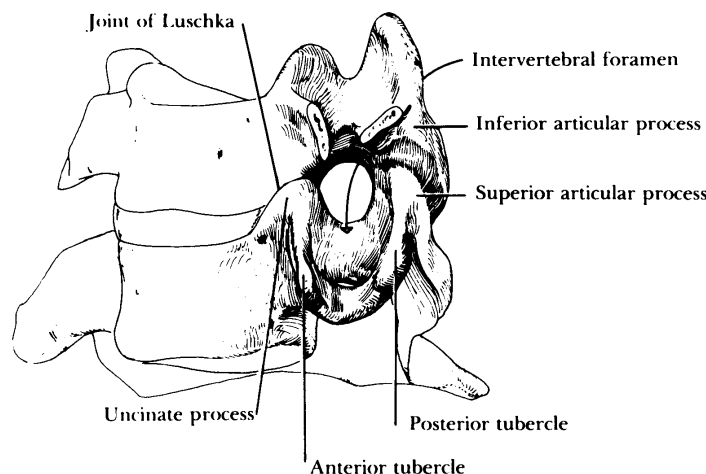


Figure 1.7: A sketch of a typical cervical functional spinal unit. Reprinted from Lestini et al., 1989. [121] with permission from Wolters Kluwer Health.

The brain and spinal cord make up the central nervous system (CNS), while the nerves that travel throughout the body make up the peripheral nervous system (PNS). The spinal cord is a dense and highly organized organ that originates at the brain stem and travels down the spinal canal. Between each vertebra, nerves originate and exit the spinal canal via the intervertebral foramina. Together the CNS and PNS transmit motor and sensory information between the brain and the body. [35]

The spinal cord is composed of two layers, grey matter in the centre and white matter which surrounds it. The grey matter gives the cord its characteristic “H” shape in cross-section and contains cell bodies, while the white matter is made up of axons. The spinal cord is surrounded by three meninges. The outer layer, called dura mater, is tough and protects the spinal cord. The thin, delicate arachnoid mater lays along the inner surface of the dura mater. The subarachnoid space, between the arachnoid mater and the spinal cord, is filled with cerebrospinal fluid. A vascular membrane called pia mater adheres to the outer surface of the spinal cord. The denticulate (or dentate) ligaments are triangular sheets of pia mater that extend from each lateral side of the spinal cord and anchor onto the dura mater. They help to tether the spinal cord in the centre of the subarachnoid space (Figure 1.8). [35, 177]

The ligaments of the cervical spine hold the joints in contact and restrict the possible motion between the vertebrae. Two ligaments are of particular interest to this thesis because they can directly interact with the spinal cord: the posterior longitudinal ligament (PLL, sometimes called the posterior common ligament), and the ligamentum flavum (LF). The PLL and LF run the length of the spine along the anterior and posterior walls of the spinal canal respectively and are adjacent to the

1.1. Cervical Spine Anatomy

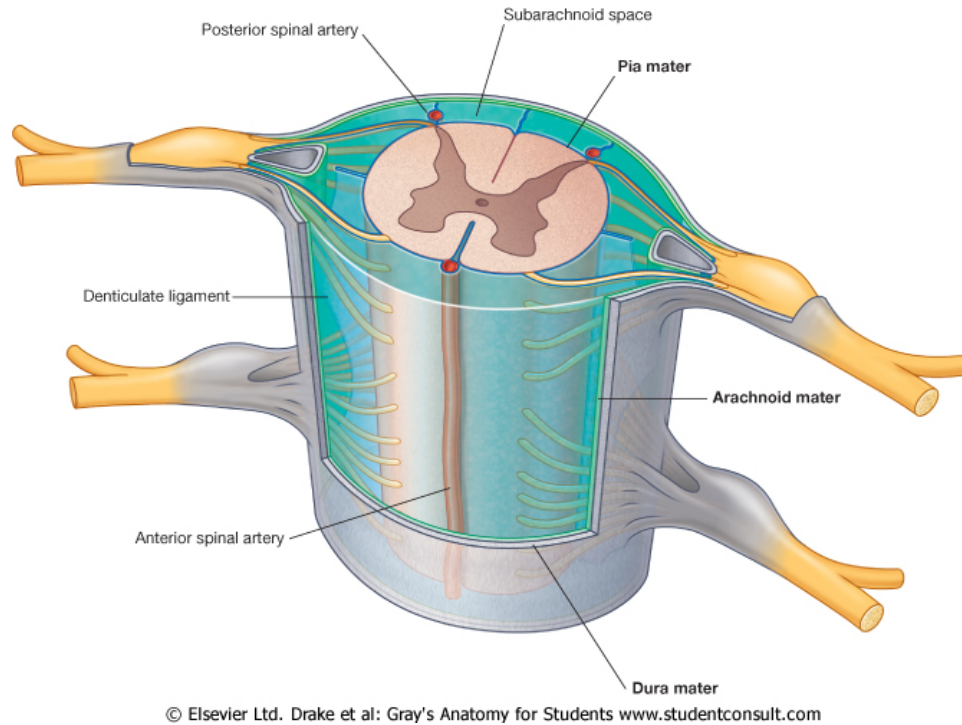


Figure 1.8: Spinal cord and related structures. Reprinted from Drake et al., 2005 [35] with permission from Elsevier.

dura mater. [35, 94, 177]

The muscles whose tendons insert directly onto the cervical spine can be broken into major groups. The spinotransversales group is primarily responsible for extending the neck and drawing the head backward. Individually, the muscles can rotate the head from side to side. The erector spinae group is responsible for extending the neck. The suboccipital muscles primarily extend and rotate the head. Other muscles of the neck counteract the muscles whose tendons insert directly onto the cervical spine and move the head in anterior directions. [35]

The vascular system contained within the cervical spine is primarily responsible for supplying blood to and from the cervical spinal cord and brain. The vertebral arteries are the largest arteries in the cervical spine. At every level of the cervical spine, segmental medullary arteries branch off of the vertebral artery to supply the anterior and the two posterior spinal arteries. Finally, the vertebral arteries reach the foramen magnum where the two arteries merge and supply the brain. The anterior and posterior spinal arteries course along the entire length of the spinal cord and supply it with blood (Figure 1.8). The spinal cord drains primarily into two veins that run along the length of the cord: the anterior spinal vein and the posterior spinal vein. These

veins drain into the internal vertebral plexus, a network that covers the external side of the dura mater and eventually drains into the major systemic veins. [35]

1.1.2 Degenerated Anatomy

Spondylosis has been extensively studied and continues to be an active area of research. [8, 14, 28, 29, 77, 93, 121, 191, 204] Degeneration leads to dysfunction of the affected anatomy, and can compromise the overall function of the spine. Spondylosis is often studied in the context of two categories of neurologic compromise: myelopathy and radiculopathy, which are due to compression of the spinal cord and the nerve roots, respectively. However, in many patients degeneration affects both the nerves and spinal cord. [77] This section will describe the spondylotic changes that are most relevant to myelopathy and SCI.

The most common forms of degeneration that directly threaten the spinal cord are intervertebral disc degeneration, and osteophyte growth (Figure 1.9). [63, 74, 76, 121, 149] Ossification of the PLL and the LF can also lead to serious injury of the spinal cord and is common in Japan but it is less common in other populations. [8, 113]

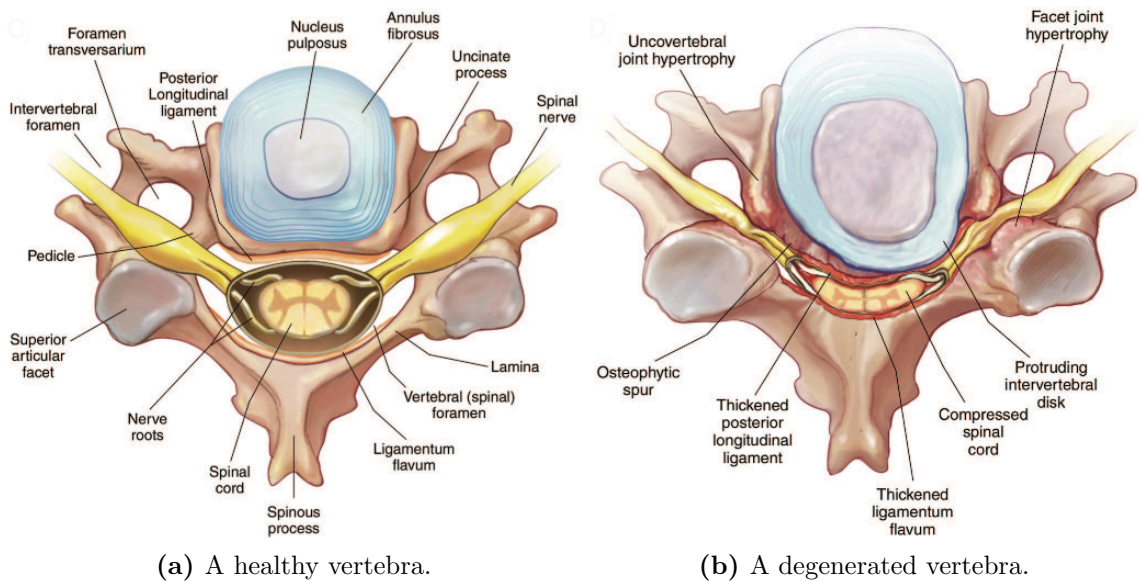


Figure 1.9: Illustrations of transverse sections of typical cervical vertebrae. A healthy vertebra (a) and a vertebra that is suffering from many types of degeneration (b). Reprinted from Tracy et al. [204] with permission from Wolters Kluwer Health.

Other types of cervical spondylosis may lead to SCI indirectly. Degeneration of the vertebral bodies includes osteoporosis, sclerosis of the endplates, and ankylosing spondylosis. Hypertrophy (enlargement) of the facet and uncovertebral joints, arthritis and other inflammatory joint disease can lead to spine dysfunction and radiculopathy (Figure 1.9). [9, 32, 39, 40, 186, 194, 204]

Spondylosis frequently affects multiple levels simultaneously and is most common in the sub-axial cervical spine. [29, 74, 77, 121, 186, 204] Degeneration is thought to be related to “wear-and-tear” on the spine and among these levels degenerative changes are most common at the most flexible FSU, which is typically C5/C6. [29, 77, 121, 186, 204]

The progression and cause of intervertebral disc degeneration is a highly complex process and an active area of research. [6, 29, 66, 121, 207, 209] Disc degeneration is characterized by disorganization of the tissue structures and loss of water content. [9, 29, 121] The various stages of disc degeneration can be visualized with magnetic resonance imaging (MRI) (Figure 1.10), which correlate well with disc height loss (visible by plane X-ray), [9, 48, 110] but there is poor correlation between degeneration grade and symptoms such as pain. [9, 76, 121, 186, 204] The cause of intervertebral disc degeneration is not known, but evidence suggests that genetics and insufficient nutrient and waste diffusion through the vertebral endplates are factors. [29, 66, 121, 209] The transport of larger solutes is aided by convective fluid-flow driven by regular loading and deformation of the discs. [45, 66] Thus spine immobility may be the cause and the consequence of disc degeneration.

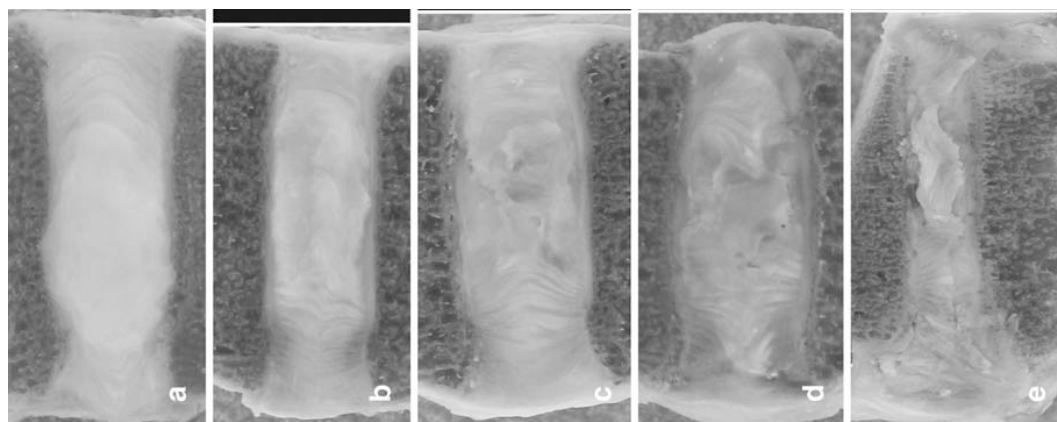


Figure 1.10: Mid-sagittal plane magnetic resonance images of intervertebral discs. Images a through e indicate increasing severity of disc degeneration. Visible changes are indicative of the grading scheme proposed by Benneker et al. Reprinted from Benneker et al. [9] with permission from Springer.

Disc degeneration can result in a loss of height, bulging or herniation of the nucleus pulposus, and an increase or a decrease in spine segment flexibility. [29, 77, 121, 204] Disc height loss can have many consequences on the surrounding structures such as reducing the size of the intervertebral foramen, endangering the nerve roots and changing the normal lordosis of the spine. [29, 77, 121] A bulging disc can protrude in any direction and can occlude the spinal canal or intervertebral foramen. If it puts pressure on the spinal cord or nerve roots a bulging disc can cause radiculopathy or myelopathy (Figure 1.9). [77, 121, 196, 204] Clinical studies using MRI have observed increased spine flexibility with mild cervical disc degeneration and reduced flexibility with more severe degeneration. [29, 121] Two studies using kinetic MRI found quantitative results supporting this relationship between cervical disc degeneration and flexibility but uncorrected repeated t-tests limited the significance of the differences found. [134, 135]

Osteophytes (bone spurs) grow radially from the margins of a vertebral body adjacent to the disc and are thought to be the body's response to vertebral instability as they tend to reduce range of motion (ROM). [8, 29, 121, 191, 204] Anterior osteophyte growth is more common and it may be so extreme that it completely changes the shape of the vertebral body (Figure 1.11). [63, 121] Severe osteophytosis can eventually lead to bridging and fusion of adjacent vertebrae. If an osteophyte grows in a posterior direction, it can endanger the spinal cord by consuming space in the vertebral canal (Figure 1.12) or it can endanger the nerve root by consuming space in the foramen (Figure 1.9). [77, 121]



Figure 1.11: Large anterior osteophytes causing locking of the vertebrae are visible in a plane X-ray image. Reprinted from Lestini et al., 1989. [121] with permission from Wolters Kluwer Health.

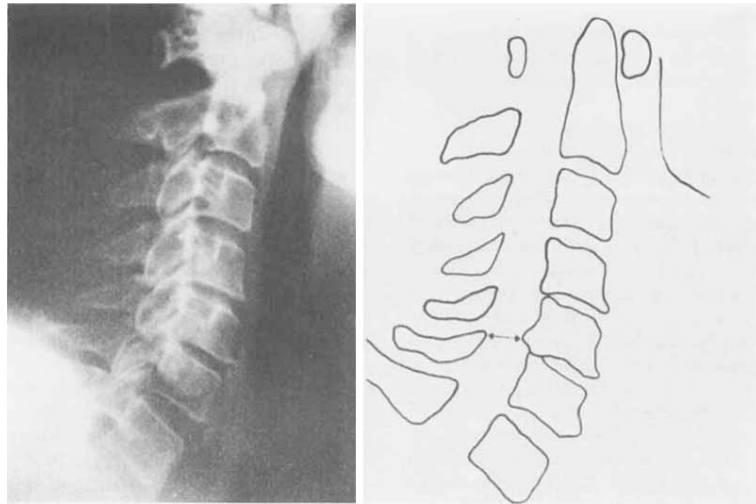


Figure 1.12: X-ray of a degenerated cervical spine. Line tracings show the minimum pincer diameter in the spinal canal has been reduced by an osteophyte growing posteriorly from the C5 vertebral body. Reprinted from Lestini et al., 1989. [121] with permission from Wolters Kluwer Health.

As the name implies, ossification of the PLL and the LF is a transformation of the

ligaments into bone-like tissue. This reduces ligament elasticity until they are eventually rigid. The cause of ossification is unclear, but contributing factors include accumulated mechanical wear and genetics. Ossified ligaments consume more space in the canal than healthy ligaments. Since ossified ligaments are less elastic, they do not conform to the contour of the spinal canal during spine motion and can reduce the available space in the canal by exacerbating ligament bulging during spine motion. Once rigid, the ligament can fracture due to minor trauma and injure the spinal cord. [8, 39, 94, 112, 113, 221]

Various forms of spondylosis often develop together and their interaction is complex. Examples include osteophytes forming around an unstable degenerated disc, or vertebral endplate sclerosis reducing nutrient diffusion, leading to a degenerated disc. [8, 29, 66, 77, 121, 207] Perception of neurologic symptoms, such as pain, due to degeneration leads to coping behaviours, and myelopathic patients are suspected to voluntarily reduce their ROM but no clear relationship between pain, pathological motion patterns, and degeneration has been found. [12, 37, 56, 135] These relationships may lead to a self-perpetuating cycle of more severe degeneration or it may reach a stable state. Even if stabilized, cervical spondylosis is better understood as a continuous process of remodelling in the context of the dynamic function of the spine.

1.2 Cervical Spine and Spinal Cord Biomechanics

1.2.1 Normal Biomechanics

Knowledge of human cervical spine biomechanics is primarily generated from experiments and observations of the spine *in vivo* and *ex vivo*. [5, 12, 13, 32, 71–73, 108, 129, 211, 217, 220] *In vivo* human studies offer the most biofidelic data, but control of the relevant variables is difficult and the methods used must not be so invasive as to harm the people involved. Thus, most *in vivo* studies depend on a variety of imaging techniques. *Ex vivo* studies use a wider selection of methods since invasiveness is not a concern, but human cadaver models deviate from the living spine they attempt to simulate, and results must always be considered in light of the relevant limitations (such as no active muscle forces, and that mechanical properties of some tissues change after death). *In vivo* and *ex vivo* animal models are highly uniform and relatively inexpensive but anatomical and biomechanical differences from the human spine must be considered. [6, 18, 19, 98, 107, 189, 192, 212, 213, 218]

Many different imaging modalities are applicable to studying spine biomechanics and each has unique strengths and weaknesses. X-ray is fast, readily available, and in-

expensive. However, X-ray is limited because it delivers an ionizing radiation dose, which puts patients at risk of harm, and it cannot effectively image soft tissue, such as the spinal cord, which is of central interest. Plane X-ray is limited to two-dimensional analysis but bi-plane imaging offers the potential for three-dimensional analysis. MRI images the spine in three-dimensions, including soft tissue, but is more expensive, time-consuming, and most devices do not allow for imaging of the spine in an upright position or allow its full flexion-extension ROM. X-ray computed tomography (CT) scanning has similar advantages and drawbacks as MRI but delivers a higher X-ray dose than a plane X-ray. Injecting contrast dye into the spinal canal allows for better X-ray imaging of the spinal cord, but myelograms are more invasive and introduce additional health risks to patients.

In vivo studies have quantified the active [37, 46, 49, 80, 87, 115, 116, 119, 124, 127, 150, 151, 165, 179, 208, 222] and passive [37, 38, 128, 134, 135] flexion-extension ROM of the cervical spine. Active ROM is caused by the subjects' muscles while passive motion is caused by an external force or the effects of gravity. Some studies visualize the individual vertebrae [37, 38, 49, 80, 87, 119, 124, 134, 135, 151, 165, 179, 208] while others only measure the total spine motion. [46, 115, 116, 127, 128, 150, 222]

Many of the mechanical characteristics of the spine have been quantified using cadaveric flexibility tests that apply a pure bending moment. [61, 133, 144, 146, 157, 159, 181] To achieve a pure bending moment, the spine must be free to rotate (in the directions orthogonal to the applied bending moment) and translate (in all three orthogonal directions) at one end of the spine. The spine displays a non-linear sigmoidal-shaped rotation response to an applied moment. The small ROM achieved with zero or very small applied moment is called the neutral zone (NZ) and is quantified by the hysteresis of the angle-moment plot of a spine during a continuous pure-moment bending test cycle (Figure 1.13). [61, 215]

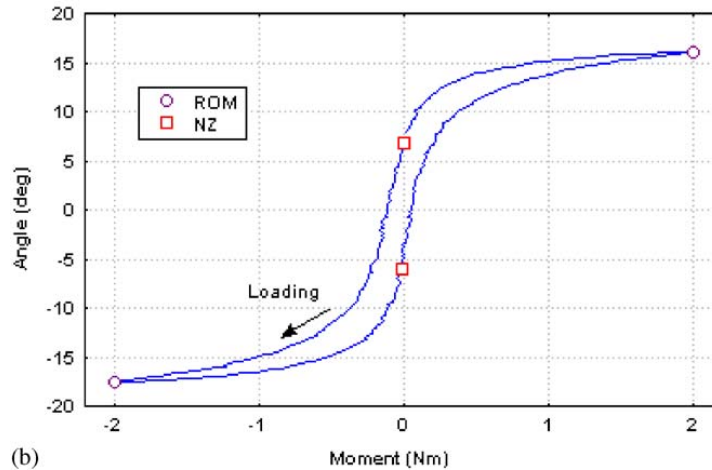


Figure 1.13: The resulting moment-angle plot during a continuous pure-moment bending test cycle of a cervical spine. Range of motion is indicated by the purple circles at the points of maximum applied moment and the neutral zone is indicated by the red squares at the points of zero applied moment. Reprinted from Goertzen et al. [61] with permission from Elsevier.

Many studies [12, 37, 38, 56, 121, 164, 165, 169, 208] have shown that during flexion-extension motion, the cervical vertebrae simultaneously rotate and translate relative to the adjacent vertebrae. The instantaneous planar motion of each vertebra can be described by a rotation about a point away from the vertebra called the instantaneous centre of rotation (COR). The location of each vertebra's instantaneous COR travels as the vertebra moves. The average COR of each vertebra is found in the inferior adjacent vertebral body (Figure 1.14).

Comparisons between *in vivo* and *ex vivo* experiments have demonstrated the need for muscle force simulation in cadaveric flexibility testing. [216] The most common muscle force simulation technique is called a follower-load [133, 160, 163] which applies axial compression using cables running along each lateral side of the spine guided through the average COR of each vertebra. By guiding the load through the COR, the static moment due to the follower load is minimized and buckling is prevented.

Due to a combination of factors, the spinal canal changes shape and size during spine motion. As a consequence of the location of each vertebra's average COR, as the spine extends the AP diameter of the vertebral canal becomes narrower in the pincer direction, and the total path length of the canal becomes shorter. [165] The pincer canal diameter (sometimes called the pincher [88] or dynamic canal diameter [71, 74]) is found between the inferior-posterior aspect of the vertebral body and the superior-anterior base of the lamina of the adjacent inferior vertebra (Figure 1.15). [121, 139,



Figure 1.14: A sketch of a mid-sagittal plane view of the cervical vertebral bodies. Anterior faces right. The dots indicate the average centre of rotation of each vertebra. The circles indicate the two standard deviation range of the instantaneous centre of rotation. Reprinted from Bogduk et al. [12] with permission from Elsevier.

176, 191] As the spine extends the posterior elements of the spine come together, tension in the PLL and LF is relieved, and those ligaments as well as the intervertebral discs bulge into the canal, reducing the AP diameter. [25, 67, 71, 165] The cumulative effect in a typical healthy adult cervical spine is a reduction of total canal volume in extension. [81]

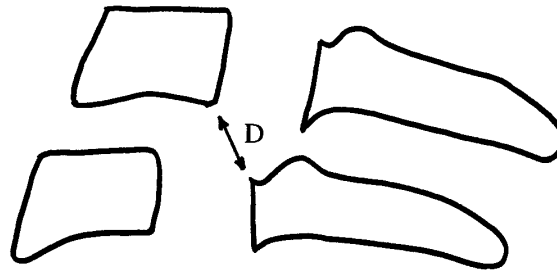


Figure 1.15: A sketch of the vertebral bodies and posterior elements of the cervical spine in the sagittal plane showing the mid-sagittal pincer diameter of the cervical spinal canal. Anterior faces left. Reprinted from Harrison et al. [71] with permission from Elsevier.

Cervical spinal canal length change during flexion-extension has been quantified and causes the spinal cord to translate and stretch. The anterior wall of two cadaver cervical spines were measured in maximum extension and maximum flexion. The length of the anterior cervical canal of the two specimens increased in flexion by 15mm and 23mm. [15] Other studies showed a increase of the anterior and posterior canal

path length of between 0% to 24% and between 28% to 61% respectively as the cervical spine rotates from full extension to full flexion. [71, 165, 183] The superior-inferior translation of the spinal cord is somewhat tethered by the brain stem, nerve roots and the denticulate ligaments. [35, 78, 177] The anterior dura mater is somewhat tethered to the PLL by friction and loose fibrous tissue. [78, 177] Thus the spinal cord must translate and stretch to conform to spine motion. [72] Cord translation up to 18mm and strain up to 17.6% was observed during flexion-extension motion of dissected cadavers. [177] More recently, the spinal cord was observed to translate 3mm and to elongate up to 6% and 10% along the anterior and posterior surfaces, respectively, from neutral to full flexion without causing injury in vivo. [223] In extension, tension of the spinal cord is relieved. [72]

In a typical healthy young spine, canal diameter changes due to spine motion are small and not harmful to the spinal cord. Change of the minimum osseous canal diameter is typically 1mm or less (in the pincer direction). [88] Canal diameter change during flexion-extension motion due to the soft tissue have been quantified in many cadaveric studies. Nuckley et al. [146, 147] observed no change, Chen et al. [25] observed disc and LF bulge consume up to 2.8mm, and Gu et al. [67] observed LF bulge up to 3.5mm. Results from Gu et al [67] were most extreme at the C5/C6 level and using an average canal diameter of 15.4mm [19, 98, 117, 158] and an average cord diameter of 6.5mm at that level [96, 97, 109], no cord compression would be expected.

The spinal cord has non-uniform, non-linear, visco-elastic material properties. [10, 21, 22, 57, 72, 83, 84, 148, 184] This allows the spinal cord to conform to spinal motion and deform to a great extent without developing significant stress or injury. In a traumatic impact scenario, applied strain and strain rates must be considered as both cause increased stress in the cord. [10, 21, 22, 57, 72, 83, 84, 148, 184] The three-dimensional stress and strain developed in the spinal cord in different loading scenarios is complicated, resulting from many components of the three-dimensional stress tensor, and the different material properties of the grey and white matter. [73, 105, 152, 156, 184] The regions of maximum Von Mises stress and principle strain have been shown to relate to the injury patterns observed in the spinal cord. [64, 73, 152, 184]

SCI criteria based on strain or deformation have been developed. [21, 51, 57, 74, 106, 152] Studies have related transverse cord compression ratio to graded pathological change [51] and neurologic dysfunction (Japanese Orthopaedic Association Score). [74] SCI was related to transverse crushing in a guinea pig model, [57, 152] and uniaxial strain in a study using puppies. [21] A threshold for SCI was also developed using a ferret model that depended on impactor velocity and cord compression. [106]

Traumatic SCI is a result of both the initial mechanical insult (primary injury) and

a cascade of events that follow as the body reacts (secondary injury). The primary injury is thought to be due to the applied stress and strain on the spinal cord tissue. This insult may also injure or interfere with the vasculature running along the spinal cord. A combination of cord stress (or strain) and inadequate blood supply (ischemia) play a significant role in SCI. [14, 26, 62, 129] Secondary injury is due to bleeding, swelling (potentially causing further ischemia), and other cellular activity causing spinal cord cell death. [8, 27, 78, 129]

Current human cadaveric studies often focus on the spinal canal and do not directly observe the spinal cord. [25, 67, 81, 88, 89, 146, 147] Previously, studies dissected spines and examined the cord's response to spine motion [15, 177, 197] but these studies are limited because the mechanical properties of the cord change rapidly after death. [22, 83, 84, 148] To address this issue, three labs (including this lab) have developed mechanical surrogate spinal cords with material properties similar to a living spinal cord. [11, 114, 171] The material properties of the cord developed in this lab were verified in quasistatic transverse compression, quasistatic longitudinal tension and dynamic transverse compression. [95, 114] With the addition of a radio-opaque contrast agent, the surrogate cord is visible by X-ray imaging.

1.2.2 Degenerated Biomechanics

Age-related degenerative changes have diverse and complicated effects on spine and spinal cord biomechanics in both traumatic and non-traumatic situations. [8, 14, 32, 39, 44, 78, 93, 156, 162, 191, 204, 210] The shape and mechanical properties of the spine can change with degeneration, which can make previously benign motions injurious for the spinal cord. Many clinical studies of elderly patients report spine fractures or SCI without fracture due to low energy impacts, [39, 68, 75, 79, 103, 112, 113, 176, 187, 201] but this author is aware of only one experimental study that relates traumatic injury with spondylosis. [31]

An SCI can occur without osseous or ligamentous injury to the spine and have often been referred to as spinal cord injury without radiographic anomaly (SCIWORA) or spinal cord injury without radiologic evidence of trauma (SCIWORET). [39, 68, 75, 79, 103, 112, 113, 176, 187, 201] However, with the advent and increasing use of MRI, the spinal cord can be directly imaged and fewer injuries fall into the SCIWORA, and SCIWORET categories. Some authors have commented that SCIWORA is becoming a misnomer, since “radiographic anomalies” can be detected using MRI in most patients with an injury. [79]

The forms of degeneration that directly threaten the spinal cord (disc degeneration, osteophytes, and ligament ossification, described above in Section 1.1.2) can all be

effectively observed with different imaging modalities. [7, 39, 204] MRI provides the most detailed images of soft tissues such as intervertebral discs. Disc bulges, herniation, dehydration, structural disorganization and disc height can be observed with MRI. [9, 121, 186, 204] Disc height, inferred by measuring vertebral endplate distance, can also be measured using X-ray. [9, 48, 50, 110, 121] Osteophytes are visible in MRI, but are clearest via X-ray (plane or CT). [7, 63, 121, 204] Ossification of the posterior longitudinal ligament (OPLL) or ossification of the ligamentum flavum (OLF) can be detected with X-ray (plane or CT), or MRI. [7, 39, 112, 113, 221] MRI is the first choice for clinical diagnosis of myelopathy or radiculopathy due to spondylosis as it can image the spinal cord and confirm if the surrounding tissue is causing compression or dysfunction. [69, 75, 112, 113, 204]

Spondylosis may lead to an overall increase or decrease in spine flexibility. Studies of lumbar intervertebral discs suggest mild degeneration causes an increase in segmental mobility but more advanced degeneration causes mobility to decrease. [132, 145] These results were consistent with finite element model results found by Rohlmann et al. [182] A cadaveric study of cervical spine motion segments with disc degeneration was less conclusive. [137] Osteophyte growth is associated with decreased spine flexibility, and may ultimately lead to vertebral fusion. [8, 29, 121, 191, 204] OPLL and OLF gradually fuses the vertebrae together reducing spine flexibility. [39, 112, 113] While these clinical observations are consistent, this author is not aware of any experimental study quantitatively relating osteophyte size, OPLL, or OLF with change in ROM. In addition, a reduction of flexibility in one region of the spine, may result in an compensatory increase in flexibility at other adjacent levels. This is seen in spondylotic patients with reduced mobility in the sub-axial cervical spine. [131]

The relationship between spine flexibility loss due to spondylosis and spine injury due to mild trauma is unclear. Spondylosis most commonly affects the sub-axial cervical spine. [29, 74, 77, 121, 186, 204, 204] When degenerated levels are less flexible, injuries due to mild trauma are frequently observed clinically at the next most mobile superior segment in the spine. [16, 32, 39, 112, 125, 194] Dens fractures are particularly common in elderly populations. [16, 92, 123, 125, 167, 194] However, one study observed injuries were more common at the next most mobile inferior segment in the spine. [113] In these cases degenerative rigidity is thought to provide some protection to the spine, but in other cases degeneration appears to make the spine brittle, and fractures have been observed at the site of ankylosing spondylitis or OPLL due to mild trauma, possibly due to concurrent osteoporosis. [32, 39, 40, 113] A rigid lever arm or hinge/fulcrum mechanism has been proposed to explain the fractures frequently observed in the upper cervical spine when inferior segments have reduced flexibility due to advanced spondylosis. [31, 32] Experimental modelling is needed to better understand the different injury mechanisms and how to protect patients in

the event of trauma. [16, 31] To the best of this author’s knowledge, only one cadaveric impact study has related injury to spondylotic features in the spine. During compression-flexion impacts, injuries were frequently located adjacent and superior to locations of degeneration. [31]

Spondylosis not only changes the quantity of spine motion but also the quality. Normal spine motion is a combination of vertebrae rotating and translating relative to each other. Disproportionate translation of two adjacent vertebrae is called spondylolisthesis. While most cases of cervical spondylolisthesis are due to trauma such as a hangman fracture (fracture of the axis pedicles), degenerative spondylolisthesis is associated with disc degeneration and facet hypertrophy. [93] This may be due to a loss of disc height causing laxity of the spine ligaments. [29] In principle, a pathologic change in the relationship between vertebral rotation and translation could be visualized as a change of the COR. [38, 208] However, due to the travel of each vertebra’s COR during normal healthy motion, in practice a healthy COR has not been successfully distinguished from a pathologic COR due to spondylosis, except in extreme cases. [56]

A pincer action between two adjacent vertebrae is the typical spondylotic SCI mechanism due to spine extension (Figure 1.15). [8, 33, 69, 71, 191] Many human cadaver studies have examined spinal canal narrowing in quasi-static extension illustrating the pincer mechanism. [25, 62, 67, 81, 88, 146, 147, 195] The normal reduction of the pincer diameter during extension may be exaggerated by pathologic vertebral motion patterns such as spondylolisthesis. Posterior osteophytes, ossification of the PLL and LF, and a bulging or herniated disc reduce the static canal diameter and exaggerate the dynamic canal diameter change that normally occurs during flexion and extension. [25, 33, 67, 71, 74, 121, 140, 197, 204] As the spine extends, the spinal canal path length decreases, spinal cord longitudinal tension relaxes, and its cross-sectional diameter increases. [71, 72, 78, 141, 183] All of these effects compound to consume the clearance space for the spinal cord in the spinal canal. This is of particular concern to people with a naturally small neural space, who have little clearance to begin with. [204] If the extension motion is due to a traumatic impact (such as a fall causing an impact to the forehead), the transverse compression would be applied at a higher speed, which would increase spinal cord stress. [10, 85, 106]

“Bowstring stretching” of the spinal cord across an anterior protrusion (such as a bulging disc or posterior osteophyte) is the typical spondylotic SCI mechanism due to spine flexion (Figure 1.16). [15, 73, 78, 156, 191] As the spine flexes, the spinal cord is stretched and pulled anteriorly due to the path length of the spinal canal becoming longer and the curvature of the spine becoming more rounded. [72, 73, 78, 140, 141, 156, 177, 191] Spondylosis may increase localized spinal cord tethering in a variety of ways causing cord stretching to be less uniformly distributed. Canal stenosis can cause

cord pinching. [78] An anterior canal protrusion (such as a bulging disc or osteophyte) can increase the friction between the dura and the PLL. [78, 177] Thickening of the dentate ligaments or narrowing of the foramen (due to any combination of causes such as a bulging disc, osteophyte growth, or disc height loss) can restrict sliding of the nerve roots, causing them to stretch with spine movement and increase their tethering effect. [29, 77, 78, 121] These factors cause bowstring stretching that causes very complicated combined loading in the spinal cord. [8, 73, 78, 156, 191] Three dimensional numerical modelling of this combined loading condition has not been conducted, but qualitative analyses [73, 78, 156] and a 2D numerical simulation [122] suggest that the shear stress would be maximum near the centre of the cord. A three-dimensional finite element model of intermittent cervical myelopathy provoked by flexion found maximum Von Mises Stress would be located in the grey matter, particularly at the anterior horn and posterior horn but the model did not include longitudinal tension of the cord. [105] These stress patterns are consistent with the centrally located cord injury associated with cervical central cord syndrome that is commonly suffered by elderly SCI patients. (The syndrome is defined as an incomplete SCI that disproportionately impairs motor function of the upper limbs, while function below the lesion is relatively preserved.) [33, 69, 92, 120, 170, 193] Additionally, compression at the anterior surface of the spinal cord may cause ischemia. [8, 15, 62, 78, 162, 191] While studies prior to 1970 using cadaveric specimens illustrated the bowstring and pincer injury mechanisms and their effects on the shape of the spinal cord and blood vessels, [15, 177, 197] the bowstring stretch injury mechanism has been somewhat neglected in current research. [78]

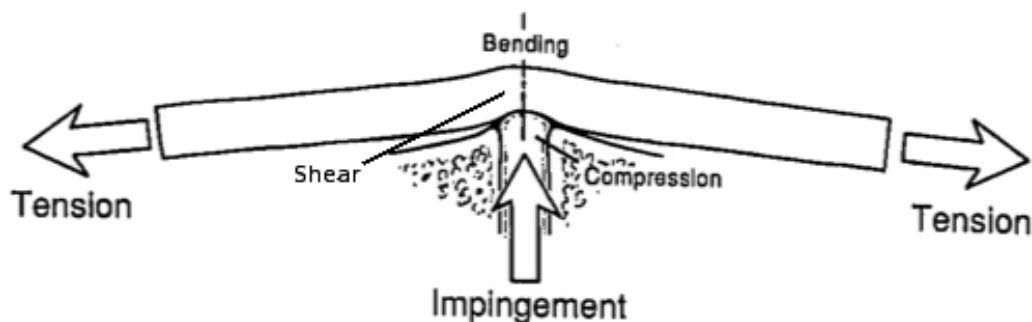


Figure 1.16: Illustration of bowstring stretching of the spinal cord due to a posterior bulging disc during spine flexion. Adapted from Panjabi et al. [156] with permission from Wolters Kluwer Health.

A need remains for further understanding of quantitative relationships between spine degeneration and cervical spine motion and SCI. There are no clear relationships between vertebral ROM, AP translation, or canal diameter change with the combined

effects of spondylosis. This requires improved quantitative *in vivo* methods to measure degenerative features and *ex vivo* experimental models to relate these features to the compression of a biofidelic spinal cord.

1.3 Study Objectives

The objectives of this thesis are part of the preliminary development of a research program that aims to quantify the relationships between spine degeneration, spine motion, and SCI tolerance and risk. Two studies are performed.

The objective of the first study is to develop an image analysis technique for quantitative analysis of cervical spine kinematic and degenerative features in plane images and to evaluate the analysis technique using a plane flexion-extension X-ray image pair. These techniques may be used in the future to measure continuous, quantitative variables that may be used to build multi-variable regression models that predict clinical SCI risk factors, such as cervical spinal canal diameter change.

The objective of the second study is to develop a new method for quantifying the effect of increasing canal stenosis on spinal cord compression during spine motion in cadaveric experimental models. This study will determine the effect of increasing canal stenosis due to an artificial osteophyte on a biofidelic surrogate cord during quasi-static motion of an *ex vivo* whole porcine cervical spine. Accuracy of surrogate spinal cord diameter measurements made via plane X-ray will be evaluated.

Chapter 2

X-ray Predictors of Cervical Spinal Canal Diameter Change

2.1 Introduction

Spinal cord injuries (SCIs), while uncommon, can have devastating effects because any damage to the central nervous system can cause widespread and permanent sensory and motor impairment. Traumatic SCI incidence is often reported between 25 to 52 people per million in North America and has a bimodal age distribution; injuries are most common in young adults (15-29 years) and the elderly (over 65 years). [30, 36, 120, 170, 193, 206] Trends indicate that injury rates are increasing among the elderly, reflecting shifting population demographics. [92, 101, 120, 170, 172, 206] These are often incomplete cord injuries and are predominately due to falls. [36, 39, 92, 101, 103, 120, 172, 172, 194, 206]

A narrow spinal canal can compress the spinal cord, which can contribute to incomplete SCI. [39, 68, 92, 103, 113, 176, 188] A spinal canal can become more narrow over time due to age-related spinal degeneration such as osteophytes (bone spurs) protruding from the vertebral body posteriorly into the spinal canal. [39, 92, 103, 113, 121, 176, 188] The spinal canal diameter can be dynamically reduced by flexion-extension motion in both traumatic and non-traumatic situations. [39, 68, 92, 103, 113, 121, 176, 188] The most significant dynamic narrowing occurs in the pincer direction between the inferior-posterior corner of a vertebral body and the superior edge of the lamina from the adjacent-inferior vertebra. This is the narrowest diameter of a spinal canal in subjects with posterior osteophytes. [121, 139, 176, 191]

Many clinical [39, 52, 71, 90, 102, 126, 168, 176, 191] and experimental [25, 67, 81, 146, 147, 195] studies have shown that the cervical spinal canal typically becomes more narrow in extension and becomes wider in flexion, but few studies have explored how canal diameter change during spine motion relates to degenerative features. Magnetic resonance imaging (MRI) was used in a series of studies to measure canal diameter and cord compression during flexion-extension motion and subjects were categorized into

groups based on disc degeneration. [134–136] Chen et al. [23] found disc degeneration grade and canal diameter in neutral MRI images could predict cord impingement in extension. Hayashi et al. [74] measured intervertebral disc space narrowing, osteophytosis, and retrolisthesis and qualitatively related them to canal diameter narrowing. They contrasted degenerative features and canal diameter change in young patients with older patients and between myelopathic patients compared to non-symptomatic subjects. Using X-ray computed tomography (CT) myelograms, they quantified the compression ratio of the spinal cord and related those results to canal narrowing and neurologic symptoms. Muhle et al. [139, 140] graded osteophyte severity and disc degeneration and compared patients’ canal diameter change and cord compression during flexion-extension motion using kinematic MR imaging. Fukui et al. [52] correlated pincer canal diameter in extension with anterior-posterior (AP) vertebral translation and with the Japanese Orthopaedic Association (JOA) score for clinical evaluation of myelopathy. Gore et al. [63] measured cervical spine features in X-ray images and correlated static canal diameter (not canal diameter change) with degenerative measures (disc space narrowing, endplate sclerosis, anterior and posterior osteophyte size) in asymptomatic people. Taken together, many different degenerative features have been compared with canal diameter change, but differences in methodology make synthesis of these results difficult. Although some of these studies showed relationships between degenerative features and canal diameter change, few used regression analyses and most did not evaluate these relationships quantitatively.

To the best of our knowledge, no study to date has used plane X-ray to quantify angular range of motion (ROM), AP translation, intervertebral disc height, osteophyte length, and spinal canal diameter change due to flexion-extension motion in the cervical spine as continuous variables so that the relationship between the variables can be quantified by linear regression. These variables could be individually correlated, or a group of variables may be used to create a multi-variable linear regression model that predicts canal diameter change during flexion-extension motion. The objective of the present study is to develop an image analysis technique for quantitative analysis of cervical spine kinematic and degenerative features in plane images and to evaluate the accuracy and precision of the technique using a plane flexion-extension X-ray image pair.

2.2 Materials and Methods

A sample flexion-extension sagittal plane X-ray image pair was used to evaluate the analysis technique (Figure 2.1). The four corners of the projected perimeter of each vertebral body were located and manually digitized. The corners were located on the

2.2. Materials and Methods

surface of the cortical shell of each vertebral body. Where an osteophyte spur was identified, the tip of the osteophyte and the estimated vertebral body corner (where the corner would be if the osteophyte was not there) were both marked. Estimated vertebral body corners were located by the thickened cortical shell in the region of an osteophyte. Additionally, the superior edge of each lamina that forms the posterior wall of the vertebral canal was marked (Figure 2.2). All landmarks were located and manually digitized by the author.

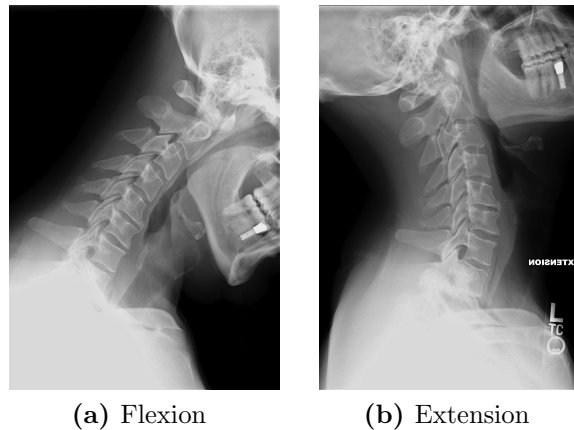


Figure 2.1: Sample flexion-extension image pair used to demonstrate analysis technique. Image source: commons.wikimedia.org [3, 4] Attribution: Stillwaterising Creative Commons CC0 1.0 Universal Public Domain Dedication.

Custom analysis scripts were written using Matlab (R2006a, The MathWorks Inc., Natick, Massachusetts, USA) that allowed manual digitization of the boney landmarks and calculated the following variables for analysis.

- Angular Range of Motion (ROM)
- Anterior-Posterior (AP) Translation
- Intervertebral Disc Height
- Spinal Canal Diameter (in flexion, in extension, and the difference)
- Osteophyte Length

Each variable was calculated for each functional spinal unit (FSU) between C2 and C7. A scale factor was estimated to convert all linear variable results into mm based on published quantitative dimensions of the cervical vertebral body. [158] The resulting vertebral body depth of the C3 to C7 vertebrae in the presently analyzed images

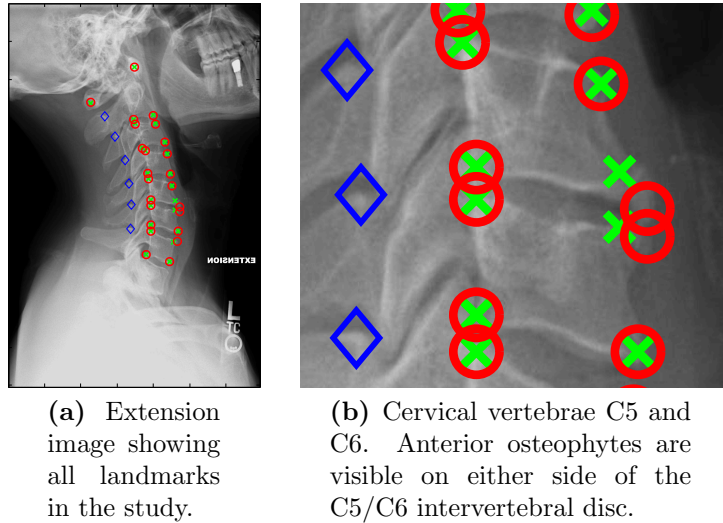


Figure 2.2: Landmarks on cervical vertebrae used for image analysis. Each red circle indicates an anatomical vertebral body corner or the tip of an osteophyte if present. Each green x indicates an estimated vertebral body corner (where the corner would be if the osteophyte was not there). These locations overlap if no osteophyte is present. The blue diamonds indicate the superior edge of the lamina.

ranged between 14 and 18mm which was within 1mm of the previously published values.

After digitizing the landmarks, ROM was calculated for each FSU using an algorithm developed by Frobin et al. [49] The four vertebral body corners were used to find a mid-line through each vertebra. If an osteophyte was present, the estimated vertebral body corners were used. The angle between each pair of adjacent lines was found. A positive angle indicated an angle opening toward the anterior, while a negative angle indicated opening to the posterior (Figure 2.3). ROM was calculated by subtracting the difference between the angle in the extension X-ray image and the flexion X-ray image. Positive ROM was defined as extension motion ($ROM = \text{Angle}_{\text{Extension}} - \text{Angle}_{\text{Flexion}}$). ROM values from each FSU were also summed to produce a representative whole-spine (C2-C7) ROM.

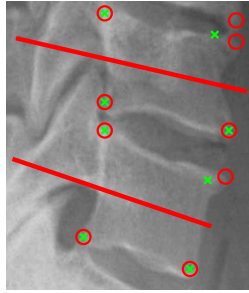


Figure 2.3: Red lines illustrate the vertebral body mid-lines used to calculate the angle between two adjacent vertebrae.

AP translation was calculated by adapting an algorithm developed by Frobin et al. [49]. The bisectrix in the present study bisects the angle created by the lines defined by the endplates of the vertebral bodies adjacent to the disc. Then, the centre-point of each vertebra was calculated by finding the average of the coordinates of the four vertebral body corner points. If an osteophyte was present, the estimated vertebral body corners were used. The centre points of each vertebra were then projected onto the bisectrix by a line perpendicular to the bisectrix. The distance between these projected points defined the dorso-ventral displacement (Figure 2.4). AP translation was defined as the difference between the dorso-ventral displacement in the flexion X-ray image and the extension X-ray image. Positive AP translation meant the superior vertebra was more posterior, relative to the inferior vertebra, in extension relative to flexion (AP translation = dorso-ventral displacement_{Extension} - dorso-ventral displacement_{Flexion}). The difference between the present method and the one developed by Frobin et al. was the definition of the bisectrix. [49]

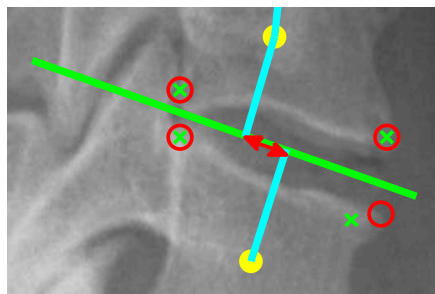


Figure 2.4: Positive dorso-ventral displacement in the extension view is illustrated by the red arrow. The yellow dots illustrate the centre point of vertebrae. The green line illustrates the bisectrix. The cyan lines illustrate the perpendicular projection of the vertebral centre point onto the bisectrix.

The intervertebral disc height was calculated by adapting an algorithm developed

2.2. Materials and Methods

by Frobin et al. [50] Using the bisectrix described above, the anterior disc height was calculated by summing the perpendicular distances from the anterior corners of the adjacent vertebral bodies to the bisectrix. Then the posterior disc height was calculated in the same manner, using the adjacent posterior vertebral body corners. If an osteophyte was present, the estimated vertebral body corner was used (Figure 2.5). A representative value for the intervertebral disc height was found by averaging the anterior and posterior disc height. Disc height values calculated in this way are expected to be insensitive to vertebral angle so the value from either the flexion or extension image can be used. However, it is not known if this representative disc height is insensitive to vertebral angle in general, so values from both flexion and extension images are reported in the present study. Frobin et al.'s method used only the anterior disc height and a correction factor to account for vertebral angle. [50]

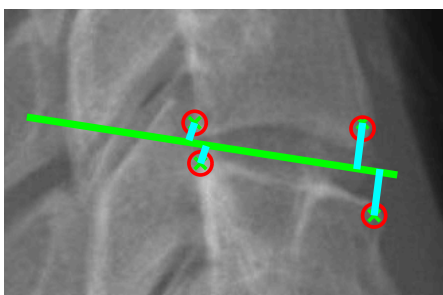


Figure 2.5: Posterior and anterior disc height are illustrated by the two pairs of cyan lines. The green line illustrates the bisectrix.

Canal diameter was measured between the inferior-posterior corner of a vertebral body and the superior edge of the lamina from the adjacent-inferior vertebra. If an osteophyte was present, the tip of the osteophyte was used (Figure 2.6). This diameter is commonly referred to as the pincer diameter and can change due to relative motion of the vertebrae. Canal diameter in flexion was subtracted from the value measured in extension to calculate canal diameter change (Canal Diameter Change = Canal Diameter_{Extension} - Canal Diameter_{Flexion}).

Osteophyte length was calculated by measuring the distance between the tip of the osteophyte and the estimated vertebral body corner. The lengths of the osteophytes growing from the four corners adjacent to an intervertebral disc were summed to give one representative value for each FSU. Osteophyte lengths were calculated in both flexion and extension and the greater of those two values for each FSU was used (Figure 2.7).

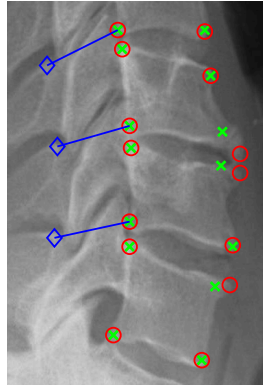


Figure 2.6: Pincer canal diameter was measured from the inferior-posterior corner of a vertebral body and the superior edge of the lamina from the adjacent-inferior vertebra. The blue lines illustrate the canal diameters.

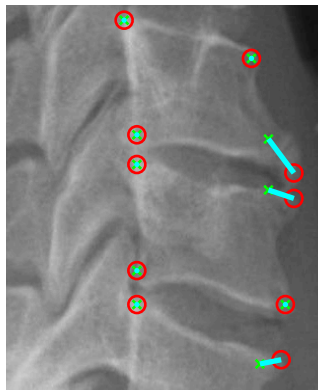


Figure 2.7: Osteophyte length is the sum of the distances measured between the tip of an osteophyte and the estimated vertebral body corner around a given intervertebral disc. Cyan lines illustrate the osteophyte length, where osteophytes exist.

2.2.1 Intra-reader Repeatability Assessment

The X-ray image pair was manually digitized by the author on two occasions more than five months apart. All kinematic and degenerative variables were calculated using each of the landmark data sets. The difference between the calculated variables illustrated intra-reader repeatability.

The repeatability of digitizing landmarks was evaluated by manually digitizing one osteophyte tip, one estimated vertebral body corner, and one lamina landmark in one image 30 times each (Figure 2.8). The procedure for digitizing the landmarks

required the user (the author) resize the image and move the mouse between each repetition. For each landmark, the average location of the cloud of digitized points was found. Then the magnitude of the vector distances from each point to the average point was found. The average distance indicated the radius of the point cloud and the repeatability of digitizing that landmark. Distances were calculated in pixels and then converted to mm using the same scaling factor as in the main study.



Figure 2.8: Dot clouds illustrate the 30 repeated digitizations for each landmark. Red dots indicate the osteophyte tip. Green dots indicates an estimated vertebral body corner. Blue dots indicate the superior edge of the lamina.

2.2.2 X-ray Image Analysis Accuracy and Precision Assessment

The calculation of all variables in this study are subject to various sources of error that can be broken into three groups: X-ray imaging, location of landmarks, and manual digitizing of points. These sources of error are described in more detail in the Discussion (Section 2.4.1). The cumulative effects of these sources of error were quantified by assessing the angular and linear measurement error.

Angular Accuracy

Angular accuracy was quantified by using the X-ray image analysis method described above to measure a known vertebral angle change. This was achieved by imaging,

2.2. Materials and Methods

with the assistance of Vancouver General Hospital Radiology, two dried human cervical spine vertebrae mounted on a simple apparatus that controlled the vertebrae's relative position (Figures 2.9 and 2.10). The dried vertebrae were mounted to carved plastic blocks that accepted the curvature of the vertebral bodies. Rubber bands provided the seating force. Vertebral body landmarks were then located and manually digitized by the author. The vertebral angle was controlled by three interchangeable wedges that were each cut with a different angle. (15° , 27.7° , 39.9°) The angle of each wedge was verified with an accuracy of $\pm 0.4^\circ$ by taking the arctangent of multiple measurements of the height and length of the wedges with digital callipers ($\pm 0.005\text{mm}$). The resulting angles calculated along the length of each wedge were consistent within $\pm 0.4^\circ$.

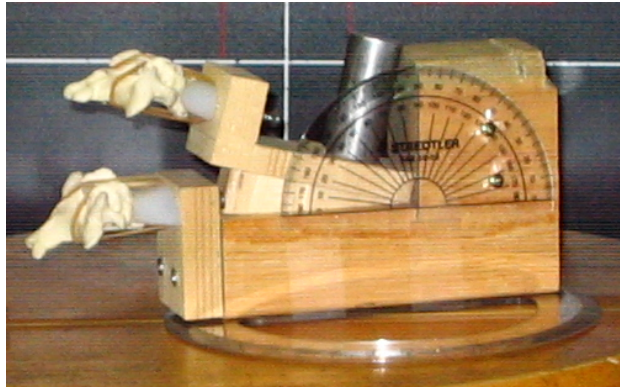


Figure 2.9: Photograph of the X-ray angular accuracy assessment apparatus. The 15° wedge is in use.

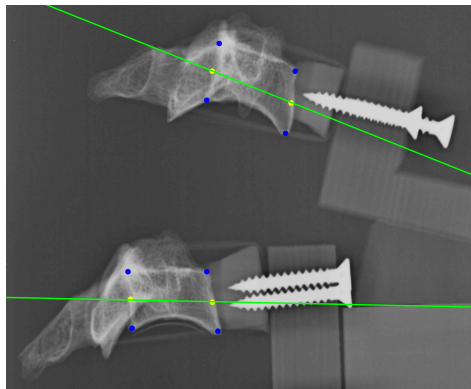


Figure 2.10: A typical angular accuracy assessment X-ray image with highlighted landmarks and geometric constructions. The 15° wedge is in use. The apparatus is positioned in-plane.

The absolute vertebral angle was not known because mounting the vertebrae onto the apparatus introduced a constant offset to the angle measured from the wedge angle. This constant offset was cancelled out by finding the difference between the vertebral angles in each different position. This subtraction replicated finding the ROM in the main study and produced three angle difference values 12.7° ($= 27.7^\circ - 15^\circ$), 12.2° ($= 39.9^\circ - 27.7^\circ$), 24.9° ($= 39.9^\circ - 15^\circ$) with an accuracy of $\pm 0.8^\circ$. These values were the best available standard against which the image analysis algorithm was compared.

Imaging with a constant wedge angle (15°) was repeated with the whole apparatus in-plane, and out-of-plane. The out-of-plane angle was increased in 5° increments by noting the angle indicated by the 360° protractor attached to the base of apparatus. ($0^\circ, 5^\circ, 10^\circ, 15^\circ$) A 15° maximum out-of-plane angle was deemed reasonable since regular hospital radiology procedures can be relied upon to keep patients' bodies and head motions reasonably aligned in-plane. [70] By subtracting the angle calculated in the out-of-plane images from the in-plane image, the error due to out-of-plane rotation was quantified.

Linear Precision

To quantify the linear precision of this study, the static vertebral canal diameter of each vertebra from the sample X-ray pair was calculated. A static canal diameter (as opposed to the pincer canal diameter that was measured in the main study) is defined by two points on a single vertebra. The static canal diameter calculated for this study was measured between the inferior-posterior corner of a vertebral body and the superior edge of the lamina of the same vertebra (Figure 2.11). Since these two points were on a rigid body, the distance between them should not change during spine motion. Any difference between the static canal diameter calculated in the flexion and extension views was due to the cumulative effects of all sources of error in the image analysis method.

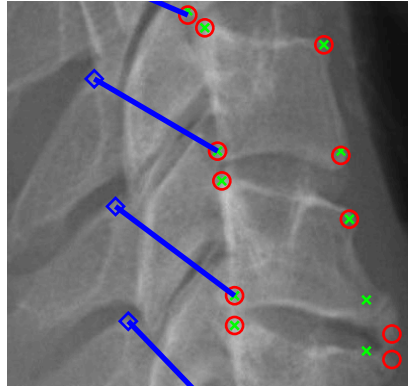


Figure 2.11: Static canal diameter, illustrated by the blue line, measured from the inferior-posterior corner of a vertebral body and the superior edge of the lamina of the same vertebra.

2.3 Results

2.3.1 X-ray Image Analysis Accuracy and Precision Assessment

Angular Accuracy

The in-plane image analysis accuracy in the main study was conservatively estimated to be $\pm 1.3^\circ$. The average error indicated by the accuracy study ($\pm 0.5^\circ$) was less than the error of the wedge angle difference itself ($\pm 0.8^\circ$) (Table 2.1). The two error values were added to produce a conservative measure of accuracy.

Table 2.1: Results of the in-plane angular accuracy study.

Wedge Angle Difference	Vertebrae Angle Difference (Calculated From X-ray Image)	Error
12.7°	13.1°	0.4°
12.2°	11.4°	0.8°
24.9°	24.5°	0.4°
	Average Error	0.5°

Angle measurements were not affected by out-of-plane rotation of up to 15° in an amount that could be meaningfully detected. The error recorded with a 5° out-of-plane rotation was marginally detectable, but as the out-of-plane angle increased, the

2.3. Results

error observed was less than the image analysis accuracy ($\pm 1.3^\circ$) (Table 2.2). Since no trend of increasing error as the out-of-plane angle increased was detected, error due to out-of-plane rotation up to 15° was dismissed.

Table 2.2: Results of the out-of-plane angular accuracy study. Vertebrae angle was measured with a constant wedge angle while out-of-plane angle increased.

Out-of-plane Angle	Error
5°	1.6°
10°	0.1°
15°	0.9°

Linear Precision

The linear average absolute-value error was approximately $\pm 0.6\text{mm}$ (Table 2.3). Since this analysis assumed a scale factor, the static canal diameter change indicates an approximate precision, and is comparable to the sample results (Section 2.3.2).

Table 2.3: Static canal diameter difference between flexion and extension views and the average of the absolute-value of the canal diameter change.

Vertebral Level	Static Canal Diameter Change (mm)
C3	0.5
C4	0.1
C5	-0.5
C6	-0.8
C7	-0.9
Average Absolute-value Error	0.6

2.3.2 Kinematic and Degenerative Variables Sample Results and Repeatability

Sample results for kinematic and degenerative variables were calculated using the flexion-extension X-ray image pair (image source: commons.wikimedia.org [3, 4]). The images were digitized on two occasions and results from both landmark data sets are summarized below (Tables 2.4 and 2.5). Based on the results of the image analysis assessment, values are reported to the nearest integer. ROM results may be compared to the angular image analysis accuracy assessment (Table 2.1). Since the linear variables were calculated using the estimated scale factor, they are approximate

2.3. Results

but they can be compared to each other (within and between variables) and to the results from the linear image analysis precision assessment (Table 2.3).

Table 2.4: Sample results for kinematic and degenerative variables using the first landmark data set.

FSU	C2	C3	C4	C5	C6
	/C3	/C4	/C5	/C6	/C7
ROM (°)	6	16	16	3	14
AP Translation (mm)	0	1	2	0	0
Disc Height, Flexion (mm)	4	5	5	3	4
Disc Height, Extension (mm)	4	5	6	5	6
Canal Diameter, Flexion (mm)	19	18	18	15	16
Canal Diameter, Extension (mm)	18	14	15	14	14
Canal Diameter Change (mm)	-1	-4	-4	-1	-2
Osteophyte Length (mm)	None	None	None	10	4

Table 2.5: Sample results for kinematic and degenerative variables using the second landmark data set.

FSU	C2	C3	C4	C5	C6
	/C3	/C4	/C5	/C6	/C7
ROM (°)	11	15	13	7	11
AP Translation (mm)	1	1	1	0	0
Disc Height, Flexion (mm)	3	4	4	3	4
Disc Height, Extension (mm)	4	5	5	4	5
Canal Diameter, Flexion (mm)	20	19	18	15	16
Canal Diameter, Extension (mm)	18	15	15	14	15
Canal Diameter Change (mm)	-2	-4	-3	-1	-1
Osteophyte Length (mm)	None	None	None	10	4

The difference between the sample results based on the first and second manual digitizations demonstrated high intra-reader repeatability for all linear results (Table 2.6) but ROM results were less repeatable. Linear results from the two digitizations were within experimental precision. Individual ROM results did differ by more than experimental accuracy, but the total ROM (when ROM from all FSU's are summed) was equal.

Table 2.6: Difference between sample results for kinematic and degenerative variables using the first and second landmark digitization data sets.

FSU	C2 /C3	C3 /C4	C4 /C5	C5 /C6	C6 /C7
ROM (°)	5	-1	-4	3	-3
AP Translation (mm)	0	0	-1	0	0
Disc Height, Flexion (mm)	0	0	-1	0	-1
Disc Height, Extension (mm)	0	0	-1	-1	-1
Canal Diameter, Flexion (mm)	0	1	0	0	0
Canal Diameter, Extension (mm)	0	0	0	0	0
Canal Diameter Change (mm)	0	0	1	0	1
Osteophyte Length (mm)	None	None	None	-1	0

The intra-reader repeatability of digitizing vertebral landmarks (osteophyte tip, estimated body corner, and lamina) ranged between ± 1.66 pixels to ± 2.36 pixels depending on the type of landmark (Table 2.7). Using the same estimated scale factor as in the main study, this is equivalent to a range of approximately ± 0.21 mm to ± 0.30 mm. These repeatability results can be compared to all other sample results, (Tables 2.4 and 2.5) and precision results (Table 2.3).

Table 2.7: Vertebral landmark intra-reader digitization repeatability.

Vertebral Landmark	Average Distance (pixels)	Average Distance (mm)
Osteophyte Tip	2.36	0.30
Estimated Body Corner	1.77	0.23
Lamina	1.66	0.21

2.4 Discussion

The image analysis technique described in the present work offers a means of measuring a combination of kinematic and degenerative cervical spine features as continuous quantitative variables. To the best of our knowledge, the combination of variables reported in the present work has not been measured as continuous quantitative variables in a single population group before.

Continuous quantitative variables may be used to create linear regression models that predict clinically relevant risk factors for cervical SCI, such as spinal canal diameter

and canal diameter change during flexion-extension motion. AP canal diameter may indicate the severity of neurologic injury after trauma. Values between 10 and 13mm have been proposed as a threshold for a stenotic canal, but there is currently no clear guideline for a compromised canal diameter or a canal diameter that would cause cord compression. [8, 14, 23, 41, 43, 52, 99, 117, 136, 175, 203] Increasing spinal canal diameter change during flexion-extension motion is considered a risk to a patient, if there is little available space for the spinal cord, because any reduction in spinal canal cross-sectional area may compress and injure the spinal cord. [8, 14, 23, 39, 42, 71, 74, 136, 139, 140, 176, 191] This space reduction and cord compression may be due to voluntary motion or motion imposed on the spine due to trauma. Myelopathic patients with a canal diameter that changes significantly due to spinal motion, would be expected to reduce their voluntary ROM to guard against painful motions, but no clear relationship between degeneration, changes in spine motion patterns or symptoms has been found. [12, 37, 56, 135]

Linear regression models indicating the relationship between the variables quantified in the present study may be characteristic of different population groups if an appropriately large and uniform sample population is chosen. These relationships would likely change with advancing age or spondylotic degeneration and could be used to compare patient groups of various conditions and ages. Comparing symptomatic and non-symptomatic patients may reveal different variable relationships, which could be used for screening of patients likely to develop symptomatic cervical myelopathy. Longitudinal studies of patients would allow for more direct comparisons. Comparing the variable relationships of patients who suffered severe SCI versus patients who suffered mild SCI due to mild trauma, may allow for screening of patients at risk of injury due to low energy trauma with advanced degeneration. The variable relationships of patients who suffered SCI due to high energy versus low energy impacts and outcomes could also be compared. Comparing variable relationships of pre- and post-operation myelopathic patients with a variety of clinical outcomes may allow for predictors of surgical success to be developed. The present image analysis could be used to relate observations from a variety of imaging modalities (such as MRI and X-ray). This may, for example, allow inferences about soft tissue, such as spinal cord compression, to be made based on analysis of sagittal plane X-rays. Previous studies have shown that intervertebral disc height correlates with the disc morphological grade observed by MRI [9, 48, 110] thus intervertebral disc height may serve as an indicator for the extent of intervertebral disc degeneration.

Comparison of regression models for different subject groups may lead to predictors of SCI injury risk, treatment effectiveness, or expected recovery after injury in elderly populations. More effective prediction tools are desired by clinicians [32, 93, 204] in particular regarding post SCI mortality in elderly patients. [55] Testing a patient

and finding a characteristic relationship of kinematic and degenerative variables may allow for early identification that he or she belongs to an at-risk population.

2.4.1 Accuracy, Precision, Repeatability and Sources of Error

While applicable to many imaging modalities, the analysis technique was evaluated using sagittal plane X-ray images. The angular accuracy, linear precision, and repeatability of this technique when applied to plane X-ray images were assessed. The sources of error that affect the present image analysis technique can be categorized into three groups: X-ray imaging, locating landmarks, and digitizing of points.

X-ray imaging error can be due to positioning the sagittal plane of patients not parallel to the image plane, inconsistent patient behaviour, out-of-plane motion, distortion due to two-dimensional projection of objects with a depth away from the image beam centre, and limitations of image resolution. Many studies depend on regular clinical imaging in both retrospective and prospective studies. Some error due to patient positioning, behaviour, and out-of-plane motion must be accepted and have been shown to be negligible when following regular procedures. [70] Distortion of features due to projecting objects with a depth onto a two-dimensional image cannot be corrected using software because it depends on the particular shape of the object and its position and orientation in the image. Analysis techniques like those developed by Frobin et al. [49, 50] minimize this effect but this author is not aware of any means to eliminate it completely. Limitations of image resolution are relative to the ratio of an image pixel to the smallest feature to be measured. This is variable, but gains in magnification are a trade-off with increased image distortion and decreased field of view. New technology with improved resolution is regularly developed and using the latest technology available is recommended.

Due to a lack of contrast and various bony features being superimposed on top of each other, the landmarks on each vertebral body may not be accurately or repeatably located. Of particular importance is the X-ray reader's ability to locate the same landmark in the flexion and extension view of the same patient. Inter- and intra-reader repeatability has served as a surrogate for X-ray landmark accuracy in past work. [47]

The present method involved the author manually digitizing points on a computer monitor. This may introduce additional error but based on the visual feedback of the digitizing scripts, consistently clicking on the intended location (such as a vertebral body) in the image was easily done and reproduced. All of the assessment methods

used for this study incorporated the final step of manual landmark digitization, so this source of error was taken into account.

The assessment of angular accuracy of the image analysis technique had both strengths and limitations. The main strength of the angular accuracy assessment was its simplicity while replicating clinical imaging procedures for cervical spine sagittal plane X-rays of patients. This was achieved by imaging a pair of dried human cervical vertebrae at the Vancouver General Hospital radiology department. The main limitation of the angular accuracy assessment was the accuracy of measuring the angle of the wedges used. The manufacture and measurements were limited because the wedges were made of wood. Measurements were particularly affected by the fragility of the thin end of each wedge. Despite this, the angle of the wedges were quantified within an error or $\pm 0.4^\circ$ which was adequate to quantify the accuracy of the main study within an error bound that compared well to previous similar studies (Section 2.4.2).

The main strength and limitation of the linear precision assessment was its use of the sample X-ray image pair. It ensured all potential sources of error were to some extent present. This assessment may be conducted on all future images from sample population groups, and will provide a reliable quantification of linear precision. Since the analyzed image pair did not include a scale reference to accurately convert measurements to millimetres, the linear precision assessment was approximate (as were the linear sample results). The linear precision of the present study is approximate because it was based on an assumed scale factor for the X-ray images that produced reasonable sizes for vertebral body depth. This error is of the same order of magnitude as the smallest values recorded for AP translation and canal diameter change. However, in symptomatic elderly patients with degenerated spines and pathological motion patterns, values of clinical relevance should be detectable.

Landmark digitization was highly repeatable and compared well to the other error assessment results. Due to the many arithmetic operations and combinations of landmarks, error would compound. For example, the precision of calculating spinal canal diameter ($\pm 0.6\text{mm}$) depended on combining a lamina landmark ($\pm 0.30\text{mm}$) and an osteophyte tip landmark ($\pm 0.21\text{mm}$). The landmark digitization repeatability assessment may have been affected by the user remembering the location digitized in the previous repetition. This effect was reduced by short delays between each repetition.

Variable calculation repeatability was assessed using two digitization data sets that were collected five months apart. Results suggested linear results are highly repeatable, but angular results are more sensitive to landmark digitization repeatability. This analysis benefited from the generous amount of time between the two digitizations of the X-ray images. The results are limited because only one X-ray pair was

analyzed with only one repetition. This limitation may be overcome if future work analyzes large samples of clinical images with multiple repetitions.

2.4.2 Comparisons to Previous Studies

The angular accuracy and linear precision of the present work ($\pm 1.3^\circ$, and approximately $\pm 0.6\text{mm}$, respectively) were similar to the precision of the image analysis technique developed by Frobin et al. [49, 50] They reported an angular precision of $\pm 2^\circ$. Linear values were reported as dimensionless variables, scaled to the nearest vertebral body, with a precision of 5%. This corresponds to an error of $\pm 0.7\text{mm}$ for a 15mm vertebral body depth. [49] Leivseth et al. [119] later evaluated the accuracy of Frobin et al.'s technique and found the accuracy to be $\pm 2.4^\circ$ and $\pm 0.78\text{mm}$, using stereophotogrammetric roentgen analysis as their gold standard.

The relationships between many different cervical degenerative variables, kinematic variables and SCIs have been studied previously including, but not limited to, the variables studied in the present work. Cervical spine ROM, [49, 74, 134–136, 139, 140, 178, 179] AP translation, [49, 50, 52, 178, 179] intervertebral disc height, [9, 50, 63, 74, 110, 178] spinal canal diameter, [23, 43, 52, 74, 99, 136, 139, 142, 174, 202, 221, 224] and osteophyte length [63, 74] have each been analyzed and compared in a variety of combinations. The cervical spinal cord has been directly measured when the imaging modality used permitted it. [23, 74, 135, 136, 139, 140, 142, 174, 202, 221] The morphological grade of the intervertebral disc is typically assigned based on qualitative evaluation of imaging. [9, 23, 110, 134, 135] Some of these variables have been compared to neurologic outcomes such as JOA score, [52, 74, 142, 221] or the American Spinal Injury Association injury grade. [43]

Past studies have reported a variety of the above mentioned clinical features as categorical and continuous variables. Studies that use categorical variables may have an easier time finding statistical differences between groups. [23, 63, 110, 134–136, 139, 140, 142] However, this often creates a situation where statistical tests must be repeated, and some of the differences may be an artifact of the multiple comparisons. Significance correction (such as the Bonferroni or Holm-Sidak correction) is needed in this situation. Regression analysis can only be applied to continuous quantitative results but assigning a numerical value to categorical variables makes regression analysis possible. [9] A particularly thorough study by Hayashi et al. [74] investigated all the variables discussed, compared different population groups and imaging modalities, but the results were a mix of continuous and categorical variables so linear regression analysis could only be performed on a subset of the results. In another study that used regression analysis, Reitman et al. [179] found shear, an-

terior and posterior displacement of the vertebrae could explain up to 90% of the variation of the ROM of 140 asymptomatic subjects but degenerative features were not examined. Various studies that used continuous variables have found statistically significant correlations between: pincer canal diameter, age, vertebral posterior slide, duration of myelopathy and JOA score; [52] spinal cord AP compression ratio and neurologic symptoms; [74] canal diameter and space available for the spinal cord (albeit moderate); [174, 202] and canal compromise and cord compression. [43] The present work makes simultaneous linear regression analysis of all the variables analyzed possible.

The sophistication of different imaging analysis techniques to measure kinematic and degenerative variables ranges. Additional complexity can address the shortcomings of simpler methods but may make the technique less applicable to clinical practice. [179] Cervical spine flexion-extension ROM has been extensively studied by plane X-ray image analysis and illustrates this range. [38, 49, 80, 119, 124, 150, 151, 164–166, 179, 208] One of the earliest image analysis techniques was developed by Penning [164, 165] who visualized segmental ROM by overlaying transparent X-ray images. He also first applied the concept of the instantaneous centre of rotation (where the relative movement of two rigid bodies is described by only a rotation about a point) to describe vertebral motion. The technique developed by Frobin et al. [49] is more complicated and calculates ROM by finding the change of intervertebral angle from flexion to extension. This technique depends on digitizing vertebral body corners which were formerly manually digitized [47] but the latest iteration was a semi-automated process that depended on a user's initial best guess. [49] This procedure was highly accurate, and improved on Penning's method because it was insensitive to radiographic distortion and was highly repeatable, but it was highly complex. Use of Frobin et al.'s technique in the present work involved adaptations that generally simplified it (including returning to manual digitization of landmarks) and further simplification would likely be needed to create a viable clinical tool.

The present image analysis algorithm used to calculate ROM, AP translation, and intervertebral disc height was based on an algorithm developed by Frobin et al. [49, 50] but there were some significant deviations (Section 2.2). The landmarks were all located and digitized manually without any computer automation. If an osteophyte was present, the estimated vertebral body corners (where the corner would be if the osteophyte was not there) and the anatomical corners were both digitized and used for calculating different variables, as appropriate. The definition of the bisectrix was revised to ensure it would always run through the disc-space between adjacent vertebrae. This was not reliable under Frobin et al.'s method if the adjacent vertebral bodies were substantially different in size or shape (due to an osteophyte or other degeneration) or if the disc space was reduced. These changes made the technique

more robust when analyzing degenerated and irregularly shaped vertebrae without diminishing the accuracy of Frobin et al.'s technique.

2.4.3 Future Considerations

The present image analysis technique is a promising method that will allow for quantification and comparison of kinematic and degenerative features of the cervical spine. Further refinements and additions to the methods are recommended to ensure high quality results if this method is applied to a sample of clinical patient images.

X-ray Imaging

Sagittal plane cervical spine flexion-extension X-rays of clinical patients can be retrospectively and prospectively analyzed. Prospective study subjects should have a scale reference marker, such as a radio-opaque disc, attached to their neck in the sagittal midline, near their C4 vertebra. The scale marker will allow for direct conversion from digital image pixels to mm for linear variables. The populations sampled should include both adult and elderly subjects with and without cervical myelopathic symptoms. If these patients have cervical spine imaging by a different modality (e.g. MRI or CT), those images should be included for analysis and comparison.

Records of the spine imaging protocol must be collected so that images can be appropriately compared. The typical plane X-ray imaging protocol followed at Vancouver General Hospital uses exposure settings of 70kV, 630mA, 16mAs. The X-ray source is 143cm from the collector plate, and each subject stands with their shoulder against the imaging plate.

Accuracy and Repeatability

Quantification of the kinematic and degenerative variables will depend on accurate and repeatable identification of landmarks on each vertebra. Collaboration with two or more orthopaedic surgeons should improve landmark location accuracy and allow for repeatability to be assessed. These surgeons will mark up the X-ray images with colour-coded dots to indicate the relevant landmarks. The colour-coded dots will then be digitized.

To better reflect the improved study method, the accuracy assessment (Section 2.2.2) should also depend on a collaborating surgeon to locate the landmarks of the dried vertebrae mounted on the simple apparatus. The apparatus could be re-imaged with

simulated soft tissue in the X-ray beam path to produce comparable contrast and with more out-of-plane angle positions.

Both intra- and inter-surgeon repeatability should be assessed. To assess the intra-surgeon repeatability of the image analysis algorithm, the collaborating surgeon, should mark a sub-set of the images a second time, some time after the images were initially marked. To assess the inter-surgeon repeatability, the same images should be marked by a different surgeon on two occasions some time apart. This surgeon must be instructed by the author but not influenced by the other collaborating surgeon. The time-gaps are to eliminate the effect of the surgeons remembering where they originally located the landmarks. All of these images would then be analyzed using the same image analysis algorithm from the main study and all of the variables for each vertebral level calculated. Two-way repeated measures analysis of variance can be used to find any significant difference between the matched differences of angles or canal diameters due to either factor. The results may be scatter-plotted against each other and deviation from a straight line with a slope of 1 would indicate less repeatability.

Statistical Analysis

Canal diameter change for each FSU level could be correlated against each variable calculated from the same FSU level. Single or multi-variable regression analyses are possible and should be tested to find effective predictors for canal diameter change. Correlations could be considered significant if their p-values are less than 0.05 after using the Holm-Sidak correction factor for repeated tests.

Doing repeated statistical tests (such as many correlations) increases the likelihood of getting a false positive error. Using the Holm-Sidak p-value correction is recommended because it is based on the actual probability of getting a false positive result. This is a more accurate correction than the more widely used Bonferonni correction which is overly conservative. [60] Bonferonni correction is more popular because it is mathematically simple, but computer-aided calculations make the additional complexity of the Holm-Sidak algorithm trivial.

An issue that would need to be resolved is deciding how many repeated correlations are considered part of one “family” of results. This determines the number of repetitions to be corrected for. It is the opinion of this author that the correlations of variables from a single vertebral level or FSU constitute a “family” if the variables from each level or FSU are analyzed in isolation from each other and if the variables analyzed at each FSU are not expected to have a mechanical impact on variables at other FSU levels. This is complicated since adjacent levels may in some cases influence each

other. For example, the flexibility of an FSU may increase to compensate for a stiff or fused adjacent level, but the causality of this effect is controversial. [8, 32, 113, 178]

Human cervical spine anatomical and biomechanical data vary to a great degree. A large sample size will be needed to find any statistically significant relationships between the many variables analyzed. A well accepted rule-of-thumb for multi-variable regressions is to include a sample population 10-times the number of variables included in the regression model. [154] Six variables (any two of the three canal diameter variables can be used simultaneously) are proposed for analysis in this study. Thus a five-variable model could be used to predict the sixth. This suggests approximately 50 patients would be needed in each sample group.

The number of subjects may need to be increased to ensure enough data is collected for variables that are observed less often. It is frequently observed in sagittal plane X-rays that lower cervical vertebrae are obscured by the patient's shoulder. If including variables from the C6 and C7 vertebrae is a priority for this study, each population group will likely need to be increased in size so that patients with obscured vertebrae can be excluded. Posterior osteophytes are observed clinically less often than anterior osteophytes and a large number of subjects may be needed to include that variable in the regression analysis. A 50% increase in sample size is recommended to allow for this, resulting in approximately 75 patients in each sample group.

Initially, a comparison between two sample groups is recommended, such as elderly symptomatic patients versus elderly non-symptomatic patients. Following this, more sample groups could be analyzed and compared such as younger adults with and without symptoms, and the same groups with different imaging modalities. These repeated comparisons will necessitate a p-value significance correction, and larger sample groups to compensate. It is difficult to estimate the sample size needed to allow for this, but considering the particularly high variability in elderly and degenerated populations, another 50% size increase is reasonable. This results in approximately 113 patients in each group.

Finally, each regression model should be verified against a second sample group of equal size. This will result in doubling the needed number of subjects for each sample group to 226 patients.

Relationships between the variables analyzed may not be linear in nature. For example, the relationship between disc degeneration and ROM in the cervical spine is inconclusive [134, 135] and in the lumbar spine the relationship is also complicated and possibly non-linear. [132, 145] The lumbar spine appears to destabilize with early disc degeneration but ROM decreases as degeneration becomes more advanced. Any such non-linear relationship would not be captured by linear regression.

Multi-variable linear regression is a powerful analysis technique but must be applied carefully. Each variable used as an input for the regression model must be linearly independent. This is a concern since degenerative features typically develop in concert, potentially as a response to each other. [8, 121, 204] Multi-variable linear regression would be appropriate if the input variables show non-linear or statistically insignificant linear relationships between them.

Many Factors Affect Cervical Spine Flexibility

Any relationship between cervical spine flexibility and the variables analyzed may be obscured by many other uncontrolled factors. These include (but are not limited to) if the patient warmed up or stretched before X-ray imaging, natural temporal variation of spine flexibility, [12] and effects of myelopathic or radiculopathic symptoms including weakness, tingling, loss of sensation and pain. [77, 121, 186] Pain is intimately related to spine degeneration and affects patients in unpredictable ways. These issues may be mitigated if the study was conducted prospectively, but they must be accepted if patient images are analyzed retrospectively.

2.5 Conclusions

There is a need for indicators of SCI risk, predictors of treatment effectiveness, expected recovery, and mortality in elderly populations. [32, 55, 93, 204] Currently, plane X-ray does not adequately detect cervical spine injuries and cannot be used alone for screening. [138] A single variable cannot encompass all the risk factors associated with making such predictions. Perhaps the quantitative relationship between a group of variables will have predictive value. Many different studies have previously related various combinations of kinematic and degenerative variables, but the combination of variables used in the present work, all measured using continuous and quantitative variables, has not been attempted.

The image analysis method described in the present work makes the simultaneous regression analysis of a new combination of kinematic and degenerative variables possible. The image analysis method was evaluated using a sample flexion-extension X-ray image pair and shown to be highly accurate and precise. Further studies using this analysis method with multiple population groups and imaging modalities are recommended to discover if there are characteristic regression relationships for each group that will allow for quantitative comparison between them.

Chapter 3

Effect of Canal Stenosis on Surrogate Cord Compression During Cervical Spine Motion

3.1 Introduction

Traumatic spinal cord injury (SCI) incidence rates for North America are often reported between 25 to 52 per million people per year. [30, 36, 120, 170, 193, 206] Among SCIs of equal severity, cervical injuries have the worst outcomes. SCI incidence has a bimodal age distribution in developed nations. [36, 120, 170, 206] The majority of people who suffer a traumatic cervical SCI are young adult males who were in an automotive accident. [30, 36, 120, 167, 170, 194, 206] The elderly population have the next highest incidence of SCI [30, 36, 120, 170, 206] and for similar injuries, elderly have worse outcomes due to other comorbidities. [33, 34, 53, 54, 92, 193, 194]

There are many differences between the elderly and younger adult populations that could be relevant to SCI, including the extent of spinal degeneration. The human spine begins degenerating as early as the age of 25, [29, 121, 191] and over time these cumulative changes can make the spine and spinal cord more vulnerable to injury. [29, 33, 39, 40, 69, 92, 103, 112, 113, 125, 176, 188, 194] This is supported by the SCI aetiology contrast between the two population groups; elderly people more commonly suffer cervical SCI due to minor trauma (such as a fall from standing) which would be trivial to younger people. [24, 92, 100, 120, 125, 167, 170, 193, 194]

One of the most common types of spinal degeneration is osteophyte bone spurs that grow from a vertebral body. [63, 74, 121, 149] Osteophytes can grow in any direction but they can threaten the spinal cord when they grow posteriorly into the spinal canal. In that case, the minimum anterior-posterior (AP) canal diameter is found in the pincer direction: between the bone spur on the inferior-posterior aspect of the vertebral body and the superior-anterior aspect of the lamina of the adjacent inferior vertebra. [71, 74, 88, 121, 139, 176, 191]

During normal cervical spine flexion-extension motion, the neural space in the spinal canal can change due to a number of different mechanisms including soft tissue bulging into the canal (such as the intervertebral disc, posterior longitudinal ligament (PLL), or ligamentum flavum (LF)), or pathologic AP vertebral translation. If the canal is already congenitally narrow or narrowed due to spinal degeneration, the spinal cord can be compressed and injured during normal motion. During a mild traumatic impact involving the head or neck, if the spine is degenerated, the neck can be forced to move to an extent that injures the spinal cord while causing minor or no osteoligamentous damage at all. [68, 92, 103, 113, 121, 123, 125, 176, 188, 194]

While many studies have investigated the effect of spinal motion on the cervical spinal canal, relatively few have done so experimentally *ex vivo*. Chen et al. [25] used radio-opaque beads attached to the PLL and the LF to measure their intrusion into the cervical spinal canal during step-wise motion induced by a combination of axial load and flexion-extension moments. Gu et al. [67] attached a strain gauge to the LF to measure how it bulged into the canal during step-wise extension motion. Holmes et al. [81] inserted a latex tube full of water into the canal and measured the displaced water during step-wise flexion-extension motion. Nuckley et al. [146, 147] used custom sensors to detect AP canal diameter change and intervertebral foramen size change during many different combinations of spinal motion and with incrementally damaged spines. Subramaniam et al. [195] measured spinal canal volume change during step-wise flexion-extension motion by measuring the pressure difference of water flowing through a tube in the spinal canal. The canal size was varied by inserting an artificial osteophyte made from a wooden craft ball and then performing a laminectomy. Since these studies did not observe the spinal cord directly, they could have missed important injury mechanisms.

Even fewer cadaveric experimental studies have directly observed the effects of cervical spinal canal occlusion and differing spinal posture on the spinal cord in the canal. Breig et al. [15] examined 40 adult cadaver cervical spines that were chemically fixed in different postures (flexion, extension, or neutral). Cervical air myelograms were used to observe the effects on the spinal cord. Reid [177] dissected cadaver specimens to investigate the effect of cord tension due to flexion of the head and anterior canal protrusions on the spinal cord. Taylor [197] visualized the cervical spinal cord in five cadavers as they were flexed and extended by adding radio opaque oil to the canal space. However, in both of these studies the positioning of the spine was not controlled and quantitative measurements of the spinal cord compression were not made. In a three-part study, Tencer et al. [198–200] measured the transverse force-displacement relationship of the spinal cord in whole human spine specimens. Using a custom designed probe equipped with a micro-loadcell at the tip, they tested the effects of many parameters including laminectomy, spine shortening and distraction, and

cervical flexion. However, the biofidelity of all of these studies was limited because all of the experiments used previously frozen or chemically fixed spinal cord specimens. Since the mechanical properties of the spinal cord change quickly after death, [22, 83, 84, 148] the spinal cord properties measured in these studies would have been different from those of a living spinal cord. Three labs (including this lab) have developed mechanical surrogate spinal cords with material properties similar to a living spinal cord. [11, 114, 171] The surrogate cords have been used in cadaveric or simulated cervical spine models in dynamic flexion-extension or impact tests.

Previous work has not quantified biofidelic spinal cord deformation in the canal of a cadaveric cervical spine specimen during continuous flexion-extension motion as a function of variable spinal canal stenosis. The objective of this study is to determine the effect of increasing canal stenosis due to an artificial osteophyte, on the compression of a biofidelic surrogate cord, during physiologic and greater-than-physiologic motion in an *ex vivo* whole porcine cervical spine. Accuracy of surrogate spinal cord diameter measurements made via X-ray will be evaluated.

3.2 Materials and Methods

3.2.1 Cadaver Specimens and Preparation

Quasistatic flexion-extension flexibility tests were carried out on six skeletally mature, fresh-frozen, cadaveric porcine cervical spine specimens (C2-T1). Approximately 36 hours in advance of testing, each specimen was removed from the freezer to give time for thawing and preparation. Anterior processes, muscle tissue, and vertebral levels other than C2 to T1 were removed.

A hole for an M8 screw was drilled into the the midline of the C5 vertebral body at an angle approaching the posterior elements of C6. A stainless steel M8 machine screw was threaded into the hole and protruded into the spinal canal (Figure 3.1). The M8 screw served as the artificial osteophyte for this study as its size and shape, when protruding into the canal, approximated a sub-set of the wide variety of shapes a biologic osteophyte can take. When most extreme, osteophytosis can completely change the shape of a vertebral body. [121] Additionally, the screw could repeatably protrude into the canal any amount desired and was radio-opaque.

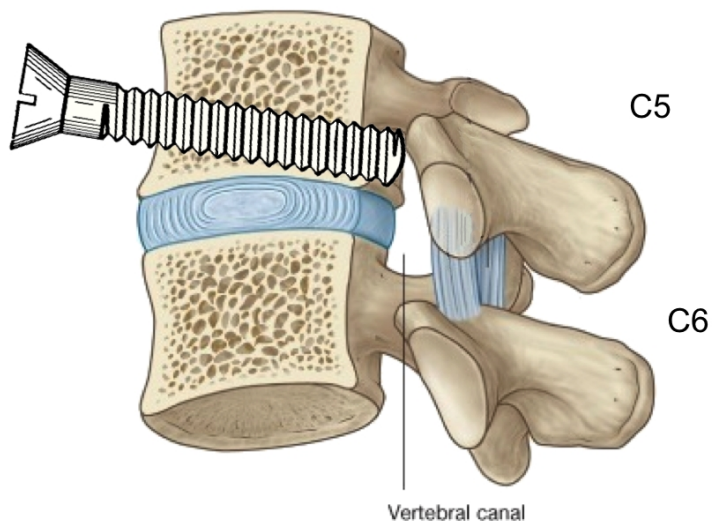


Figure 3.1: Illustration of the artificial osteophyte design. An M8 machine screw protrudes into the vertebral canal through the C5 vertebral body. Adapted from Drake et al., 2005 [35] with permission from Elsevier.

The biological spinal cord was removed from the spinal canal and replaced by a radio-opaque surrogate cord. The surrogate spinal cord (initially developed by Kroeker [114]) was made from QM Skin 30, a 2-part translucent moulding rubber (ACC Silicones Ltd, UK). It was made radio-opaque by adding powdered barium sulphate so that its position and size could be observed inside the spinal canal during testing via fluoroscopy. The surrogate cord has material properties similar to a living spinal cord, validated in quasistatic transverse compression, dynamic transverse compression, and quasistatic tension in the longitudinal direction. [95, 114]

The surrogate cord was moulded into a cylinder with an elliptical cross-section (major diameter: 11.8mm; minor diameter: 6.5mm). The cross-sectional dimensions were based on average values found in previously published studies. [96, 97, 109] The surrogate cord was anchored in place at C2 and T1 where the spine was potted in polymethylmethacrylate (PMMA). The PMMA was set around a wood screw threaded into each end of the surrogate cord. The PMMA blocks were moulded parallel to the endplates of the vertebrae so that they encased the vertebrae but did not interfere with spinal motion at that level.

Eye hooks, used to guide follower load cables (Section 3.2.2), were screwed into the

lateral sides of each vertebrae and the PMMA potting. Sagittal plane X-rays were used to ensure the hooks were affixed symmetrically and roughly one third of the AP width of the spine from the anterior surface of the spine, which minimized any bending moment applied by the compressive follower load. [133]

Figure 3.2 shows a typical spine specimen before and after preparation. After preparations were completed, each spine was wrapped in gauze, moistened with saline, sealed in a plastic bag, and refrigerated overnight. At all times, specimens were kept moist with a saline solution and cared for according to recommended guidelines. [214, 215]



Figure 3.2: A typical spine specimen before and after preparation.

3.2.2 Quasi-static Flexion-extension Tests with a Follower Load

Flexibility tests were carried out using a custom-designed spine machine, located at the ARTORG Research Center at the University of Bern. Pure moment bending of the spine was accomplished by applying a torque to the cranial end of the spine (generated by one of 3 orthogonal rotational actuators EC40 BL D 120W KL 2WE, Maxon Motors, Switzerland) while releasing all three translational degrees of freedom at the caudal end of the spine. The spine machine design and function was described previously by Gédet et al. [58] The rate of bending was 1° per second until a moment limit was reached. A 2.5Nm and a 3.75Nm moment limit were used. These moment limits were intended to move the spine through a physiologic range of motion (ROM) and a non-injurious greater-than-physiologic ROM, respectively. Using a 2.5Nm moment limit with a porcine cervical spine was recommended by Schmidt et al. [189] when simulating a human physiologic ROM.

Load and rotation data was synchronously collected at 10Hz. Load data was collected by a six-axis load cell (MC3A 1000, AMTI, Watertown, MA, USA) located at the caudal end of the spine, between the spine and the machine crosshead. Rotation data

3.2. Materials and Methods

was collected by the encoder in the spine machine rotational actuator (Figure 3.3).

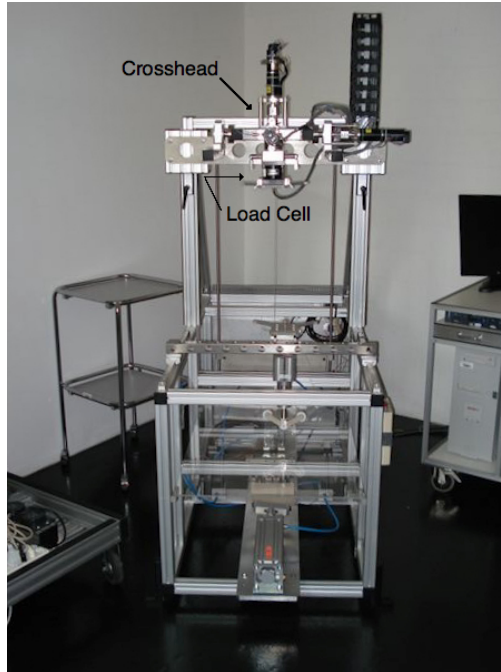


Figure 3.3: ARTORG Research Center spine machine. (University of Bern, Switzerland.)

To improve the biofidelity of the tests, a 100N axial compression follower load simulated the effect of neck musculature. [133, 160, 163] The force was applied using a cable guided by eye hooks located on the lateral sides of each vertebra. This guided the force near the approximate balance point of each vertebra, which reduced the eccentricity of the force to nearly zero, and the force remained close to pure compression even while the spine moved during flexibility testing. [133, 163] Prior to the flexibility testing, the follower load setup of each spine was tested by increasing the compressive load until the load cell read 100N in the axial direction. All spines were stable and did not buckle, nor flex or extend significantly. This indicated that the load passed close to the balance point of each vertebra. The 6-axis load cell was used to record the static moment exerted on the spine when the follower load was applied (Table 3.1). The static moment was subtracted from the moment limits used during flexibility testing.

3.2. Materials and Methods

Table 3.1: Static moments due to the follower loads.

Specimen	Static Moment (Nm)
A	0.61
B	0.57
C	0.53
D	0.60
E	0.50
F	0.55

The 2.5Nm moment limit flexibility test was repeated with canal occlusion increased in increments of 25% of the canal diameter until the artificial osteophyte made contact with the surrogate cord when the spine was in a neutral position. If 50% canal occlusion or 75% canal occlusion would have caused noticeable cord compression in the neutral position, the amount of artificial osteophyte intrusion was reduced so that the artificial osteophyte only just contacted the surrogate cord. These canal occlusion judgements were made during testing using X-ray. Due to the variation in spinal canal size, (Table 3.2) the maximum canal intrusion for three of the specimens was greater than 50% and for three it was less. Both the perpendicular and pincer canal diameters of each specimen at the C5 vertebral level were measured using boney landmarks found in plane X-rays taken before testing (Figure 3.4).

Table 3.2: Specimen sagittal canal diameters measured at vertebral level C5. (All values in mm.)

Specimen	Perpendicular Canal Diameter	Pincer Canal Diameter
A	12.9	15.0
B	13.2	15.3
C	15.3	18.5
D	11.7	17.5
E	11.3	15.0
F	12.7	14.3
Human Average	15.4 ± 1 [19, 98, 117, 158]	

3.2. Materials and Methods

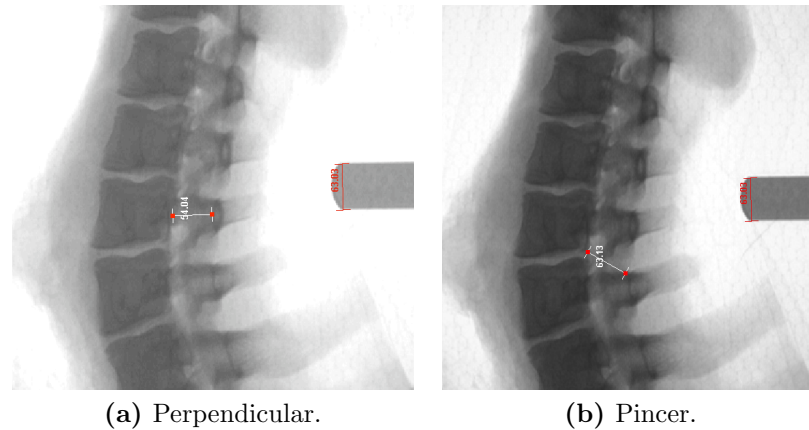


Figure 3.4: Representative X-ray images of the spine specimens illustrating the landmarks used to measure canal diameter. The canal diameter of each specimen was measured in the perpendicular and pincer direction. A 15mm scale reference was included in each image to convert canal diameter measurements to millimetres.

After all tests using the 2.5Nm moment limit, the final flexibility test had a 3.75Nm moment limit and 25% canal occlusion. This increased moment limit was 50% greater than the limit recommended by Schmidt et al. [189] to simulate human physiologic ROM, and was intended to induce a greater-than-physiologic motion without causing osteoligamentous damage. The two most flexible specimens exceeded the ROM of the spine machine before the 3.75Nm moment limit was reached. These tests were excluded from analysis because the pure moment testing condition was violated. Table 3.3 summarizes which specimens were tested in which manner.

Table 3.3: Test conditions carried out on each specimen.

Test Condition	Specimens Tested
0% canal occlusion. Moment limit: 2.5Nm	A,B,C,D,E,F (All)
25% canal occlusion. Moment limit: 2.5Nm	A,B,C,D,E,F (All)
50% canal occlusion. Moment limit: 2.5Nm	C,D,F
Maximum canal occlusion. Moment limit: 2.5Nm	A,B,C,D,E,F (All)
25% canal occlusion. Moment limit: 3.75Nm	A,B,D,F

For each test, the spine was subjected to four cycles of continuous flexion-extension up to the moment limit in each direction. The moment limit was offset by the static

moment due to the follower load (Table 3.1). The first 1.5 cycles served as pre-conditioning. This was necessary to accommodate C-arm imaging (Section 3.2.3). Motion and load data were collected during the third cycle.

3.2.3 X-ray Imaging and Analysis

A fluoroscope (Siremobil Iso-C, Siemens AG, Germany) was used to image the position and size of the surrogate cord during testing. The C-arm was positioned so that the spine was imaged in the sagittal plane (Figure 3.5). To image the spine in the centre of the field of view during full flexion and full extension, the C-arm needed to be moved between two positions during testing. As a result, X-ray imaging during each test was done immediately before and after the 3rd cycle of flexion-extension bending (Figure 3.6).

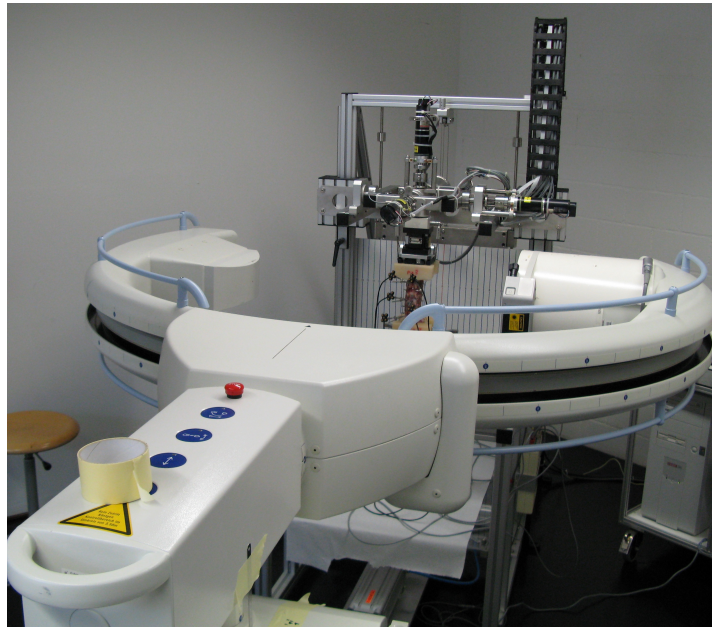


Figure 3.5: C-arm in position around spine machine.

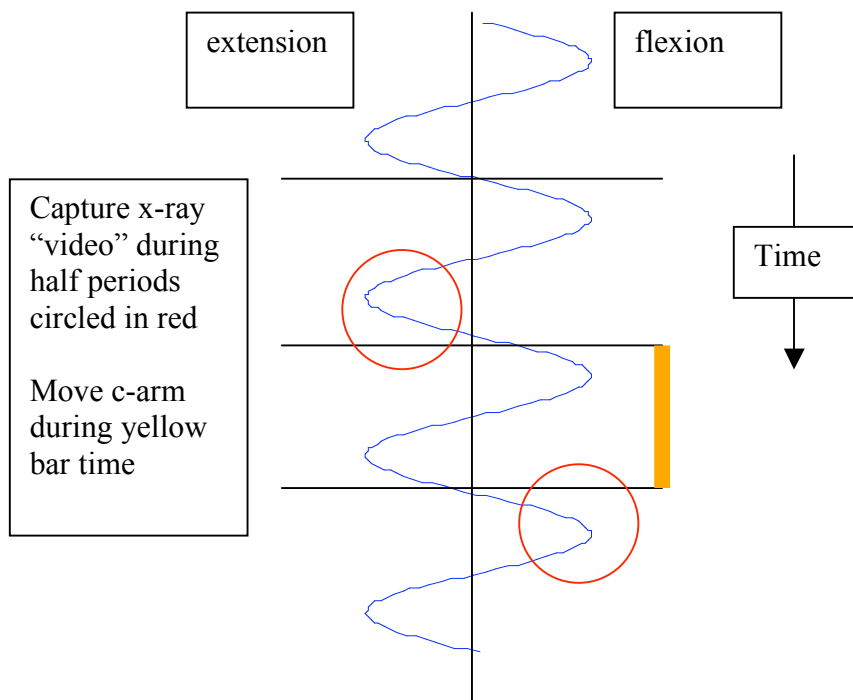


Figure 3.6: X-ray imaging timing compared to flexion-extension loading sequence.

The C-arm imaged continuously with an exposure of 50kV and 0.3mA. Images were output to a computer frame-grabber PCI card (Meteor-2/4, Fabrimex Systems AG, Germany) which collected still images at a variable rate between 10-14 frames per second, using Fabrimex sView V1.0 software. Although the X-ray images were not synchronized to the other data collected, they were time-stamped so that the images could be related to the events of each test.

Three X-ray images from each flexibility test were selected for analysis (maximum flexion, maximum extension, and neutral pose). The following features in each image were manually segmented using Analyze (Version 8.1, Biomedical Imaging Resource, Mayo Clinic, Rochester, Minnesota, USA) and a WACOM touch screen tablet (Cintiq 21UX Version 1.08, WACOM Co. Ltd.): Anterior and posterior margins of surrogate spinal cord, superior and inferior margins of artificial osteophyte, C4 landmark, C5 posterior margin, C6 landmark (Figure 3.7).

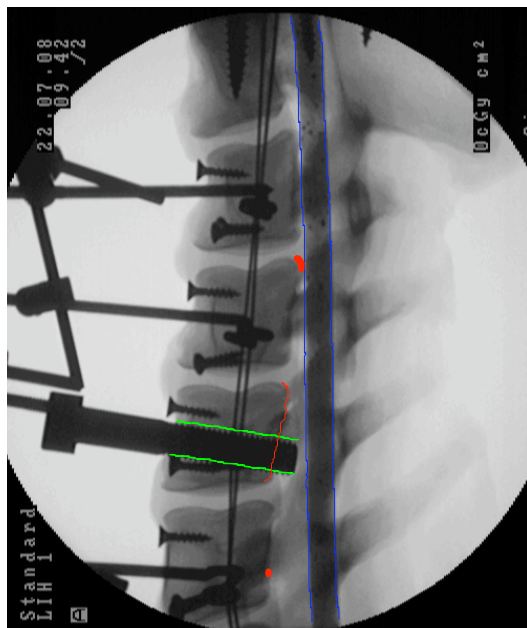


Figure 3.7: Typical C-arm X-ray image segmentation. (Specimen B, 25% canal occlusion, neutral pose.) Blue lines: anterior and posterior margins of surrogate spinal cord. Green lines: superior and inferior margins of artificial osteophyte. Red dots: C4 and C6 landmarks. Red line: C5 posterior margin.

The pixel coordinates of the segmented landmarks were used as inputs for custom written analysis scripts created using Matlab (R2006a, The MathWorks Inc., Natick, Massachusetts, USA). All analysis was two-dimensional and assumed only sagittal plane motion. This assumption was considered valid as all the segmented landmarks were in the mid-sagittal plane and no out-of-plane motion was observed during the flexion-extension tests. Since the artificial osteophyte was circular in cross-section, was located in the mid-sagittal plane, and had a known physical diameter, it was used as a scale reference to relate millimetres to pixels.

The minimum AP diameter of the surrogate cord along its length was calculated by finding the point on the posterior margin of the cord that was the closest to each point along the anterior margin of the cord. The cord diameter near the artificial osteophyte was calculated by averaging the AP diameters that were immediately adjacent to the artificial osteophyte (Figure 3.8). The overall cord diameter was calculated by averaging the diameters that were contained within minimally distorted region but excluding the region near the artificial osteophyte. (Details of the minimally distorted region are given in Section 3.2.4.) The difference between the surrogate cord diameter near the artificial osteophyte and the overall cord diameter was calculated and referred to as the “cord diameter difference”.

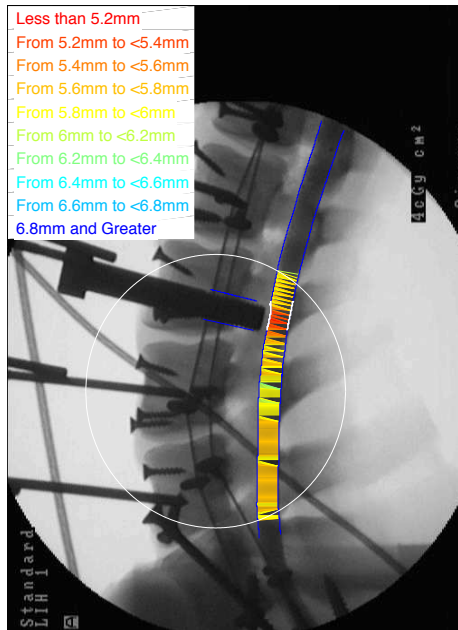


Figure 3.8: A series of colour-coded line segments plotting the minimum distance from the anterior margin of the surrogate cord to the corresponding closest point on the posterior margin. The line segments are colour-coded based on their length as indicated in the legend from less than 5.2mm to greater than 6.8mm. The surrogate cord margins are highlighted by a blue line. The region of the surrogate cord near the artificial osteophyte is highlighted in white. The white circle marks the perimeter inside of which image distortion was undetectable (Section 3.2.4).

3.2.4 Image Analysis Accuracy and Distortion Quantification

Image analysis accuracy was quantified by finding the diameter of a surrogate spinal cord that was compressed a known amount. A micrometer was used to compress the surrogate cord with an accuracy of $\pm 0.001\text{mm}$ (Figure 3.9). These cord diameter values were considered the ground truth against which the image analysis method was verified. Six different values of compression were applied to the surrogate cord ranging between 0mm to 1.5mm. At each stage of cord compression, the cord was imaged using X-ray with a cadaver spine in the X-ray beam path. This produced X-ray images where the contrast at the margins of the surrogate cord more accurately resembled the contrast in the images from the main study. All of the optical parameters of the main study were replicated. As was done for the main study, an M8 machine screw was used as a scale reference.

3.2. Materials and Methods



Figure 3.9: Accuracy assessment set-up. The micrometer was used to compress surrogate cord.

The X-ray images were analyzed using the same technique that was used in the main study. The surrogate cord and the machine screws were manually segmented and then the diameter of the cord was found along its length (Figure 3.10). The local minimum diameter value where the cord was compressed by the micrometer was recorded and compared to the diameter read from the micrometer. The difference between values measured by X-ray image analysis and the micrometer is the accuracy of the X-ray image analysis technique.

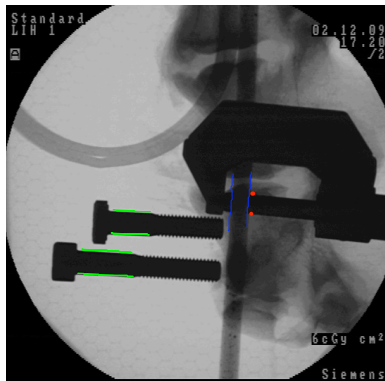


Figure 3.10: X-ray image of the micrometer compressing the surrogate cord. A spine specimen is visible. Blue lines are the margins of the surrogate spinal cord. Green lines are the margins of M8 machine screws. Red dots are the limits of the compressed region of the surrogate cord to be analyzed.

Pincushion distortion causes non-uniform image magnification. This distortion has a minimal effect near the centre of the image, but becomes more significant closer to

the edges. An X-ray image of equally spaced dots was used to assess the effects of distortion (Figure 3.11). The centre-to-centre distance between each dot was manually measured using software (GNU Image Manipulation Program Version 2.2, The GIMP Development Team). A perimeter from the centre of the image was found, inside of which distortion effects could not be detected. Outside of the perimeter, the distortion effects would affect image accuracy. Thus all analysis in the main study was confined within this perimeter (marked as a white circle in X-ray images).

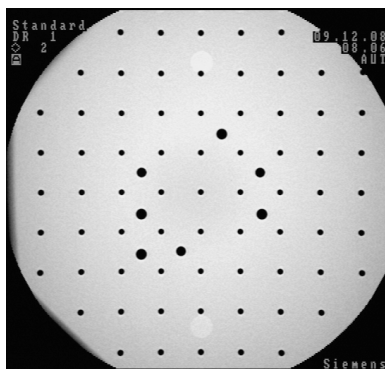


Figure 3.11: Calibration grid X-ray image used for this study.

3.3 Results

3.3.1 Image Analysis Accuracy and Distortion Quantification

The average absolute difference between the surrogate cord diameters measured using the X-ray image analysis technique and those measured using the micrometer was less than the size of one pixel at the current magnification (Table 3.4). At the current image magnification, one pixel was equivalent to 0.25mm. Due to the manual segmentation techniques used, accuracy could not be better than image resolution. Thus a conservative estimate of image analysis accuracy was $\pm 0.25\text{mm}$.

Pincushion distortion could not be detected within an ellipse near the centre of the X-ray images (Figure 3.12). The distance between all of the dots contained in the ellipse was uniform. The distance between the dots outside of the ellipse was detectably larger. Results where the compressed region of the surrogate cord was located outside of this perimeter were excluded.

Table 3.4: X-ray image analysis technique accuracy. (All values in mm.)

Actual Cord Diameter	Image Analysis Diameter	Difference
6.659	6.49	0.16
6.457	6.48	-0.02
6.157	6.01	0.15
5.655	5.17	0.48
5.356	5.58	-0.22
5.150	5.16	-0.01
Absolute Average:		0.18

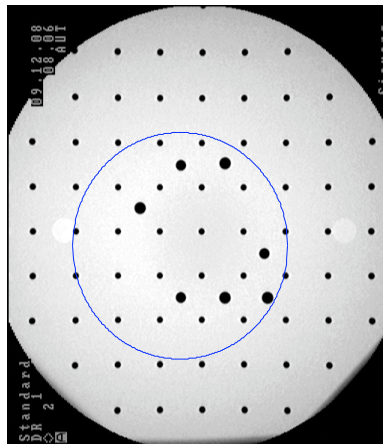


Figure 3.12: The ellipse illustrates the conservative perimeter in the X-ray images where pincushion distortion begins to have a measurable effect on the magnification. No distortion could be detected inside this perimeter.

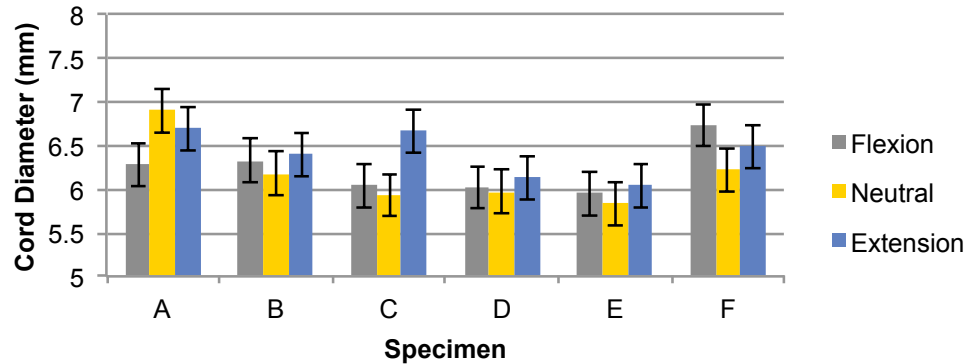
3.3.2 Surrogate Cord Compression

The artificial osteophyte was qualitatively observed to compress the surrogate cord during spinal motion in five of six specimens. Quantitative verification of surrogate cord diameter change exceeded experimental error in only two specimens. Results from each specimen are reported individually because of high inter-specimen variability compared to small cord diameter changes.

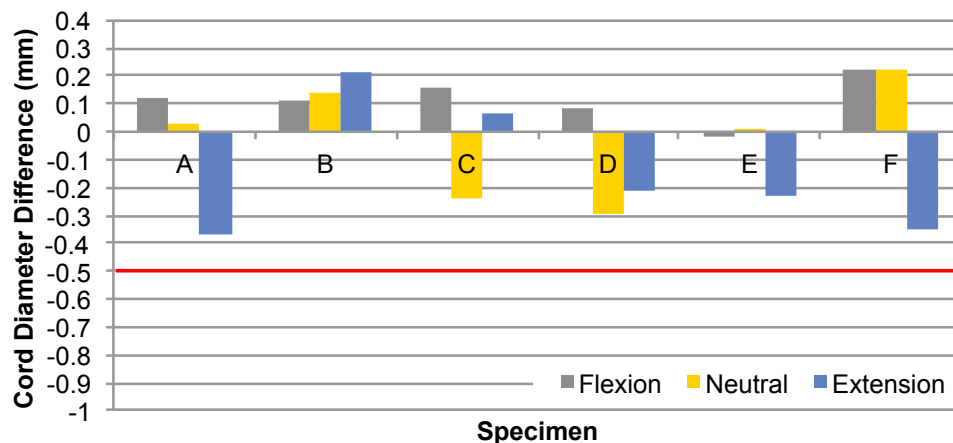
When the artificial osteophyte was flush with the anterior wall of the spinal canal (0% canal intrusion, Figure 3.13a) and when it was advanced 25% into the canal (Figure 3.14a), changes in the cord diameter near the artificial osteophyte due to

3.3. Results

spinal motion were detected. Upon visual inspection of the X-rays, no surrogate cord interaction with the artificial osteophyte was observed. The quantitative changes measured were likely due to stretching and twisting of the cord. Small fluctuations of the surrogate cord diameter difference values (Figure 3.13b and 3.14b) were also recorded but were less than the error associated with those values, and were likely an artifact of the image resolution.



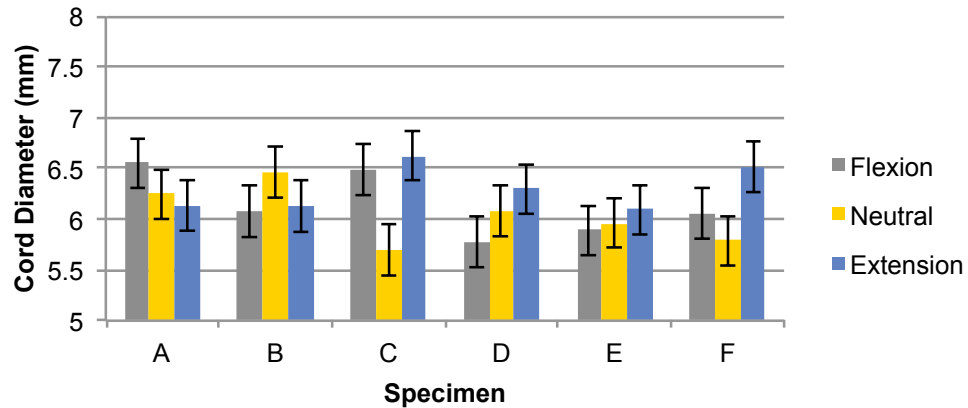
(a) Surrogate cord diameter near the artificial osteophyte. Error bars indicate accuracy ($\pm 0.25\text{mm}$). No cord compression due to the artificial osteophyte was qualitatively observed.



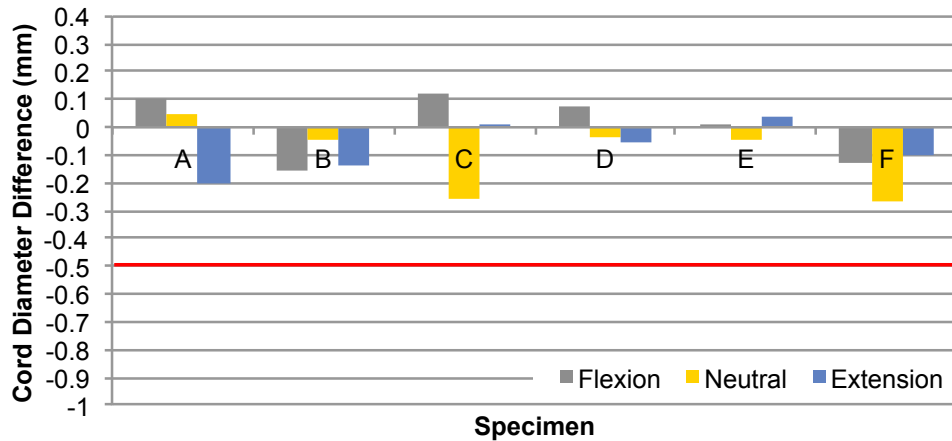
(b) Difference between the surrogate cord diameter near the artificial osteophyte and the overall cord diameter. Negative values indicate the surrogate cord was narrower near the artificial osteophyte compared to the rest of the cord. Red line indicates accuracy ($\pm 0.5\text{mm}$).

Figure 3.13: Quantitative surrogate cord results for all specimens with the artificial osteophyte at 0% canal occlusion in the neutral posture, tested to a 2.5Nm moment limit.

3.3. Results



(a) Surrogate cord diameter near the artificial osteophyte. Error bars indicate accuracy (± 0.25 mm). No cord compression due to the artificial osteophyte was qualitatively observed.



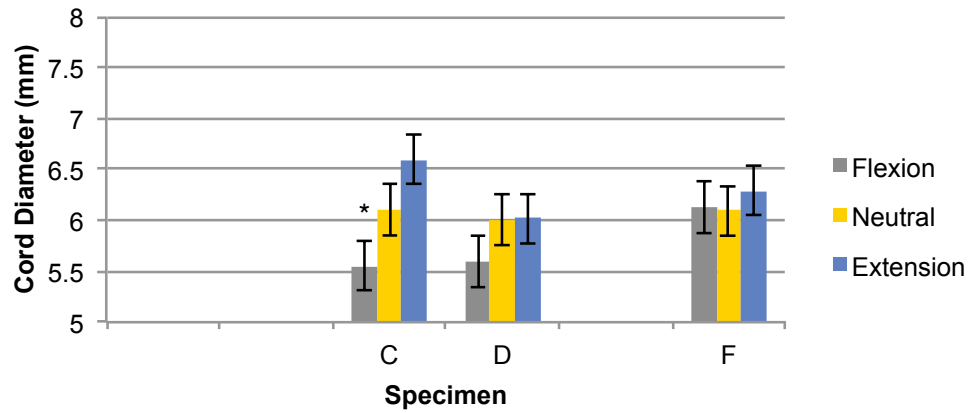
(b) Difference between the surrogate cord diameter near the artificial osteophyte and the overall cord diameter. Negative values indicate the surrogate cord was narrower near the artificial osteophyte compared to the rest of the cord. Red line indicates accuracy (± 0.5 mm).

Figure 3.14: Quantitative surrogate cord results for all specimens with the artificial osteophyte at 25% canal occlusion in the neutral posture, tested to a 2.5Nm moment limit.

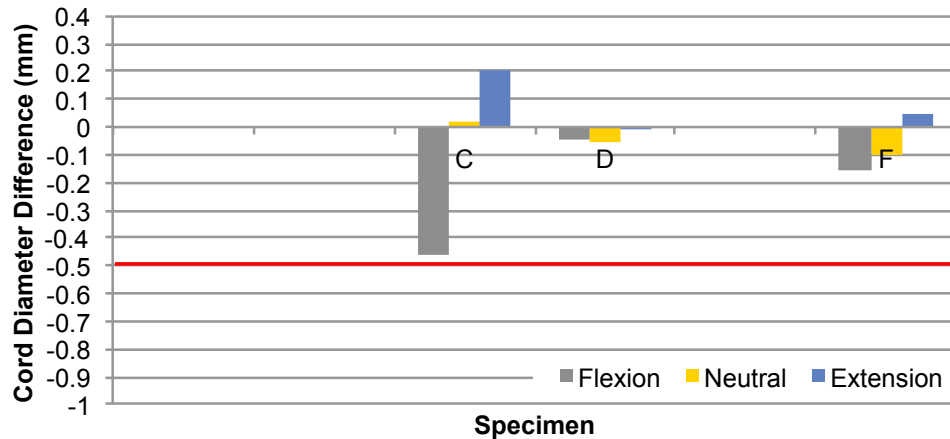
Only specimens C, D and F were tested with 50% canal occlusion. When specimens A, B and E were subjected to 50% canal occlusion, surrogate cord compression in the neutral pose was observed at the time of testing, and those tests were aborted. Specimens C and D showed a noticeable change in surrogate cord diameter near the artificial osteophyte due to spinal flexion (Figure 3.15a). However, visual inspection of the X-rays revealed that the surrogate cord of only specimen C was compressed due

3.3. Results

to the artificial osteophyte. Specimen D showed uniform diameter reduction due to stretching (Figure 3.16). This result could not be corroborated by the surrogate cord diameter difference. While the cord diameter difference value was noticeably larger for specimen C in flexion, it did not exceed the 0.5mm measurement error (Figure 3.15b).



(a) Surrogate cord diameter near the artificial osteophyte. Error bars indicate accuracy ($\pm 0.25\text{mm}$). Star indicates qualitatively observed cord compression due to the artificial osteophyte.



(b) Difference between the surrogate cord diameter near the artificial osteophyte and the overall cord diameter. Negative values indicate the surrogate cord was narrower near the artificial osteophyte compared to the rest of the cord. Red line indicates accuracy ($\pm 0.5\text{mm}$).

Figure 3.15: Quantitative surrogate cord results for all specimens with the artificial osteophyte at 50% canal occlusion in the neutral posture, tested to a 2.5Nm moment limit.

3.3. Results

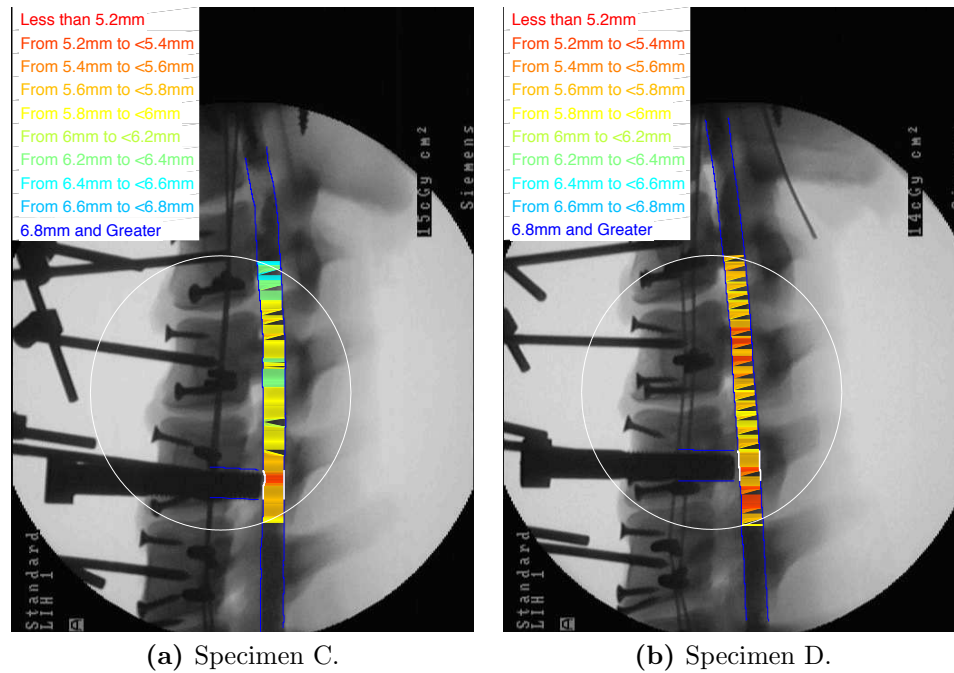


Figure 3.16: Specimens C and D full flexion X-ray images with 50% canal intrusion, and 2.5Nm moment limit. Colour-coded line segments indicate the surrogate cord AP diameter as per the legend. The surrogate cord in specimen C is compressed by the artificial osteophyte while the surrogate cord in specimen D is uniformly stretched.

During visual inspection of the X-ray images from tests where the artificial osteophyte was advanced to maximum occlusion, surrogate cord compression was observed in specimens A, C, and F during extension, (Figures 3.17, 3.18 and 3.19) and in specimens B and D during flexion (Figures 3.20 and 3.21).

3.3. Results

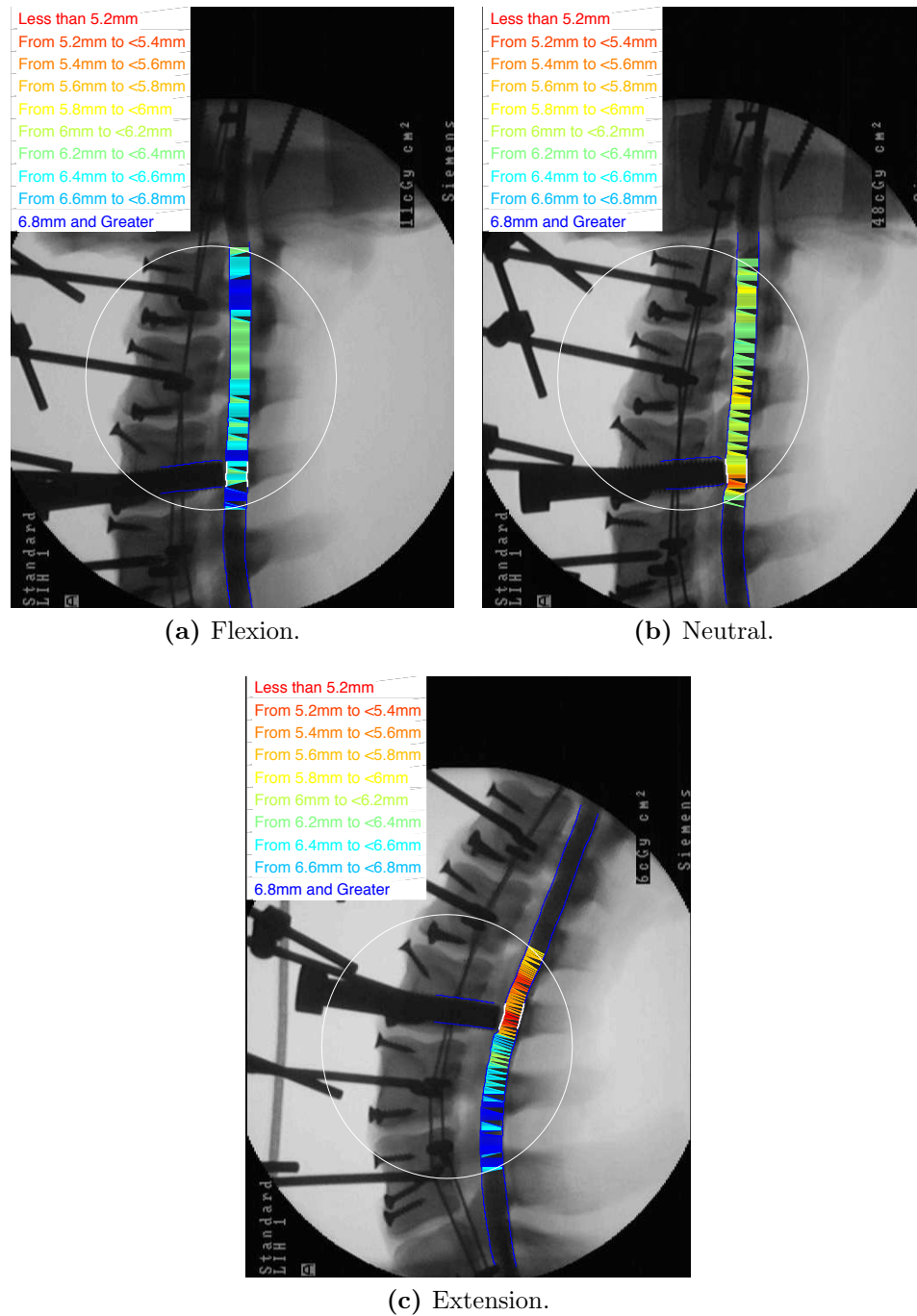


Figure 3.17: Specimen A flexion, neutral, and extension X-ray images with maximum canal occlusion, and a 2.5Nm moment limit. Colour-coded line segments indicate the surrogate cord AP diameter as per the legend. Cord compression is visible in the neutral pose and cord compression increases in extension. In extension the cord appears to be tethered and stretched between the artificial osteophyte and the superior end of the specimen.

3.3. Results

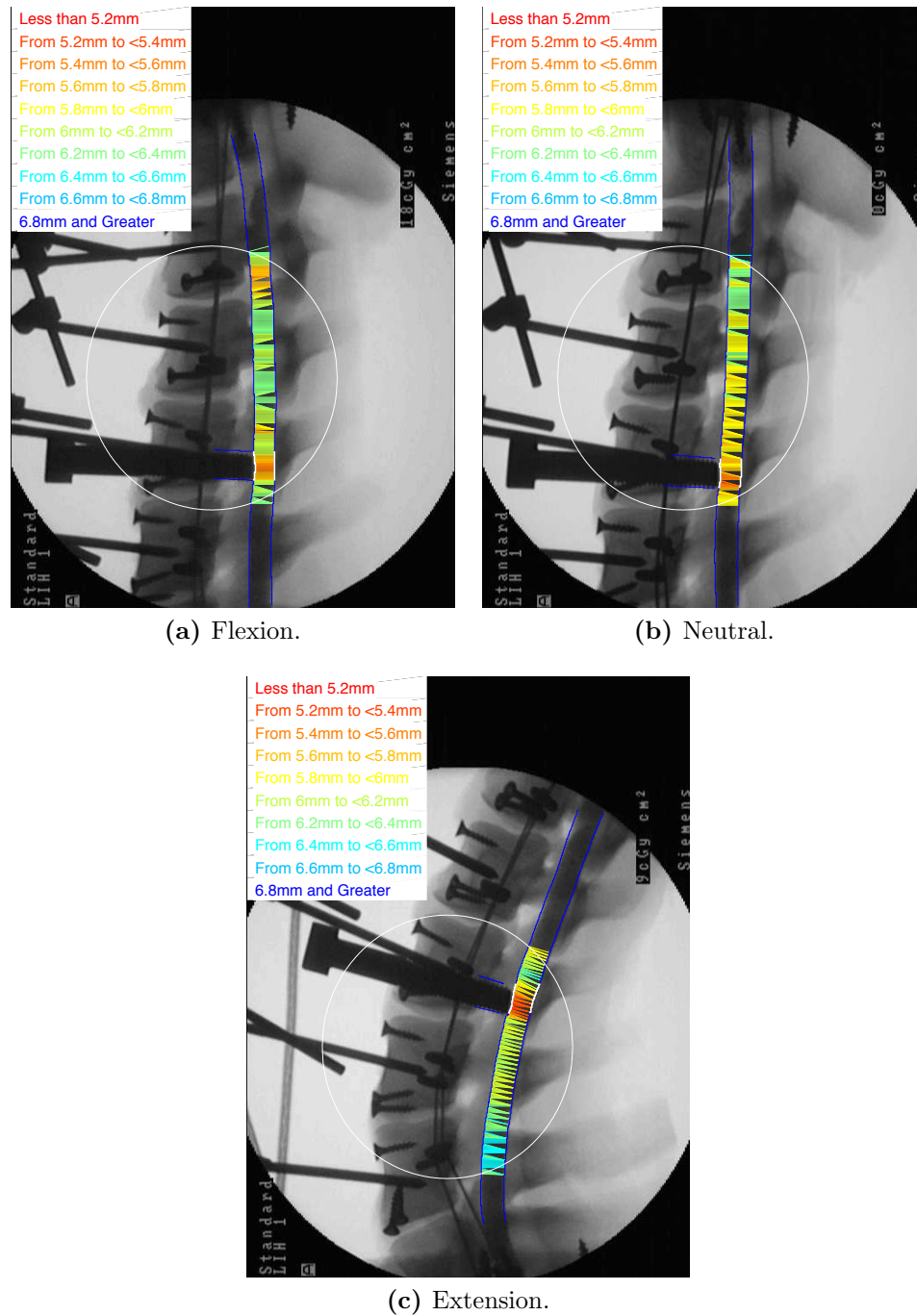


Figure 3.18: Specimen C flexion, neutral, and extension X-ray images with maximum canal occlusion, and a 2.5Nm moment limit. Colour-coded line segments indicate the surrogate cord AP diameter as per the legend. Cord compression is visible when the spine was in a neutral pose and cord compression increases as the spine extends.

3.3. Results

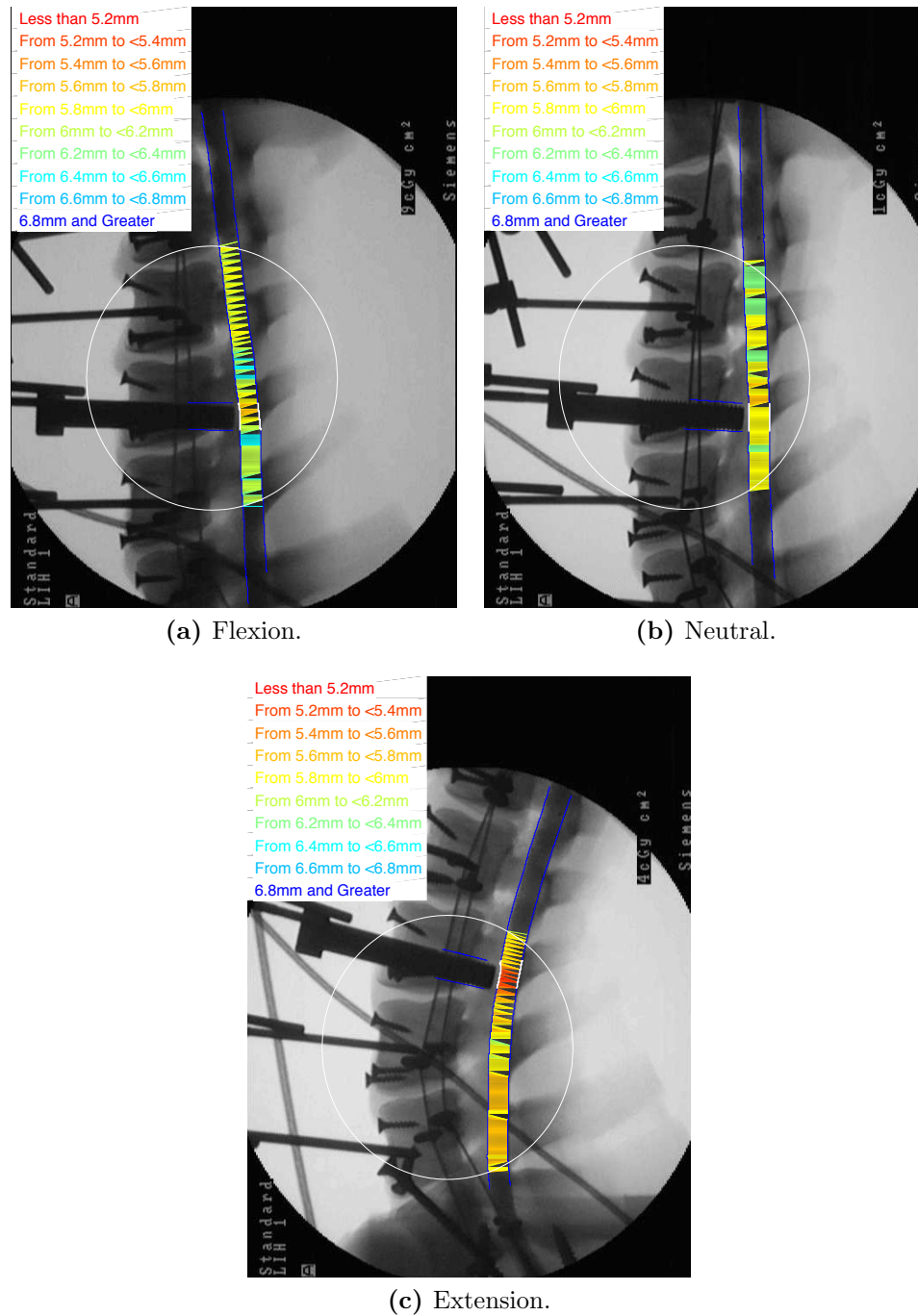


Figure 3.19: Specimen F flexion, neutral, and extension X-ray images with maximum canal occlusion, and a 2.5Nm moment limit. Colour-coded line segments indicate the surrogate cord AP diameter as per the legend. Cord compression increases as the spine extends.

3.3. Results

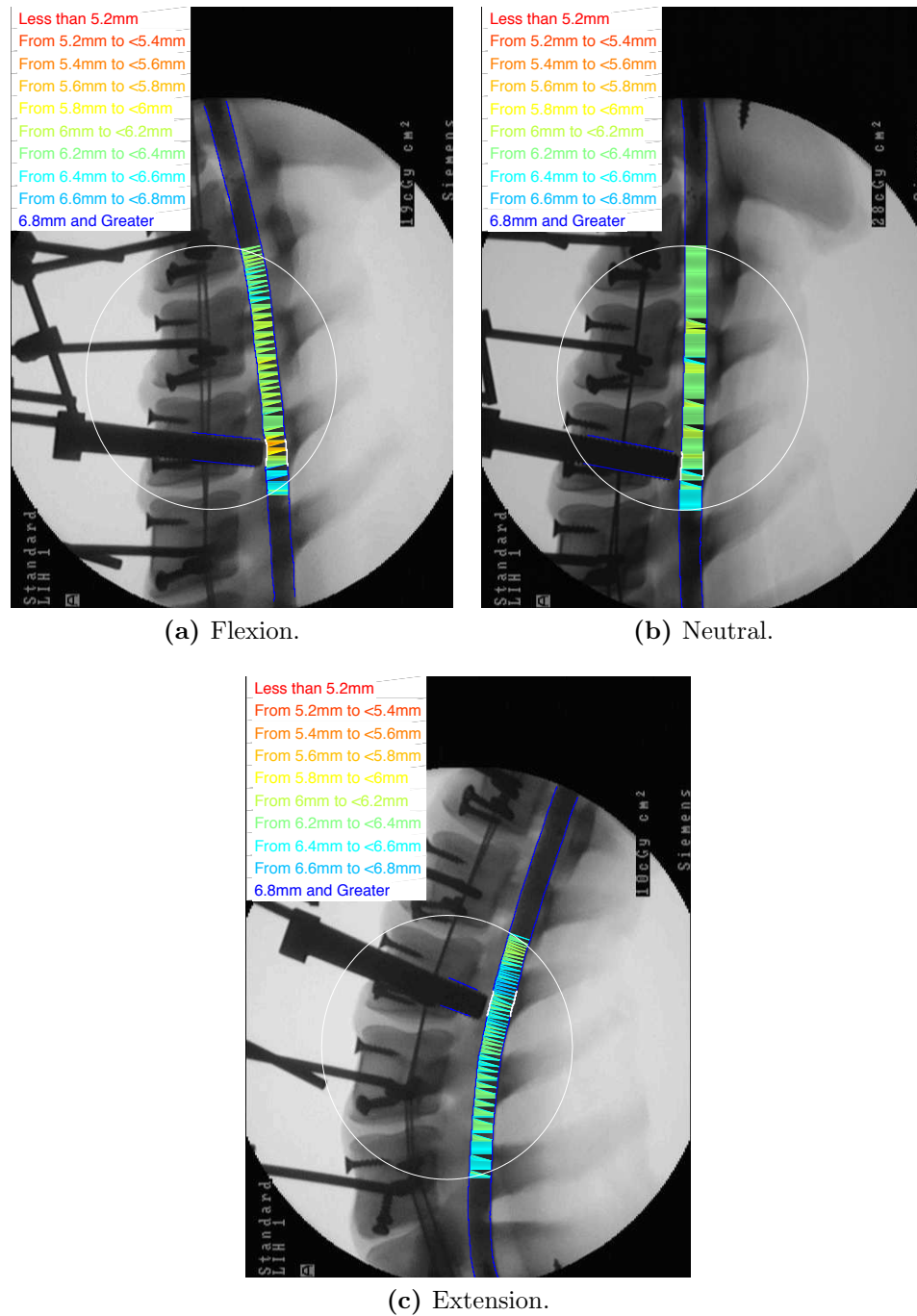


Figure 3.20: Specimen B flexion, neutral, and extension X-ray images with maximum canal occlusion, and a 2.5Nm moment limit. Colour-coded line segments indicate the surrogate cord AP diameter as per the legend. Cord compression increases as the spine flexes.

3.3. Results

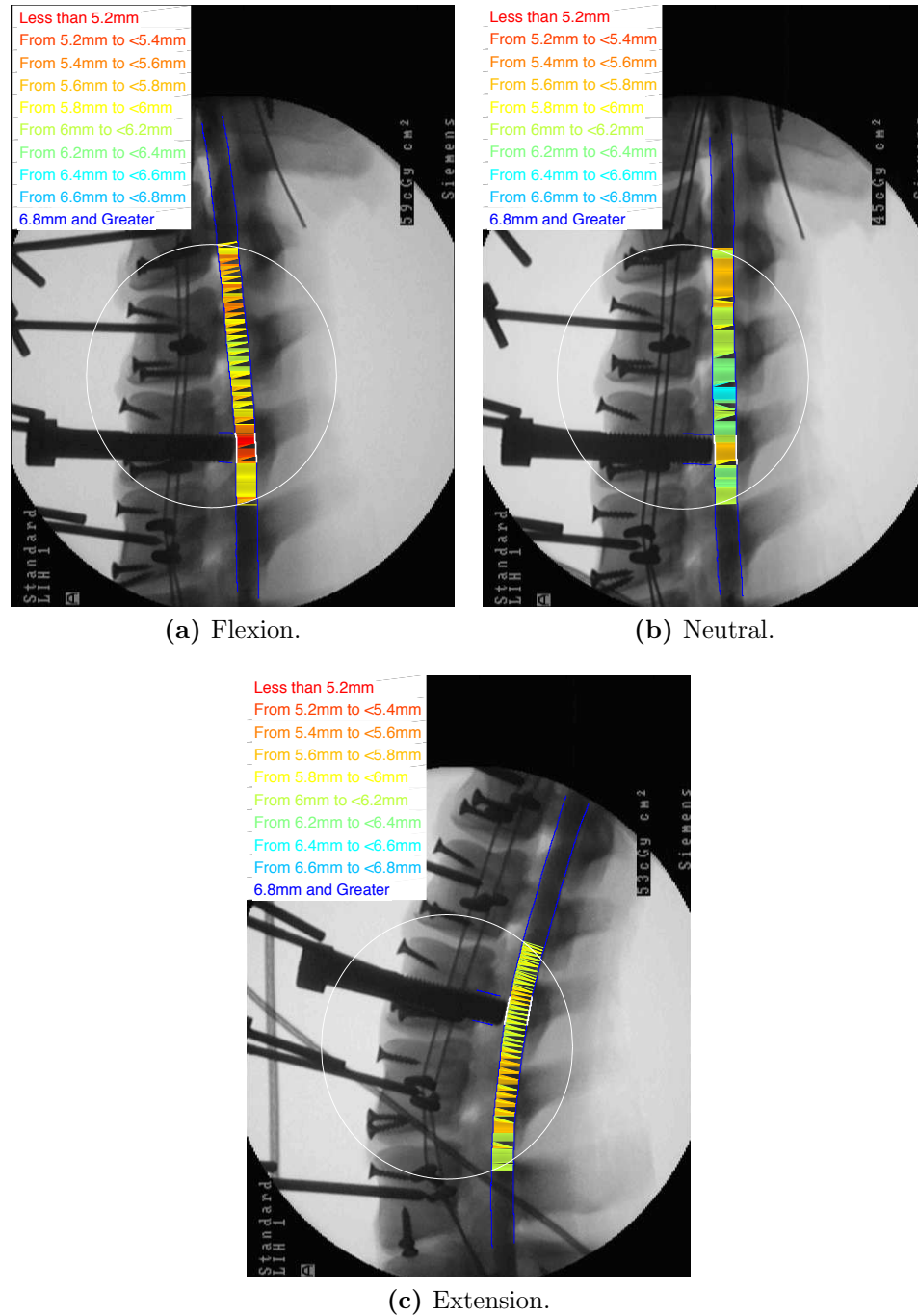
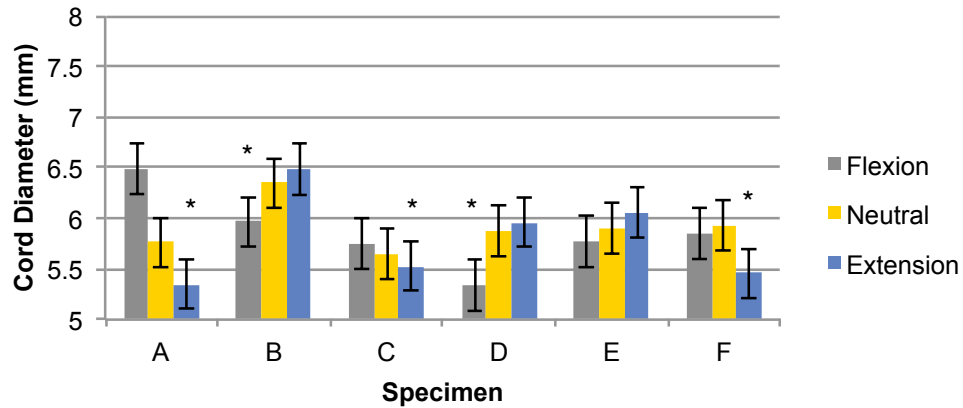


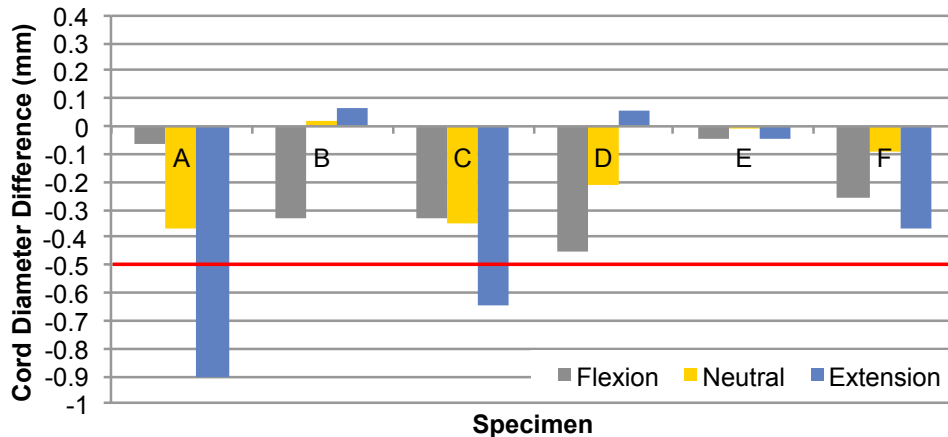
Figure 3.21: Specimen D flexion, neutral, and extension X-ray images with maximum canal occlusion, and a 2.5Nm moment limit. Colour-coded line segments indicate the surrogate cord AP diameter as per the legend. Cord compression increases as the spine flexes.

3.3. Results

Due to the small amounts of cord compression measured, the quantitative results are not conclusive for all specimens. When comparing the cord diameter values measured near the artificial osteophyte, (Figure 3.22a) cord compression is suggested in specimens A and F in extension and specimens B and D in flexion. The relative magnitudes of the cord diameter differences (Figure 3.22b) for specimens A, B, C, D, and F support the visual observations but only the results for specimens A and C exceeded the measurement error.



(a) Surrogate cord diameter near the artificial osteophyte. Error bars indicate accuracy ($\pm 0.25\text{mm}$). Star indicates qualitatively observed cord compression due to the artificial osteophyte.



(b) Difference between the surrogate cord diameter near the artificial osteophyte and the overall cord diameter. Negative values indicate the surrogate cord was narrower near the artificial osteophyte compared to the rest of the cord. Red line indicates accuracy ($\pm 0.5\text{mm}$).

Figure 3.22: Quantitative surrogate cord results for all specimens with the artificial osteophyte at maximum canal occlusion in the neutral posture, tested to a 2.5Nm moment limit.

While best efforts were made at the time of testing to not compress the surrogate cord when the spine was in a neutral pose, visual inspection of the X-ray images with colour-coded cord diameters showed that the cord was compressed in the neutral pose when testing specimens A and C. Both of these specimens showed increased cord compression when the spine was extended.

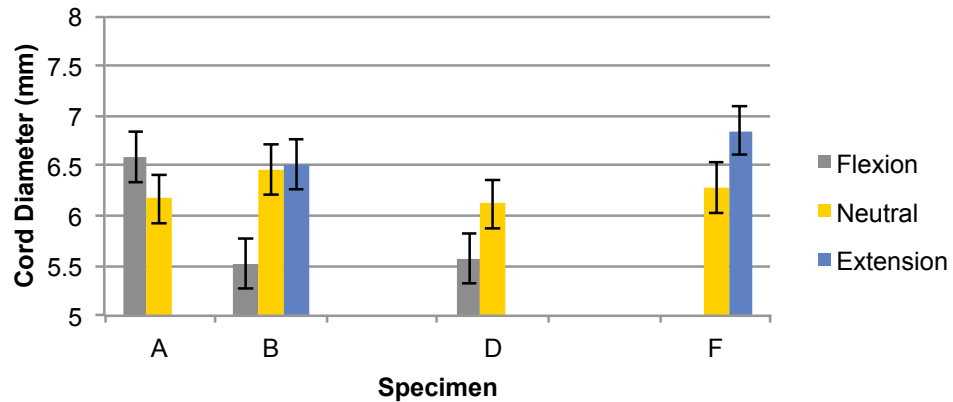
3.75Nm moment limit tests with 25% canal occlusion were conducted on only 4 of the 6 specimens tested (A, B, D, and F) because of limitations of the spine machine. Specimens C and E were more flexible than the other spines and did not reach the 3.75Nm moment limit within the motion limit of the machine. Due to the increased moment limit, all specimens moved through an increased ROM. As a result, the region of interest (area around the surrogate cord near the artificial osteophyte) of some images was not centred, and pincushion image distortion affected those surrogate cord diameter measurements. Those test results (Test A-Extension, D-Extension, and F-Flexion) were excluded from further analysis and are not reported.

During all 3.75Nm moment limit tests with 25% canal occlusion, the surrogate cord diameter changed as the spine moved through its ROM (Figure 3.23a). However, visual inspection of the X-ray images showed that the artificial osteophyte did not compress the surrogate cord and all cord diameter changes were due to uniform stretching of the surrogate cord. These observations are supported by the small surrogate cord diameter difference values (Figure 3.23b).

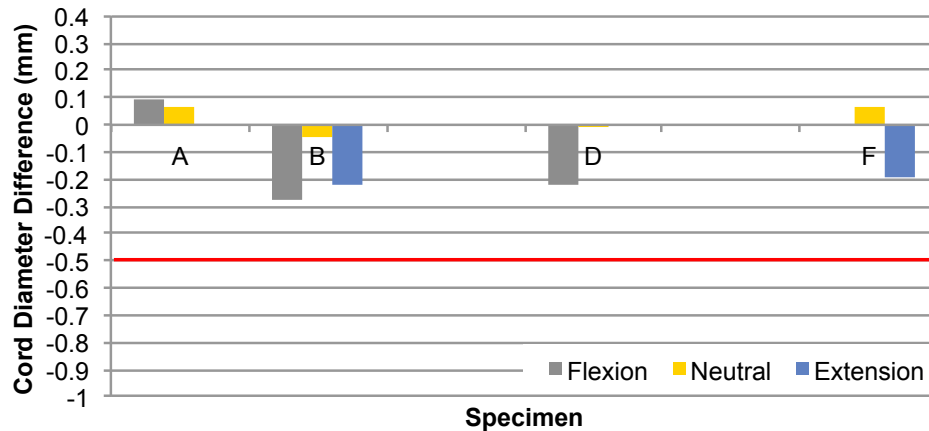
3.3.3 Range of Motion

All tests with the same moment limit produced a highly repeatable ROM (Figure 3.24). Repeated tests on the same specimen produced similar results, as were results across specimens.

3.3. Results



(a) Surrogate cord diameter near the artificial osteophyte. Error bars indicate accuracy (± 0.25 mm). No cord compression due to the artificial osteophyte was qualitatively observed.



(b) Difference between the surrogate cord diameter near the artificial osteophyte and the overall cord diameter. Negative values indicate the surrogate cord was narrower near the artificial osteophyte compared to the rest of the cord. Red line indicates accuracy (± 0.5 mm).

Figure 3.23: Quantitative surrogate cord results for all specimens with the artificial osteophyte at 25% canal occlusion in the neutral posture, tested to a 3.75Nm moment limit.

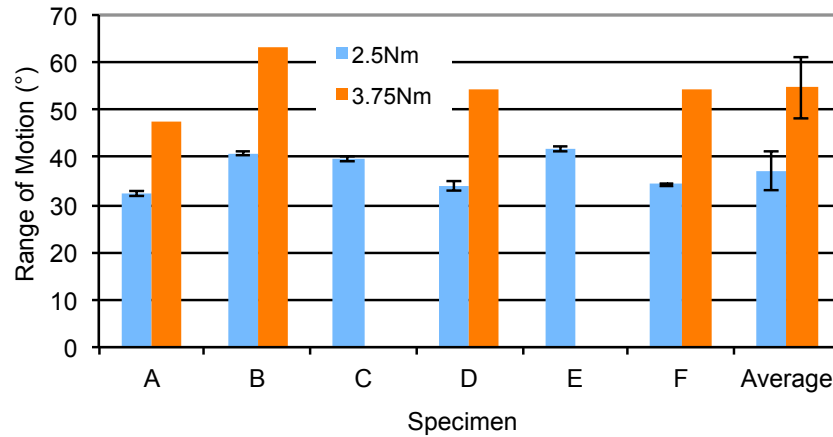


Figure 3.24: Specimen range of motion results. Repeated 2.5Nm tests results were averaged. Error bars indicate standard deviations. Specimens C and E were not tested at 3.75Nm.

3.4 Discussion

The present study examined the effect of canal occlusion on spinal cord compression during flexion-extension spine motion. By using a radio-opaque surrogate cord inside a whole porcine cervical spine with a continuously adjustable artificial osteophyte, spinal cord deformation was directly observed using X-ray. It was observed that an artificial osteophyte can compress the surrogate cord when the spine is either extended or flexed. In extension, cord compression was due to the spinal canal narrowing. In this posture, the surrogate cord was pinched between the posterior elements of the spinal canal and the artificial osteophyte. In flexion, cord compression was due to the cord becoming stretched along the anterior wall of the spinal canal. When the artificial osteophyte protruded into the spinal canal, it caused longitudinal cord stretching and local transverse compression.

This study illustrates the importance of observing the spinal cord when studying cervical spondylotic myelopathy and traumatic SCI in the presence of spinal degeneration. Spinal cord compression in flexion may not be apparent from only observing the spinal canal space and the tissues surrounding the spinal cord. If the spinal canal is occluded, hyper-flexion due to impact may compress and injure the spinal cord.

Enhancing our understanding of SCI mechanisms can improve prevention and treatment strategies. Informing medical practitioners (such as doctors, nurses, physiotherapists, first responders) that the spinal cord can be jeopardized in either flexion

or extension when canal space is occluded, may help prevent SCI during medical interventions.

3.4.1 Comparisons to Previous Studies

Cervical spondylotic myelopathy and spinal cord biomechanics have been studied extensively both clinically and experimentally. Clinical studies [17, 39, 40, 52, 104, 126, 139–141, 176, 223] and case reports [42, 90, 91, 104, 111, 168, 188, 197] document SCIs and neurological deficits due to cord compression in both flexion and extension. SCI mechanisms in both flexion and extension have also been described in many review articles [14, 32, 71–73, 78, 156, 166, 191, 210] but experimental research has primarily focused on spinal canal constriction during extension while often neglecting stretch-associated SCI that can occur during flexion. [78]

Many different experimental cadaver studies have measured cervical spinal canal diameter change during spine motion. [25, 67, 81, 88, 146, 147, 195] When canal diameter change was detected, these studies consistently found that canal diameter decreased as the spine extended. Thus conclusions regarding cord compression could only be made about canal occlusion in extension. Ivancic et al. [89] found the canal diameter was reduced a small amount in flexion because they defined their pincer canal diameter opposite to the typical definition. These studies did not detect cord compression in flexion because the spinal cord or a surrogate were not observed.

Few cadaveric experimental studies have observed the effects of cervical spondylotic myelopathy on the spinal cord in the canal. Breig et al. [15] observed the spinal cord in 42 cadaveric cervical spines using air myelograms. By manually flexing and extending the spines they demonstrated the bow-string spinal cord compression mechanism during spine flexion in specimens that had a spondylotic ridge. Reid [177] also examined the behaviour of the spinal cord in cadaveric specimens during flexion and extension of the head. He simulated the effects of an anterior protrusion into the canal (such as an osteophyte) by pulling the cord posteriorly 3mm. Based on the loads applied, he estimated that the pressure on the spinal cord would be sufficient to cause injury. Taylor [197] observed cervical spinal cord compression due to bulging of the LF during extension.

Few previous studies have artificially introduced canal stenosis in their experimental cervical spine models. [62, 195, 198–200] Gooding et al. [62] induced anterior cervical spinal cord ischemia *in vivo* to dogs using specially designed screws protruding into the spinal canal through the vertebral body. They found that the induced ischemia accounted for observed myelopathy. Subramaniam et al. [195] occluded the spinal canal of human cadaveric cervical spines during step-wise flexion-extension testing

using hemispherical craft balls sewn into the canal. In a three-part study using whole human cadaveric spines, Tencer et al. [198–200] observed the effects of anterior canal occlusion by pushing a probe into the spinal canal through a hole in the vertebral bodies of C3, T7, T12, and L3 (but most experiments focused on the T12 level). The probe displacement was controlled by a linearly variable differential transformer. A micro-loadcell was mounted at the tip of the probe that contacted the spinal cord. They found that the transverse force-displacement relationship of the spinal cord in the canal was not affected by laminectomy or spine shortening. The contact force for a given amount of transverse displacement was increased by distraction and flexion. These results indicated that clinical posterior decompression interventions (such as a laminectomy) would have no effect on a spinal cord that is compressed by an anterior canal occlusion, such as an osteophyte. Spine flexion and distraction, which are sometimes applied as therapeutic interventions, could make spinal cord compression worse. The present work supports these findings as cord compression observed in flexion did not involve the posterior elements thus posterior decompression would have no effect.

The biofidelity of all biomechanical studies that test cadaveric spinal cords is limited because the mechanical properties of the spinal cord change quickly after death, [22, 83, 84, 148] and to mitigate this limitation some authors used a biofidelic surrogate cord. [11, 171, 185] Pintar et al. [171] instrumented a gelatine surrogate cord with pressure sensors to quantify the effect of a burst fracture spine injury on a spinal cord. Bilston et al. [11] used a surrogate cord in a biofidelic mechanical model of the cervical spine and head to quantify the strain and strain-rate induced in the spinal cord during traumatic flexion-extension motion. Saari et al. [185] used a surrogate spinal cord in a cadaveric cervical spine with a surrogate head to quantify spinal cord deformation during head-first impact. All of the studies used dynamic test conditions to simulate injury mechanism, and none modelled a stenotic canal. However, results from Bilston et al. [11] support the findings of the present study as they observed axial cord stretch in flexion and axial cord compression in extension.

The pincer (in extension) and bowstring stretching (in flexion) spondylotic SCI mechanisms can cause complicated stress and strain patterns in the cord that can cause injury or neurologic dysfunction. [8, 69, 71–73, 105, 156, 191] Previous studies have related the extent of SCI to cord compression, [21, 51, 57, 74, 106, 152] but the injury thresholds developed would not directly translate to the complicated loading scenarios in the present work. None the less, some published relationships can offer some insight into expected neurologic outcomes due to the cord compression observed in the present study.

The present study observed localized AP surrogate cord diameter change in multiple specimens, but the extent of cord diameter change never exceeded 1mm (roughly 15%

diameter change). Cursory bench-top measurements of a surrogate cord with 1mm of AP compression resulted in a compression ratio (the ratio of the sagittal diameter to the transverse diameter) of 0.46.

Fujiwara et al. [51] and Hayashi et al. [74] related cord compression ratio to graded pathological change and neurologic dysfunction respectively. Neurologic dysfunction was graded using the Japanese Orthopaedic Association (JOA) score. The compression ratio of the surrogate cord may have resulted in a grade 1 pathological change according to Fujiwara et al.'s scale and was outside the range of data collected by Hayashi et al. However, extrapolating Hayashi et al.'s correlation, a compression ratio of 0.46 would predict a JOA score of 10 (out of a maximum score of 17, where 17 indicates no neurologic dysfunction).

SCI criteria developed by Kearney et al. [106] incorporated impactor velocity and cord compression. The compression measured in the present study is below the range of compression results reported by Kearney et al. and it was conducted quasi-statically. However, the constant velocity-compression curves reported by Kearney et al. suggest even if the compression observed in the present study was applied with a velocity of up to 7m/s there would likely be full recovery if any cord injury was suffered.

Transverse cord compression has also been related to injury. A clinical study of magnetic resonance images of patients with a cervical SCI without evidence of boney injury suggests that cord compression at the narrowest region of the cord is mild and likely non-injurious if the cord retains at least 2/3 of the cord diameter at C1. [75] Studies by Galle et al. [57] and Ouyang [152] graded the resulting injury to guinea pig spinal cords due to transverse crushing. These results suggest that the 15% spinal cord diameter change observed in the present study would not be injurious.

The present study displayed highly repeatable ROM results. While the intent of using the 2.5Nm and 3.75Nm moment limits was to produce physiologic and greater-than-physiologic ROM (respectively), all the results appear to be similar to or less than normal physiologic ROM results published in previous cadaveric flexibility studies that applied moments to a human spine (Figure 3.25). One possible explanation for this difference is the previous studies applied step-wise loading while the present study applied a continuously varying moment with a constant velocity. Continuous loading protocols have been shown to produce smaller ranges of motion than step-wise loading. [61]

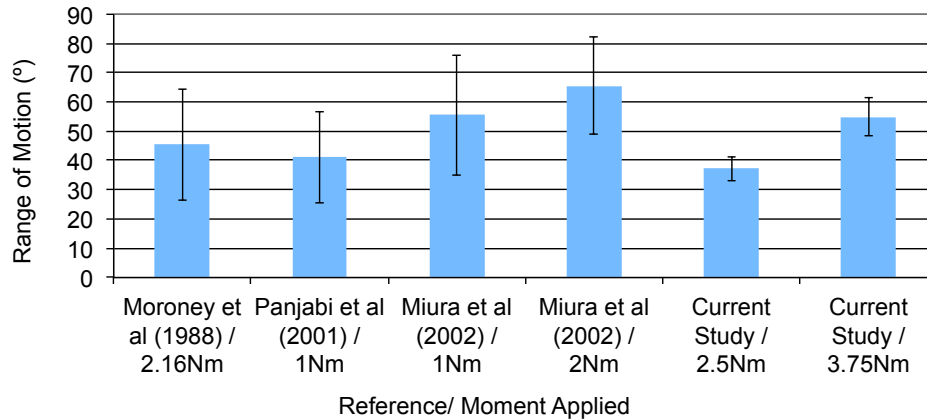


Figure 3.25: Range of motion of the present study compared to previous pure moment cadaver studies. Error bars indicate standard deviation of average results. Miura et al. [133] and Panjabi et al. [160] tested whole spine specimens (C2-T1), while Moroney et al. [137] tested multiple functional spinal units from the lower cervical spine (C2-T1).

3.4.2 Limitations

Fresh frozen cervical porcine spines were used in this study as a model for living human cervical spines. Human and porcine spines have many anatomical similarities that are relevant to this study. Both species have the same number of cervical vertebrae and the vertebrae are similar in size and shape. The cervical spinal AP canal diameter of porcine specimens is similar but often narrower than a typical human. [19] Comparison between the canal diameters of the specimens used in the previous study and previously published human averages, found the same trend (Table 3.2). Furthermore, the differences were less important since canal occlusion was controlled by the artificial osteophyte.

There are numerous notable differences between human and porcine anatomy. Porcine vertebral endplates are more flat, while human endplates are more saddle-shaped. In a neutral pose, porcine spines typically have a greater lordotic curve. (20° in human versus 44° in porcine spines.) [19] In the porcine cervical spine, the spinous processes on C2 and C7 are larger than those found in human vertebrae. [19] The lower cervical porcine vertebrae have large anterior processes that the human does not have (Figure 3.26) and in the present study they were removed during preparation. Facet orientation in the porcine cervical spine is different compared to the human cervical spine, and more resembles the facet joint orientation found in the human lumbar spine. [154, 219]

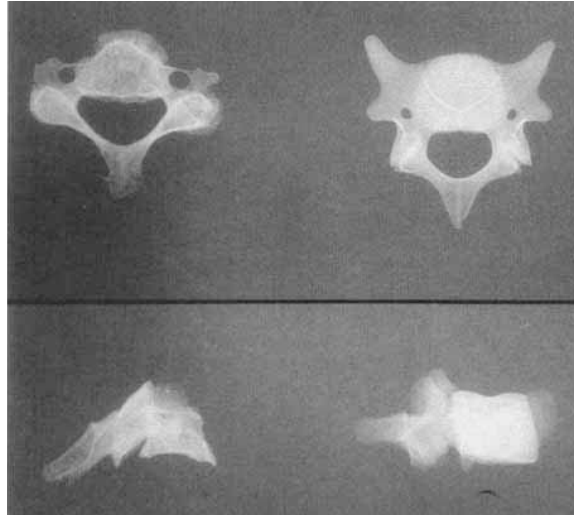


Figure 3.26: Axial and lateral radiographic comparisons of a human cervical vertebra (left), a porcine cervical vertebra (right). Adapted from Oxland et al, 1991. [154] with permission from John Wiley and Sons.

Despite these differences, many authors have concluded that the porcine cervical spine is an acceptable surrogate for the human cervical spine. Schmidt et al. [189] repeated tests on human and porcine cervical spine specimens and found the biomechanical properties of the two species were very similar in the flexion-extension direction. However, they also found that the porcine spine is not a suitable model for the human cervical spine when tested in lateral bending or axial rotation. This is likely due to the difference in facet joint angle causing different coupled motion. Numerous authors have used the porcine cervical spine as a biomechanical model for the human cervical spine in trauma [59, 161, 205] and implant tests. [65, 143, 180]

Using porcine spines reduced the inter-specimen variation usually found when repeating tests using human cadavers. Using specimens that had no natural degeneration and an artificial osteophyte allowed the effects of canal diameter to be isolated.

While some authors have found that freezing and thawing may have a small but significant effect on the mechanical properties of cadaveric porcine spines, [20, 82] these storage and handling conditions conformed to previously established recommendations and should not have adversely affected this study. [214, 215]

Surrogate cord deformations observed in this study were small compared to the resolution of the X-ray images and the image analysis accuracy. While the cord diameter measurements were accurate within $\pm 0.25\text{mm}$ (1 pixel), this error accumulated when comparing multiple cord diameter values. Image resolution could have been improved

by increasing image magnification, but that would have restricted the image field of view. Reducing the field of view would have been undesirable, and the image magnification used was considered the best available compromise. While the image resolution and cord deformation measurement accuracy limited the analysis of the present study, the resolution and accuracy were sufficient to show that the cord deformations produced would not be expected to injure a living spinal cord. If the surrogate cord had been compressed a clinically injurious amount, the present analysis would likely have been able to detect the compression.

ROM results are not from the same period of flexibility testing as the surrogate cord compression results. The ROM results are from the third cycle of spine flexion-extension motion while the X-ray images were collected during the last half of the second cycle and the first half of the fourth cycle. This was necessary to collect centred images of the surrogate cord during maximum spine flexion and extension. Thus the ROM results cannot be directly compared to the cord compression results.

The surrogate spinal cord was moulded into an elliptical shape with dimensions matching average values for human spinal cords [96, 97, 109] in an effort to make the surrogate cord more biofidelic than previous versions used in this lab. [95, 114, 185] The minor axis of the cord was aligned with the sagittal plane when the cord was anchored into place. However, the cord may have twisted during testing which would have increased the projected AP diameter measured in the X-rays. The cord would be more likely to twist when it was not in contact with the canal wall or artificial osteophyte and when the cord was axially compressed due to reduction of the spinal canal length due to extension. Contact with the artificial osteophyte or the anterior or posterior canal wall would tend to re-align the minimum diameter of the surrogate cord with the sagittal plane. Twisting and stretching is a likely explanation for measured cord diameter changes when the artificial osteophyte was not near the surrogate cord. The influence of twisting appears to be minimal when cord compression due to the artificial osteophyte was observed, because the cord diameter never appeared to be greater than the minor diameter of the surrogate cord mould.

The mechanical environment of the surrogate spinal cord in the present study deviated from the environment of a biological cord in a living spine. A living spinal cord in the spinal canal is surrounded by soft tissue including dura mater, and cerebrospinal fluid (CSF). The living spinal cord is somewhat constrained along its length by nerve roots and denticulate ligaments branching out of the canal between each vertebral level. The surrogate spinal cord in the present study was tested in an otherwise empty spinal canal and was only tethered at the cranial and caudal ends of the specimen. Tethering along the surrogate cord's length was rejected as no practical method could be devised that would resemble the mechanical properties of biological nerve roots. Introduction of dura mater and CSF was outside of the scope of this study.

The artificial osteophyte does not have a bar-like shape that is typical of most osteophytes observed clinically. However, biological osteophyte shapes vary greatly and the shape of the artificial osteophyte used in this study resembles a subset of the osteophytes observed clinically.

The ARTORG spine machine depends on linear motion of the inferior end of the spine during pure moment testing to release the translation degree of freedom. Due to limitations of the range of this linear motion, only four of the six specimens could be tested with the 3.75Nm moment limit. Excluding the two most flexible specimens may have biased the results toward spines with a smaller ROM.

3.4.3 Future Work

Future experimental studies investigating cervical spondylotic myelopathy should address the limitations of this study. This may include using imaging equipment with a higher resolution. Many different measures may be taken to remedy the confounding effect of an elliptical surrogate cord shape such as multi-planar X-ray or other three-dimensional imaging techniques. Adding more biofidelic constraints on the surrogate spinal cord (such as nerve roots or dura mater with simulated CSF) will likely produce a more biofidelic response and greater amounts of cord compression. The artificial osteophyte may be refined to more closely resemble the size and shape of typical osteophytes. Other forms of spinal degeneration may also be simulated to control and observe the interactions that occur in clinical patients (e.g. damaging ligaments or discs to induce local excessive spine flexibility, or simulating a bulging disc). Modifications to the experimental apparatus would allow for continuous X-ray imaging without the need for realignment and testing up to a greater ROM including spine failure. This work should be conducted on human spines so that other motion patterns besides flexion-extension can be studied.

Other extensions of this work may provide a better understanding of cervical spondylotic myelopathy and traumatic injury. Future work may include equipping the tip of the artificial osteophyte with a load cell so that direct comparison to previous work by Tencer et al. [198–200] would be possible. This could also provide insight into the stress and strain induced in the surrogate spinal cord. Using a string coated with lead-based paint, a thin radio-opaque line could be painted on the anterior and posterior surface of the spinal canal. This would allow sagittal plane X-ray to visualize soft tissue bulging. Automatic image segmentation would allow video analysis of the cord compression during testing. Since a stenotic spinal canal (a common feature of a spondylotic cervical spine) can cause myelopathy when the spine is flexed or extended, the pincer or bowstring stretch injury mechanism likely play a role during

low energy traumatic impact injury. To better understand this injury mechanism a dynamic *ex vivo* study, using human cadaver specimens outfitted with an artificial osteophyte and surrogate spinal cord, is needed.

3.5 Conclusions

A new technique for modelling degenerative cervical spinal canal stenosis and quantifying compression of a surrogate spinal cord was developed and evaluated. Canal stenosis was modelled using a continuously adjustable artificial osteophyte in a porcine cadaver spine. Surrogate cord compression was quantified using a custom-written image analysis algorithm. The image analysis algorithm accuracy was evaluated and cord diameter could be measured with an accuracy of $\pm 0.25\text{mm}$. These techniques may be applicable to studies simulating spondylosis in dynamic cadaver experiments.

This study quantified the effect of increasing canal stenosis on a biofidelic surrogate cord during physiologic motion in an *ex vivo* porcine cervical spine. Canal occlusion was shown to cause surrogate cord compression in either flexion or extension, depending on the specimen, only when the osteophyte occluded 50% or all available space in the canal. While cord compression increased with increasing canal stenosis, the extent of cord compression was very small. One possible explanation for this result is the specimens were otherwise free from degeneration. In a typical elderly clinical patient with cervical spondylotic myelopathy, many types of degeneration are present (e.g. disc and facet joint degeneration with osteophytes) and the interaction between these factors likely play a role in the extent to which the spinal cord is compromised.

This study illustrated the typical spondylotic SCI due to flexion: a bowstring stretching mechanism over an osteophyte protruding from the anterior of the spinal canal. Few experimental cadaveric studies have observed it and none with a biofidelic spinal cord.

Chapter 4

Integrated Discussion

The present work developed and evaluated methods for an ongoing research program that aims to quantify relationships between spine degeneration, spine motion, and spinal cord injury (SCI). Two complementary studies were conducted that analyzed sagittal plane flexion-extension X-ray images of cervical spines.

In the first study (Chapter 2), an image analysis technique was developed that quantitatively measured kinematic and degenerative cervical spine features as continuous variables. Angular range of motion (ROM), anterior-posterior (AP) translation, intervertebral disc height, pincer spinal canal diameter (in flexion, in extension, and the difference), and osteophyte length were calculated for each functional spinal unit using manually digitized osseous landmarks. The technique was evaluated using a publicly available sample sagittal plane flexion-extension X-ray image pair. The angular accuracy and linear precision were found to be $\pm 1.3^\circ$ and approximately $\pm 0.6\text{mm}$ respectively.

In the second study (Chapter 3), the effects of increasing canal stenosis on the spinal cord during flexion-extension motion was modelled using an artificial osteophyte and a surrogate spinal cord in an *ex vivo* porcine cervical spine. Full flexion, full extension, and neutral sagittal plane X-ray images of the spine during testing were manually segmented and analyzed to quantify transverse spinal cord diameter change. Due to the image resolution, spinal cord diameters could be measured accurately within $\pm 0.25\text{mm}$ and cord diameter differences could be measured within $\pm 0.5\text{mm}$. The artificial osteophyte was qualitatively observed to compress the surrogate spinal cord during either full flexion or full extension in five of the six specimens when the artificial osteophyte occluded all available space in the spinal canal not taken by the surrogate cord when the spine was in a neutral pose (maximum canal occlusion). However, the amount of cord compression was always small and could only be quantitatively detected above the experimental error in two specimens. Observed cord compression demonstrated the typical spondylotic SCI mechanisms: bowstring stretching in flexion and pincer in extension.

The sample results from the first study compare well with the parameters tested in the second study. The total ROM (from C2-C7) from the first study was 55° . The

average total ROM from the second study when the maximum moment limit was 2.5Nm and 3.75Nm were 37° and 55°, respectively. Osteophytes were observed in the sample X-ray image pair at the C5/C6 and C6/C7 levels. This is typical as C5/C6 is the most common level for osteophytes to develop [29, 77, 121, 186, 204] and hence the level where the artificial osteophyte was inserted into the porcine cadaver model.

4.1 Comparisons to Previous Studies

To the best of our knowledge, both studies make new contributions to the methodology or results of previous work, and the accuracy performance of each study compares well with previous studies.

The combination of variables in the first study has not been quantitatively measured simultaneously as continuous variables in a single population group before. The present set of variables analyzed were selected because they can all be observed using plane X-ray and thus by any imaging modality used for biomechanical analysis. Various subsets of the variables measured in the present work have been analyzed in past work as continuous or categorical variables. [63, 110, 134–136, 139, 140, 142] The present image analysis technique produces quantitative, continuous results which allows regression analysis to test the relationships between all of the kinematic and degenerative variables studied.

The accuracy and precision of the present methodology is roughly equal to comparable studies. [49, 50, 118, 119] The present method for analyzing ROM, AP translation, and intervertebral disc height was based on work by Frobin et al. [49, 50] which was later evaluated by Leivseth et al. [118, 119] The angular accuracy and linear precision of the present work ($\pm 1.3^\circ$, and approximately $\pm 0.6\text{mm}$, respectively) compares well to Leivseth et al.'s evaluation of Frobin et al.'s accuracy ($\pm 2.4^\circ$ and $\pm 0.78\text{mm}$, respectively).

The second study's methodology includes many improvements over similar past studies. Less recent cadaver studies that examined the effect of canal stenosis and spine motion on the spinal cord used the biological cord. [15, 177, 197–200] A three-part series of studies using whole cadaver spines [198–200] and an *in vivo* study using dogs [62] experimentally occluded the spinal canal from the anterior in a manner similar to the present work. Since spinal cord material properties change rapidly after death, [22, 83, 84, 148] results of the cadaver studies would differ from the response of a living cord. The *in vivo* study using dogs did not test the effects of spine motion nor was the dog model meant to simulate the biomechanics of a human spine. More recent cadaveric studies have quantified cervical spinal canal diameter change

during spine motion [25, 67, 81, 88, 89, 146, 147] including one study that experimentally introduced an artificial canal obstruction. [195] However, these studies did not have a spinal cord in the canal, so the bowstring stretch cord injury mechanism was neglected. The present work used a porcine cadaveric spine and a surrogate spinal cord with mechanical properties similar to a living human spine [189] and spinal cord, [95, 114] respectively. The artificial osteophyte and surrogate spinal cord were directly observed during testing via X-ray and both the bowstring stretching (in flexion) and pincer (in extension) injury mechanisms were successfully modelled.

The accuracy of the second study's image analysis technique would be sensitive enough to detect injurious cord compression based on previously published cord injury thresholds. [51, 57, 74, 75, 106, 152] The cord compression that was quantitatively detected in the present work never exceeded more than 1mm of compression (roughly 15% diameter change or an AP compression ratio of 0.46) and would likely not have been injurious even if the compression happened at speeds up to 7m/s. [51, 57, 74, 75, 106, 152]

4.2 Strengths and Limitations

The two studies comprising this thesis have many similar strengths and limitations since they both depend on plane X-ray image analysis. All analysis was limited to two dimensions and assumed no significant out-of-plane motion. This was an acceptable assumption as out-of-plane motion in clinical studies has been shown to be negligible when following regular procedures, [70] and no out-of-plane motion was observed during the cadaver testing. Plane X-ray does not effectively image biological soft tissue, which limited the possible observations and measurements made in each of the studies. In the first study, the variables analyzed were all based on hard tissue landmarks visible via plane X-ray. This precluded observation of bulging ligaments or discs into the canal space, which can significantly compress the spinal cord during flexion-extension motion. [25, 67] Furthermore, the spinal cord could not be observed. This limitation was overcome by the second study because the surrogate spinal cord was radio-opaque and could be directly observed by plane X-ray.

The image analysis technique developed for the first study has many strengths. It may be applied to any sagittal plane image of the cervical spine and produces a set of continuous variables that quantify kinematic and degenerative features. This makes regression analysis of the results possible. By depending on manual segmentation, even highly degenerated spines can be digitized.

Depending on manual digitization was also a limitation of the first study. Man-

ual digitization may have limited repeatability, but the small sample of image pairs (n=1) used to evaluate the methods precluded any repeatability assessment. Manual segmentation is time consuming and will limit the number of images that can be analyzed.

Strengths of the second study included the highly reproducible test conditions and control of the independent variable that were a result of using healthy adult porcine spines free of age-related degeneration. Test conditions, including applied loading, specimen preparation and mounting, and positioning of the artificial osteophyte, were carefully controlled and the ROM results indicate that each spine flexibility test was similar. Thus the observed cord compression could be directly attributed to the independently controlled canal occlusion due to the artificial osteophyte.

Using porcine cadaver spines free of age-related degeneration in the second study was also a limitation. Cervical porcine cadaver spines have similar mechanical properties to human cervical spines when tested in flexion-extension but are not as biofidelic as human cadaver spines. The lack of dramatic surrogate cord compression during testing may have been a consequence of biomechanical differences between human spines and porcine spines or because the spines tested were otherwise free from age-related degeneration. Clinical studies report osteophytes typically develop in human spines as a response to excess spine flexibility, often due to a degenerated disc. [8, 29, 121, 191, 204] Injurious spondylotic spinal cord compression is likely due to the interaction of many types of degeneration simultaneously affecting the spine.

4.3 Future Work

The methods developed in both studies may be applied in answering many future research questions.

The image analysis methods from first study can be used to analyze sagittal plane images using many different imaging modalities and potentially find correlations between the kinematic (ROM, AP translation, canal diameter change) and degenerative features (canal diameter, osteophyte size, disc height). Multi-variable regression models may be the most effective means of predicting clinical risk factors for spondylotic SCI such as canal diameter change due to flexion-extension motion. Features that are uniquely visible to some imaging modalities (such as disc degeneration classified by magnetic resonance imaging) may be correlated to other features visible in other imaging modalities. Comparisons between young, elderly, myelopathic, post-surgery, and post-traumatic injury patients may reveal differences that can be used to screen at-risk patients. Patients found to be at high risk of spondylotic SCI may be able

to take actions to prevent falls, which are the leading cause of SCI for the elderly population. [24, 33, 36, 69, 92, 100, 120, 170, 193]

The artificial osteophyte and the surrogate spinal cord are an effective means to visualize both of the typical spondylotic SCI mechanisms (bowstring stretching and pincer) in a cadaver spine model. Future cadaver tests may include other forms of simulated degeneration such as damaging ligaments or discs to induce local excessive spine flexibility, or simulating a bulging disc. These techniques may be applied to low energy dynamic impact testing that would simulate the falls that most commonly injure elderly patients. [24, 33, 36, 69, 92, 100, 120, 170, 193] The surrogate spinal cord may be improved by including nerve roots (with appropriate tethering), dura mater and simulated cerebrospinal fluid. Adding a load sensor to the tip of the artificial osteophyte would provide valuable information about the force applied to the spinal cord.

Finally, the studies may be combined by using the image analysis methods from the first study on degenerated cadaveric spine specimens tested with the artificial osteophyte and the surrogate spinal cord. Future cadaveric specimens will include spines from elderly people who have extensive age-related degeneration (apart from any simulated degeneration). Comparison and combination of results from repeated tests may be difficult if the biomechanics are significantly affected by the age-related degeneration. Quantitative relationships between spine kinematics and degenerative features derived from samples of clinical patients may account for differences seen in the cadaveric specimens. Future studies of clinical images and multi-factor impact cadaveric experiments that employ the image analysis methods from both of the present studies are recommended. In such a study, large sample sizes will be required to maintain statistical significance.

4.4 Conclusions

This thesis analyzed X-ray images to quantify cervical spine kinematic and degenerative features (Chapter 2) and to quantify the effect of increasing canal stenosis during spine motion on a surrogate spinal cord in cadaveric specimens (Chapter 3). The image analysis techniques developed in both studies were evaluated and found to be highly accurate and precise.

Results from the second study suggest that increasing canal stenosis causes increased cord compression in flexion and extension; however, without other degeneration, normal spine motion is unlikely to injure the spinal cord, even if all available canal space is consumed by an osteophyte. This study demonstrated the flexion bowstring

4.4. Conclusions

stretching SCI mechanism which has rarely been demonstrated in a cadaveric experimental study and never with a biofidelic surrogate cord. If interested in spinal cord compression, it is important to directly observe the spinal cord in the canal. Observing only the canal is not sufficient.

When evaluating the effects of cervical spondylosis on SCI, the interactions of many different degenerative features need to be considered. Establishing causal relationships in light of so many confounding factors is difficult. This was demonstrated by the limited positive results of the second study. The methods developed in the first study may help guide this research by finding statistical relationships between spine kinematics, degenerative features, and SCI.

Bibliography

- [1] Rick hansen institute spinal cord injury registry sci facts, Accessed July 2, 2011. URL <http://www.rickhansenregistry.org/en/news-and-resources/sci-facts.html>.
- [2] Statistics canada: Economic and financial data, Accessed May 24, 2012. URL <http://www.statcan.gc.ca/tables-tableaux/sum-som/101/cst01/dsbbcan-eng.htm>.
- [3] Wikimedia cervical spine extension image, Accessed March 19, 2012. URL https://commons.wikimedia.org/wiki/File:Cervical_Xray_Extension.jpg.
- [4] Wikimedia cervical spine flexion image, Accessed March 19, 2012. URL https://commons.wikimedia.org/wiki/File:Cervical_Xray_Extension_view.jpg.
- [5] Michael A Adams and Patricia Dolan. Spine biomechanics. *J Biomech*, 38(10): 1972–83, Oct 2005. doi: 10.1016/j.jbiomech.2005.03.028.
- [6] Mauro Alini, Stephen M Eisenstein, Keita Ito, Christopher Little, A Annette Kettler, Koichi Masuda, James Melrose, Jim Ralphs, Ian Stokes, and Hans Joachim Wilke. Are animal models useful for studying human disc disorders/degeneration? *Eur Spine J*, 17(1):2–19, Jan 2008. doi: 10.1007/s00586-007-0414-y.
- [7] G Alker. Neuroradiology of cervical spondylotic myelopathy. *Spine (Phila Pa 1976)*, 13(7):850–3, Jul 1988.
- [8] Darryl C Baptiste and Michael G Fehlings. Pathophysiology of cervical myelopathy. *Spine J*, 6(6 Suppl):190S–197S, 2006. doi: 10.1016/j.spinee.2006.04.024.
- [9] Lorin M Benneker, Paul F Heini, Suzanne E Anderson, Mauro Alini, and Keita Ito. Correlation of radiographic and mri parameters to morphological and biochemical assessment of intervertebral disc degeneration. *Eur Spine J*, 14(1): 27–35, Feb 2005. doi: 10.1007/s00586-004-0759-4.

- [10] L E Bilston and L E Thibault. The mechanical properties of the human cervical spinal cord in vitro. *Ann Biomed Eng*, 24(1):67–74, 1996.
- [11] LE Bilston and LE Thibault. Biomechanics of cervical spinal cord injury in flexion and extension: a physical model to estimate spinal cord deformations. *International Journal of Crashworthiness*, 2(2):207–218, 1997.
- [12] N Bogduk and S Mercer. Biomechanics of the cervical spine. i: Normal kinematics. *Clin Biomech (Bristol, Avon)*, 15(9):633–48, Nov 2000.
- [13] N. Bogduk and N. Yoganandan. Biomechanics of the cervical spine part 3: minor injuries. *Clinical Biomechanics*, 16(4):267–275, 2001. ISSN 0268-0033.
- [14] H H Bohlman and S E Emery. The pathophysiology of cervical spondylosis and myelopathy. *Spine (Phila Pa 1976)*, 13(7):843–6, Jul 1988.
- [15] A. Breig, I. Turnbull, and O. Hassler. Effects of mechanical stresses on the spinal cord in cervical spondylosis. a study on fresh cadaver material. *Journal of neurosurgery*, 25(1):45, 1966. ISSN 0022-3085.
- [16] K. Brodin. Neck injuries among the elderly in sweden. *Injury Control and Safety Promotion*, 10(3):155–164, 2003. ISSN 1566-0974.
- [17] D.C. Burke. Hyperextension injuries of the spine. *Journal of Bone and Joint Surgery-British Volume*, 53(1):3, 1971.
- [18] I. Busscher, A.J. van der Veen, J.H. van Die
”en, I. Kingma, G.J. Verkerke, and A.G. Veldhuizen. In vitro biomechanical characteristics of the spine: a comparison between human and porcine spinal segments. *Spine*, 35(2):E35, 2010. ISSN 0362-2436.
- [19] Iris Busscher, Joris J W Ploegmakers, Gijsbertus J Verkerke, and Albert G Veldhuizen. Comparative anatomical dimensions of the complete human and porcine spine. *Eur Spine J*, 19(7):1104–14, Jul 2010. doi: 10.1007/s00586-010-1326-9.
- [20] J P Callaghan and S M McGill. Frozen storage increases the ultimate compressive load of porcine vertebrae. *J Orthop Res*, 13(5):809–812, 1995. ISSN 0736-0266 (Print). doi: 10.1002/jor.1100130522.
- [21] G.L. Chang, T.K. Hung, A. Bleyaert, and P.J. Jannetta. Stress-strain measurement of the spinal cord of puppies and their neurological evaluation. *The Journal of Trauma*, 21(9):807, 1981.

- [22] G.L. Chang, T.K. Hung, and W.W. Feng. An in-vivo measurement and analysis of viscoelastic properties of the spinal cord of cats. *Journal of biomechanical engineering*, 110:115, 1988.
- [23] C.J. Chen, H.L. Hsu, C.C. Niu, T.Y. Chen, M.C. Chen, Y.C. Tseng, Y.C. Wong, and L.J. Wang. Cervical degenerative disease at flexion-extension mr imaging: Prediction criteria. *Radiology*, 227(1):136, 2003. ISSN 0033-8419.
- [24] H Y Chen, S S Chen, W T Chiu, L S Lee, C I Hung, C L Hung, Y C Wang, C C Hung, L S Lin, Y H Shih, and C Y Kuo. A nationwide epidemiological study of spinal cord injury in geriatric patients in taiwan. *Neuroepidemiology*, 16(5):241–7, 1997.
- [25] I H Chen, A Vasavada, and M M Panjabi. Kinematics of the cervical spine canal: changes with sagittal plane loads. *J Spinal Disord*, 7(2):93–101, Apr 1994.
- [26] Anthony M Choo, Jie Liu, Clarrie K Lam, Marcel Dvorak, Wolfram Tetzlaff, and Thomas R Oxland. Contusion, dislocation, and distraction: primary hemorrhage and membrane permeability in distinct mechanisms of spinal cord injury. *J Neurosurg Spine*, 6(3):255–66, Mar 2007. doi: 10.3171/spi.2007.6.3.255.
- [27] Anthony M Choo, Jie Liu, Marcel Dvorak, Wolfram Tetzlaff, and Thomas R Oxland. Secondary pathology following contusion, dislocation, and distraction spinal cord injuries. *Exp Neurol*, 212(2):490–506, Aug 2008. doi: 10.1016/j.expneurol.2008.04.038.
- [28] C R Clark. Cervical spondylotic myelopathy: history and physical findings. *Spine (Phila Pa 1976)*, 13(7):847–9, Jul 1988.
- [29] M D Connell and S W Wiesel. Natural history and pathogenesis of cervical disk disease. *Orthop Clin North Am*, 23(3):369–80, Jul 1992.
- [30] R A Cripps, B B Lee, P Wing, E Weerts, J Mackay, and D Brown. A global map for traumatic spinal cord injury epidemiology: towards a living data repository for injury prevention. *Spinal Cord*, Nov 2010. doi: 10.1038/sc.2010.146.
- [31] J F Cusick, N Yoganandan, F Pintar, and M Gardon. Cervical spine injuries from high-velocity forces: a pathoanatomic and radiologic study. *J Spinal Disord*, 9(1):1–7, Feb 1996.
- [32] Joseph F Cusick and Narayan Yoganandan. Biomechanics of the cervical spine 4: major injuries. *Clin Biomech (Bristol, Avon)*, 17(1):1–20, Jan 2002.

- [33] L Y Dai. Acute central cervical cord injury: the effect of age upon prognosis. *Injury*, 32(3):195–9, Apr 2001.
- [34] M J DeVivo, P L Kartus, R D Rutt, S L Stover, and P R Fine. The influence of age at time of spinal cord injury on rehabilitation outcome. *Arch Neurol*, 47(6):687–91, Jun 1990.
- [35] Richard L. Drake, Wayne Vogl, Adam W. M Mitchell, and Henry Gray. *Gray's anatomy for students*. Elsevier/Churchill Livingstone, Philadelphia, 2005. ISBN 0443066124.
- [36] Donna M Dryden, L Duncan Saunders, Brian H Rowe, Laura A May, Niko Yianakoulias, Lawrence W Svenson, Donald P Schopflocher, and Donald C Voaklander. The epidemiology of traumatic spinal cord injury in alberta, canada. *Can J Neurol Sci*, 30(2):113–21, May 2003.
- [37] J Dvorak, D Froehlich, L Penning, H Baumgartner, and M M Panjabi. Functional radiographic diagnosis of the cervical spine: flexion/extension. *Spine (Phila Pa 1976)*, 13(7):748–55, Jul 1988.
- [38] J Dvorak, M M Panjabi, J E Novotny, and J A Antinnes. In vivo flexion/extension of the normal cervical spine. *J Orthop Res*, 9(6):828–34, Nov 1991. doi: 10.1002/jor.1100090608.
- [39] S Ehara and T Shimamura. Cervical spine injury in the elderly: imaging features. *Skeletal Radiol*, 30(1):1–7, Jan 2001.
- [40] Thomas Einsiedel, Andreas Schmelz, Markus Arand, Hans-Joachim Wilke, Florian Gebhard, Erich Hartwig, Michael Kramer, Rainer Neugebauer, Lothar Kinzl, and Markus Schultheiss. Injuries of the cervical spine in patients with ankylosing spondylitis: experience at two trauma centers. *J Neurosurg Spine*, 5(1):33–45, Jul 2006. doi: 10.3171/spi.2006.5.1.33.
- [41] J A Epstein. The surgical management of cervical spinal stenosis, spondylosis, and myeloradiculopathy by means of the posterior approach. *Spine (Phila Pa 1976)*, 13(7):864–9, Jul 1988.
- [42] J A Epstein, R Carras, R A Hyman, and S Costa. Cervical myelopathy caused by developmental stenosis of the spinal canal. *J Neurosurg*, 51(3):362–7, Sep 1979. doi: 10.3171/jns.1979.51.3.0362.
- [43] M.G. Fehlings, S.C. Rao, C.H. Tator, G. Skaf, P. Arnold, E. Benzel, C. Dickman, B. Cuddy, B. Green, P. Hitchon, et al. The optimal radiologic method

- for assessing spinal canal compromise and cord compression in patients with cervical spinal cord injury: Part ii: results of a multicenter study. *Spine*, 24(6): 605, 1999. ISSN 0362-2436.
- [44] Stephen J Ferguson and Thomas Steffen. Biomechanics of the aging spine. *Eur Spine J*, 12 Suppl 2:S97–S103, Oct 2003. doi: 10.1007/s00586-003-0621-0.
- [45] Stephen J Ferguson, Keita Ito, and Lutz P Nolte. Fluid flow and convective transport of solutes within the intervertebral disc. *J Biomech*, 37(2):213–21, Feb 2004.
- [46] Virgilio F Ferrario, Chiarella Sforza, Graziano Serrao, GianPiero Grassi, and Erio Mossi. Active range of motion of the head and cervical spine: a three-dimensional investigation in healthy young adults. *J Orthop Res*, 20(1):122–9, Jan 2002. doi: 10.1016/S0736-0266(01)00079-1.
- [47] W. Frobin, P. Brinckmann, M. Biggemann, M. Tillotson, and K. Burton. Precision measurement of disc height, vertebral height and sagittal plane displacement from lateral radiographic views of the lumbar spine. *Clin Biomech (Bristol, Avon)*, 12 Suppl 1:S1–S63, 1997.
- [48] W Frobin, P Brinckmann, M Kramer, and E Hartwig. Height of lumbar discs measured from radiographs compared with degeneration and height classified from mr images. *Eur Radiol*, 11(2):263–9, 2001.
- [49] W Frobin, G Leivseth, M Biggemann, and P Brinckmann. Sagittal plane segmental motion of the cervical spine. a new precision measurement protocol and normal motion data of healthy adults. *Clin Biomech (Bristol, Avon)*, 17(1): 21–31, Jan 2002.
- [50] W Frobin, G Leivseth, M Biggemann, and P Brinckmann. Vertebral height, disc height, posteroanterior displacement and dens-atlas gap in the cervical spine: precision measurement protocol and normal data. *Clin Biomech (Bristol, Avon)*, 17(6):423–31, Jul 2002.
- [51] K Fujiwara, K Yonenobu, K Hiroshima, S Ebara, K Yamashita, and K Ono. Morphometry of the cervical spinal cord and its relation to pathology in cases with compression myelopathy. *Spine (Phila Pa 1976)*, 13(11):1212–6, Nov 1988.
- [52] K Fukui, O Kataoka, T Sho, and M Sumi. Pathomechanism, pathogenesis, and results of treatment in cervical spondylotic myelopathy caused by dynamic canal stenosis. *Spine (Phila Pa 1976)*, 15(11):1148–52, Nov 1990.

- [53] Julio C Furlan and Michael G Fehlings. The impact of age on mortality, impairment, and disability among adults with acute traumatic spinal cord injury. *J Neurotrauma*, 26(10):1707–17, Oct 2009. doi: 10.1089/neu.2009-0888.
- [54] Julio C Furlan, Deepa Kattail, and Michael G Fehlings. The impact of comorbidities on age-related differences in mortality after acute traumatic spinal cord injury. *J Neurotrauma*, 26(8):1361–7, Aug 2009. doi: 10.1089/neu.2008-0764.
- [55] Julio C Furlan, Michael B Bracken, and Michael G Fehlings. Is age a key determinant of mortality and neurological outcome after acute traumatic spinal cord injury? *Neurobiol Aging*, 31(3):434–46, Mar 2010. doi: 10.1016/j.neurobiolaging.2008.05.003.
- [56] F K Fuss. Sagittal kinematics of the cervical spine—how constant are the motor axes? *Acta Anat (Basel)*, 141(1):93–6, 1991.
- [57] Beth Galle, Hui Ouyang, Riyi Shi, and Eric Nauman. Correlations between tissue-level stresses and strains and cellular damage within the guinea pig spinal cord white matter. *J Biomech*, 40(13):3029–33, 2007. doi: 10.1016/j.jbiomech.2007.03.014.
- [58] P. Gédet, P.A. Thistlethwaite, and S.J. Ferguson. Minimizing errors during in vitro testing of multisegmental spine specimens: Considerations for component selection and kinematic measurement. *Journal of biomechanics*, 40(8):1881–1885, 2007.
- [59] Saif A Ghole, Paul C Ivancic, Yasuhiro Tominaga, S Elena Gimenez, and Manohar M Panjabi. Incremental and single trauma produce equivalent sub-failure soft tissue injury of the cervical spine. *Clin Biomech (Bristol, Avon)*, 19(8):784–9, Oct 2004. doi: 10.1016/j.clinbiomech.2004.06.001.
- [60] S.A. Glantz. *Primer of biostatistics*. McGraw-Hill Medical, 2005.
- [61] Darrell J Goertzen, Chris Lane, and Thomas R Oxland. Neutral zone and range of motion in the spine are greater with stepwise loading than with a continuous loading protocol. an in vitro porcine investigation. *J Biomech*, 37(2):257–61, Feb 2004.
- [62] M R Gooding, C B Wilson, and J T Hoff. Experimental cervical myelopathy. effects of ischemia and compression of the canine cervical spinal cord. *J Neurosurg*, 43(1):9–17, Jul 1975. doi: 10.3171/jns.1975.43.1.0009.

- [63] D R Gore, S B Sepic, and G M Gardner. Roentgenographic findings of the cervical spine in asymptomatic people. *Spine (Phila Pa 1976)*, 11(6):521–4, 1986.
- [64] Carolyn Y Greaves, Mohamed S Gadala, and Thomas R Oxland. A three-dimensional finite element model of the cervical spine with spinal cord: an investigation of three injury mechanisms. *Ann Biomed Eng*, 36(3):396–405, Mar 2008. doi: 10.1007/s10439-008-9440-0.
- [65] M.R. Grubb, B.L. Currier, J.S. Shih, V. Bonin, J.J. Grabowski, and E. Chao. Biomechanical evaluation of anterior cervical spine stabilization. *Spine*, 23(8): 886, 1998.
- [66] Thijs Grunhagen, Aboufazel Shirazi-Adl, Jeremy C T Fairbank, and Jill P G Urban. Intervertebral disk nutrition: a review of factors influencing concentrations of nutrients and metabolites. *Orthop Clin North Am*, 42(4):465–77, vii, Oct 2011. doi: 10.1016/j.ocl.2011.07.010.
- [67] Rui Gu, Qingsan Zhu, Ye Lin, Xiaoyu Yang, Zhongli Gao, and Yasuhisa Tanaka. Dynamic canal encroachment of ligamentum flavum: an in vitro study of cadaveric specimens. *J Spinal Disord Tech*, 19(3):187–90, May 2006. doi: 10.1097/01.bsd.0000190816.28682.83.
- [68] SK Gupta, K. Rajeev, VK Khosla, and BS Sharma. Spinal cord injury without radiographic abnormality in adults. *Spinal cord: the official journal of the International Medical Society of Paraplegia*, 37(10):726, 1999. ISSN 1362-4393.
- [69] E M Hagen, J A Aarli, and M Gronning. The clinical significance of spinal cord injuries in patients older than 60 years of age. *Acta Neurol Scand*, 112(1):42–7, Jul 2005. doi: 10.1111/j.1600-0404.2005.00430.x.
- [70] D E Harrison, D D Harrison, and S J Troyanovich. Reliability of spinal displacement analysis of plain x-rays: a review of commonly accepted facts and fallacies with implications for chiropractic education and technique. *J Manipulative Physiol Ther*, 21(4):252–66, May 1998.
- [71] D.E. Harrison, R. Cailliet, D.D. Harrison, S.J. Troyanovich, and S.O. Harrison. A review of biomechanics of the central nervous system—part i: spinal canal deformations resulting from changes in posture. *Journal of manipulative and physiological therapeutics*, 22(4):227–234, 1999. ISSN 0161-4754.
- [72] D.E. Harrison, R. Cailliet, D.D. Harrison, S.J. Troyanovich, and S.O. Harrison. A review of biomechanics of the central nervous system—part ii: Spinal cord

- strains from postural loads. *Journal of manipulative and physiological therapeutics*, 22(5):322–332, 1999. ISSN 0161-4754.
- [73] D.E. Harrison, R. Cailliet, D.D. Harrison, S.J. Troyanovich, and S.O. Harrison. A review of biomechanics of the central nervous system—part iii: Spinal cord stresses from postural loads and their neurologic effects. *Journal of manipulative and physiological therapeutics*, 22(6):399–410, 1999. ISSN 0161-4754.
- [74] H Hayashi, K Okada, J Hashimoto, K Tada, and R Ueno. Cervical spondylotic myelopathy in the aged patient. a radiographic evaluation of the aging changes in the cervical spine and etiologic factors of myelopathy. *Spine (Phila Pa 1976)*, 13(6):618–25, Jun 1988.
- [75] K Hayashi, K Yone, H Ito, M Yanase, and T Sakou. Mri findings in patients with a cervical spinal cord injury who do not show radiographic evidence of a fracture or dislocation. *Paraplegia*, 33(4):212–5, Apr 1995. doi: 10.1038/sc.1995.47.
- [76] J F Healy, B B Healy, W H Wong, and E M Olson. Cervical and lumbar mri in asymptomatic older male lifelong athletes: frequency of degenerative findings. *J Comput Assist Tomogr*, 20(1):107–12, 1996.
- [77] J G Heller. The syndromes of degenerative cervical disease. *Orthop Clin North Am*, 23(3):381–94, Jul 1992.
- [78] Fraser C Henderson, Jennian F Geddes, Alexander R Vaccaro, Eric Woodard, K Joel Berry, and Edward C Benzel. Stretch-associated injury in cervical spondylotic myelopathy: new concept and review. *Neurosurgery*, 56(5):1101–13; discussion 1101–13, May 2005.
- [79] Gregory W Hendey, Allan B Wolfson, William R Mower, Jerome R Hoffman, and National Emergency X-Radiography Utilization Study Group. Spinal cord injury without radiographic abnormality: results of the national emergency x-radiography utilization study in blunt cervical trauma. *J Trauma*, 53(1):1–4, Jul 2002.
- [80] H. Hino, K. Abumi, M. Kanayama, and K. Kaneda. Dynamic motion analysis of normal and unstable cervical spines using cineradiography: an in vivo study. *Spine*, 24(2):163, 1999. ISSN 0362-2436.
- [81] A Holmes, Z H Han, G T Dang, Z Q Chen, Z G Wang, and J Fang. Changes in cervical canal spinal volume during in vitro flexion-extension. *Spine (Phila Pa 1976)*, 21(11):1313–9, Jun 1996.

- [82] Michio Hongo, Ralph E Gay, Jui-Ting Hsu, Kristin D Zhao, Brice Ilharreborde, Lawrence J Berglund, and Kai-Nan An. Effect of multiple freeze-thaw cycles on intervertebral dynamic motion characteristics in the porcine lumbar spine. *J Biomech*, 41(4):916–20, 2008. doi: 10.1016/j.jbiomech.2007.11.003.
- [83] T K Hung and G L Chang. Biomechanical and neurological response of the spinal cord of a puppy to uniaxial tension. *J Biomech Eng*, 103(1):43–7, Feb 1981.
- [84] T K Hung, G L Chang, H S Lin, F R Walter, and L Bunegin. Stress-strain relationship of the spinal cord of anesthetized cats. *J Biomech*, 14(4):269–76, 1981.
- [85] Kazuhiko Ichihara, Toshihiko Taguchi, Itsuo Sakuramoto, Shunichi Kawano, and Shinya Kawai. Mechanism of the spinal cord injury and the cervical spondylotic myelopathy: new approach based on the mechanical features of the spinal cord white and gray matter. *J Neurosurg*, 99(3 Suppl):278–85, Oct 2003.
- [86] Z.N. Irwin, M. Arthur, R.J. Mullins, and R.A. Hart. Variations in injury patterns, treatment, and outcome for spinal fracture and paralysis in adult versus geriatric patients. *Spine*, 29(7):796, 2004. ISSN 0362-2436.
- [87] Takahiro Ishii, Yoshihiro Mukai, Noboru Hosono, Hironobu Sakaura, Yoshikazu Nakajima, Yoshinobu Sato, Kazuomi Sugamoto, and Hideki Yoshikawa. Kinematics of the upper cervical spine in rotation: in vivo three-dimensional analysis. *Spine (Phila Pa 1976)*, 29(7):E139–44, Apr 2004.
- [88] Shigeki Ito, Manohar M Panjabi, Paul C Ivancic, and Adam M Pearson. Spinal canal narrowing during simulated whiplash. *Spine (Phila Pa 1976)*, 29(12):1330–9, Jun 2004.
- [89] Paul C Ivancic, Manohar M Panjabi, Yasuhiro Tominaga, Adam M Pearson, S Elena Gimenez, and Travis G Maak. Spinal canal narrowing during simulated frontal impact. *Eur Spine J*, 15(6):891–901, Jun 2006. doi: 10.1007/s00586-005-0985-4.
- [90] Y Iwasaki, H Abe, T Isu, and K Miyasaka. Ct myelography with intramedullary enhancement in cervical spondylosis. *J Neurosurg*, 63(3):363–6, Sep 1985. doi: 10.3171/jns.1985.63.3.0363.
- [91] Y Iwasaki, K Tashiro, S Kikuchi, M Kitagawa, T Isu, and H Abe. Cervical flexion myelopathy: a "tight dural canal mechanism". case report. *J Neurosurg*, 66(6):935–7, Jun 1987. doi: 10.3171/jns.1987.66.6.0935.

- [92] Pascal Jabbour, Michael Fehlings, Alexander R Vaccaro, and James S Harrop. Traumatic spine injuries in the geriatric population. *Neurosurg Focus*, 25(5):E16, 2008. doi: 10.3171/FOC.2008.25.11.E16.
- [93] Sheng-Dan Jiang, Lei-Sheng Jiang, and Li-Yang Dai. Degenerative cervical spondylolisthesis: a systematic review. *Int Orthop*, 35(6):869–75, Jun 2011. doi: 10.1007/s00264-010-1203-5.
- [94] R M Johnson, E S Crelin, A A White, 3rd, M M Panjabi, and W O Southwick. Some new observations on the functional anatomy of the lower cervical spine. *Clin Orthop Relat Res*, (111):192–200, Sep 1975.
- [95] Claire F Jones, Shannon G Kroeker, Peter A Cripton, and Richard M Hall. The effect of cerebrospinal fluid on the biomechanics of spinal cord: an ex vivo bovine model using bovine and physical surrogate spinal cord. *Spine (Phila Pa 1976)*, 33(17):E580–8, Aug 2008. doi: 10.1097/BRS.0b013e31817ecc57.
- [96] T Kameyama, Y Hashizume, T Ando, and A Takahashi. Morphometry of the normal cadaveric cervical spinal cord. *Spine (Phila Pa 1976)*, 19(18):2077–81, Sep 1994.
- [97] T Kameyama, Y Hashizume, and G Sobue. Morphologic features of the normal human cadaveric spinal cord. *Spine (Phila Pa 1976)*, 21(11):1285–90, Jun 1996.
- [98] F Kandziora, R Pflugmacher, M Scholz, K Schnake, M Lucke, R Schröder, and T Mittlmeier. Comparison between sheep and human cervical spines: an anatomic, radiographic, bone mineral density, and biomechanical study. *Spine (Phila Pa 1976)*, 26(9):1028–37, May 2001.
- [99] J D Kang, M P Figgie, and H H Bohlman. Sagittal measurements of the cervical spine in subaxial fractures and dislocations. an analysis of two hundred and eighty-eight patients with and without neurological deficits. *J Bone Joint Surg Am*, 76(11):1617–28, Nov 1994.
- [100] P. Kannus, S. Niemi, M. Palvanen, and J. Parkkari. Continuously increasing number and incidence of fall-induced, fracture-associated, spinal cord injuries in elderly persons. *Archives of internal medicine*, 160(14):2145, 2000.
- [101] Pekka Kannus, Mika Palvanen, Seppo Niemi, and Jari Parkkari. Alarming rise in the number and incidence of fall-induced cervical spine injuries among older adults. *J Gerontol A Biol Sci Med Sci*, 62(2):180–3, Feb 2007.

- [102] L Kaplan and F Kennedy. The effect of head posture on the manometrics of the cerebrospinal fluid in cervical lesions: a new diagnostic test. *Brain*, 73(3): 337–45, 1950.
- [103] Hiroshi Kato, Akio Kimura, Ryo Sasaki, Naoyuki Kaneko, Munekazu Takeda, Akiyoshi Hagiwara, Shinji Ogura, Takashi Mizoguchi, Tetsuya Matsuoka, Hidehumi Ono, Kenji Matsuura, Kazuhide Matsushima, Shigeki Kushimoto, Akira Fuse, Toshio Nakatani, Masaaki Iwase, Junmei Fudoji, and Takeshi Kasai. Cervical spinal cord injury without bony injury: a multicenter retrospective study of emergency and critical care centers in japan. *J Trauma*, 65(2):373–9, Aug 2008. doi: 10.1097/TA.0b013e31817db11d.
- [104] Y. Kato, Y. Imajo, T. Kanchiku, T. Kojima, H. Kataoka, and T. Taguchi. Dynamic electrophysiological examination of cervical flexion myelopathy. *Journal of Neurosurgery: Pediatrics*, 9(2), 2008.
- [105] Yoshihiko Kato, Hideo Kataoka, Kazuhiko Ichihara, Yasuaki Imajo, Takanori Kojima, Shunichi Kawano, Daisuke Hamanaka, Kentaro Yaji, and Toshihiko Taguchi. Biomechanical study of cervical flexion myelopathy using a three-dimensional finite element method. *J Neurosurg Spine*, 8(5):436–41, May 2008. doi: 10.3171/SPI/2008/8/5/436.
- [106] P A Kearney, S A Ridella, D C Viano, and T E Anderson. Interaction of contact velocity and cord compression in determining the severity of spinal cord injury. *J Neurotrauma*, 5(3):187–208, 1988.
- [107] A Kettler, L Liakos, B Haegele, and H-J Wilke. Are the spines of calf, pig and sheep suitable models for pre-clinical implant tests? *Eur Spine J*, 16(12): 2186–92, Dec 2007. doi: 10.1007/s00586-007-0485-9.
- [108] A I King. Fundamentals of impact biomechanics: Part i—biomechanics of the head, neck, and thorax. *Annu Rev Biomed Eng*, 2:55–81, 2000. doi: 10.1146/annurev.bioeng.2.1.55.
- [109] H-Y Ko, J H Park, Y B Shin, and S Y Baek. Gross quantitative measurements of spinal cord segments in human. *Spinal Cord*, 42(1):35–40, Jan 2004. doi: 10.1038/sj.sc.3101538.
- [110] Frode Kolstad, Gunnar Myhr, Kjell Arne Kvistad, Oystein P Nygaard, and Gunnar Leivseth. Degeneration and height of cervical discs classified from mri compared with precise height measurements from radiographs. *Eur J Radiol*, 55(3):415–20, Sep 2005. doi: 10.1016/j.ejrad.2005.02.005.

- [111] P Kothari, B Freeman, M Grevitt, and R Kerslake. Injury to the spinal cord without radiological abnormality (sciwo) in adults. *J Bone Joint Surg Br*, 82(7):1034–7, Sep 2000.
- [112] I Koyanagi, Y Iwasaki, K Hida, M Akino, H Imamura, and H Abe. Acute cervical cord injury without fracture or dislocation of the spinal column. *J Neurosurg*, 93(1 Suppl):15–20, Jul 2000.
- [113] Izumi Koyanagi, Yoshinobu Iwasaki, Kazutoshi Hida, Hiroyuki Imamura, Shin Fujimoto, and Minoru Akino. Acute cervical cord injury associated with ossification of the posterior longitudinal ligament. *Neurosurgery*, 53(4):887–91; discussion 891–2, Oct 2003.
- [114] Shannon G Kroeker, Philip L Morley, Claire F Jones, Lynne E Bilston, and Peter A Cripton. The development of an improved physical surrogate model of the human spinal cord–tension and transverse compression. *J Biomech*, 42(7):878–83, May 2009. doi: 10.1016/j.jbiomech.2009.01.036.
- [115] K A Kuhlman. Cervical range of motion in the elderly. *Arch Phys Med Rehabil*, 74(10):1071–9, Oct 1993.
- [116] Charles A Lantz, Geoffrey Klein, Jasper Chen, Anne Mannion, Alan B Solinger, and Jiri Dvorak. A reassessment of normal cervical range of motion. *Spine (Phila Pa 1976)*, 28(12):1249–57, Jun 2003. doi: 10.1097/01.BRS.0000065573.94975.27.
- [117] Michael J Lee, Ezequiel H Cassinelli, and K Daniel Riew. Prevalence of cervical spine stenosis. anatomic study in cadavers. *J Bone Joint Surg Am*, 89(2):376–80, Feb 2007. doi: 10.2106/JBJS.F.00437.
- [118] G Leivseth, P Brinckmann, W Frobin, R Johnsson, and B Strömqvist. Assessment of sagittal plane segmental motion in the lumbar spine. a comparison between distortion-compensated and stereophotogrammetric roentgen analysis. *Spine (Phila Pa 1976)*, 23(23):2648–55, Dec 1998.
- [119] Gunnar Leivseth, Frode Kolstad, Oystein P Nygaard, Björn Zoega, W Frobin, and P Brinckmann. Comparing precision of distortion-compensated and stereophotogrammetric roentgen analysis when monitoring fusion in the cervical spine. *Eur Spine J*, 15(6):774–9, Jun 2006. doi: 10.1007/s00586-005-0929-z.
- [120] Brian Lenahan, John Street, Brian K Kwon, Vanessa Noonan, Hongbin Zhang, Charles G Fisher, and Marcel F Dvorak. The epidemiology of traumatic spinal cord injury in british columbia, canada. *Spine (Phila Pa 1976)*, 37(4):321–9, Feb 2012. doi: 10.1097/BRS.0b013e31822e5ff8.

- [121] W F Lestini and S W Wiesel. The pathogenesis of cervical spondylosis. *Clin Orthop Relat Res*, (239):69–93, Feb 1989.
- [122] D N Levine. Pathogenesis of cervical spondylotic myelopathy. *J Neurol Neurosurg Psychiatry*, 62(4):334–40, Apr 1997.
- [123] I H Lieberman and J K Webb. Cervical spine injuries in the elderly. *J Bone Joint Surg Br*, 76(6):877–81, Nov 1994.
- [124] R M Lin, K H Tsai, L P Chu, and P Q Chang. Characteristics of sagittal vertebral alignment in flexion determined by dynamic radiographs of the cervical spine. *Spine (Phila Pa 1976)*, 26(3):256–61, Feb 2001.
- [125] F M Lomoschitz, C C Blackmore, S K Mirza, and F A Mann. Cervical spine injuries in patients 65 years old and older: epidemiologic analysis regarding the effects of age and injury mechanism on distribution, type, and stability of injuries. *AJR Am J Roentgenol*, 178(3):573–7, Mar 2002.
- [126] Masaaki Machino, Yasutsugu Yukawa, Keigo Ito, Hiroaki Nakashima, and Fumihiko Kato. Dynamic changes in dural sac and spinal cord cross-sectional area in patients with cervical spondylotic myelopathy: cervical spine. *Spine (Phila Pa 1976)*, 36(5):399–403, Mar 2011. doi: 10.1097/BRS.0b013e3181d2510b.
- [127] Eva-Maj Malmström, Mikael Karlberg, Per Anders Fransson, Agneta Melander, and Måns Magnusson. Primary and coupled cervical movements: the effect of age, gender, and body mass index. a 3-dimensional movement analysis of a population without symptoms of neck disorders. *Spine (Phila Pa 1976)*, 31(2):E44–50, Jan 2006.
- [128] P McClure, S Siegler, and R Nobilini. Three-dimensional flexibility characteristics of the human cervical spine in vivo. *Spine (Phila Pa 1976)*, 23(2):216–23, Jan 1998.
- [129] John W McDonald and Cristina Sadowsky. Spinal-cord injury. *Lancet*, 359(9304):417–25, Feb 2002. doi: 10.1016/S0140-6736(02)07603-1.
- [130] S Mercer and N Bogduk. The ligaments and annulus fibrosus of human adult cervical intervertebral discs. *Spine (Phila Pa 1976)*, 24(7):619–26; discussion 627–8, Apr 1999.
- [131] H Mihara, K Ohnari, M Hachiya, S Kondo, and K Yamada. Cervical myelopathy caused by c3-c4 spondylosis in elderly patients: a radiographic analysis of pathogenesis. *Spine (Phila Pa 1976)*, 25(7):796–800, Apr 2000.

- [132] M Mimura, M M Panjabi, T R Oxland, J J Crisco, I Yamamoto, and A Vasavada. Disc degeneration affects the multidirectional flexibility of the lumbar spine. *Spine (Phila Pa 1976)*, 19(12):1371–80, Jun 1994.
- [133] Takehiko Miura, Manohar M Panjabi, and Peter A Cripton. A method to simulate in vivo cervical spine kinematics using in vitro compressive preload. *Spine (Phila Pa 1976)*, 27(1):43–8, Jan 2002.
- [134] Masashi Miyazaki, Soon Woo Hong, Seung Hwan Yoon, Jun Zou, Benjamin Tow, Ahmet Alanay, Jean-Jacques Abitbol, and Jeffrey C Wang. Kinematic analysis of the relationship between the grade of disc degeneration and motion unit of the cervical spine. *Spine (Phila Pa 1976)*, 33(2):187–93, Jan 2008. doi: 10.1097/BRS.0b013e3181604501.
- [135] Yuichiro Morishita, Shinichi Hida, Masashi Miyazaki, Soon-Woo Hong, Jun Zou, Feng Wei, Masatoshi Naito, and Jeffrey C Wang. The effects of the degenerative changes in the functional spinal unit on the kinematics of the cervical spine. *Spine (Phila Pa 1976)*, 33(6):E178–82, Mar 2008. doi: 10.1097/BRS.0b013e318166f059.
- [136] Yuichiro Morishita, Masatoshi Naito, Henry Hymanson, Masashi Miyazaki, Guizhong Wu, and Jeffrey C Wang. The relationship between the cervical spinal canal diameter and the pathological changes in the cervical spine. *Eur Spine J*, 18(6):877–83, Jun 2009. doi: 10.1007/s00586-009-0968-y.
- [137] S P Moroney, A B Schultz, J A Miller, and G B Andersson. Load-displacement properties of lower cervical spine motion segments. *J Biomech*, 21(9):769–79, 1988.
- [138] W R Mower, J R Hoffman, C V Pollack, Jr, M I Zucker, B J Browne, A B Wolfson, and NEXUS Group. Use of plain radiography to screen for cervical spine injuries. *Ann Emerg Med*, 38(1):1–7, Jul 2001. doi: 10.1067/mem.2001.115946.
- [139] C Muhle, J Metzner, D Weinert, A Falliner, G Brinkmann, M H Mehdorn, M Heller, and D Resnick. Classification system based on kinematic mr imaging in cervical spondylitic myelopathy. *AJNR Am J Neuroradiol*, 19(9):1763–71, Oct 1998.
- [140] C Muhle, D Weinert, A Falliner, J Wiskirchen, J Metzner, M Baumer, G Brinkmann, and M Heller. Dynamic changes of the spinal canal in patients with cervical spondylosis at flexion and extension using magnetic resonance imaging. *Invest Radiol*, 33(8):444–9, Aug 1998.

- [141] C Muhle, J Wiskirchen, D Weinert, A Falliner, F Wesner, G Brinkmann, and M Heller. Biomechanical aspects of the subarachnoid space and cervical cord in healthy individuals examined with kinematic magnetic resonance imaging. *Spine (Phila Pa 1976)*, 23(5):556–67, Mar 1998.
- [142] K Nagata, K Kiyonaga, T Ohashi, M Sagara, S Miyazaki, and A Inoue. Clinical value of magnetic resonance imaging for cervical myelopathy. *Spine (Phila Pa 1976)*, 15(11):1088–96, Nov 1990.
- [143] R J Nasca, J M Hollis, J E Lemons, and T A Cool. Cyclic axial loading of spinal implants. *Spine (Phila Pa 1976)*, 10(9):792–8, Nov 1985.
- [144] Roger W Nightingale, V Carol Chancey, Danielle Ottaviano, Jason F Luck, Laura Tran, Michael Prange, and Barry S Myers. Flexion and extension structural properties and strengths for male cervical spine segments. *J Biomech*, 40(3):535–42, 2007. doi: 10.1016/j.jbiomech.2006.02.015.
- [145] Christina A Niosi and Thomas R Oxland. Degenerative mechanics of the lumbar spine. *Spine J*, 4(6 Suppl):202S–208S, 2004. doi: 10.1016/j.spinee.2004.07.013.
- [146] David J Nuckley, Mark A Konodi, Geoffrey C Raynak, Randal P Ching, and Sohail K Mirza. Neural space integrity of the lower cervical spine: effect of normal range of motion. *Spine (Phila Pa 1976)*, 27(6):587–95, Mar 2002.
- [147] David J Nuckley, Mark A Konodi, Geoffrey C Raynak, Randal P Ching, Jens R Chapman, and Sohail K Mirza. Neural space integrity of the lower cervical spine: effect of anterior lesions. *Spine (Phila Pa 1976)*, 29(6):642–9, Mar 2004.
- [148] R J Oakland, R M Hall, R K Wilcox, and D C Barton. The biomechanical response of spinal cord tissue to uniaxial loading. *Proc Inst Mech Eng H*, 220(4):489–92, May 2006.
- [149] Eijiro Okada, Morio Matsumoto, Daisuke Ichihara, Kazuhiro Chiba, Yoshiaki Toyama, Hirokazu Fujiwara, Suketaka Momoshima, Yuji Nishiwaki, Takeshi Hashimoto, Jun Ogawa, Masahiko Watanabe, and Takeshi Takahata. Aging of the cervical spine in healthy volunteers: a 10-year longitudinal magnetic resonance imaging study. *Spine (Phila Pa 1976)*, 34(7):706–12, Apr 2009. doi: 10.1097/BRS.0b013e31819c2003.
- [150] N R Ordway, R Seymour, R G Donelson, L Hojnowski, E Lee, and W T Edwards. Cervical sagittal range-of-motion analysis using three methods. cervical range-of-motion device, 3space, and radiography. *Spine (Phila Pa 1976)*, 22(5):501–8, Mar 1997.

- [151] N R Ordway, R J Seymour, R G Donelson, L S Hojnowski, and W T Edwards. Cervical flexion, extension, protrusion, and retraction. a radiographic segmental analysis. *Spine (Phila Pa 1976)*, 24(3):240–7, Feb 1999.
- [152] Hui Ouyang, Beth Galle, Jianming Li, Eric Nauman, and Riyi Shi. Biomechanics of spinal cord injury: a multimodal investigation using ex vivo guinea pig spinal cord white matter. *J Neurotrauma*, 25(1):19–29, Jan 2008. doi: 10.1089/neu.2007.0340.
- [153] L M Overton and J W Grossman. Anatomical variations in the articulation between the second and third cervical vertebrae. *J Bone Joint Surg Am*, 34-A(1):155–61, Jan 1952.
- [154] T R Oxland, M M Panjabi, E P Southern, and J S Duranceau. An anatomic basis for spinal instability: a porcine trauma model. *J Orthop Res*, 9(3):452–62, May 1991. doi: 10.1002/jor.1100090318.
- [155] G P Pal and R V Routil. A study of weight transmission through the cervical and upper thoracic regions of the vertebral column in man. *J Anat*, 148:245–61, Oct 1986.
- [156] M Panjabi and A White, 3rd. Biomechanics of nonacute cervical spinal cord trauma. *Spine (Phila Pa 1976)*, 13(7):838–42, Jul 1988.
- [157] M M Panjabi, D J Summers, R R Pelker, T Videman, G E Friedlaender, and W O Southwick. Three-dimensional load-displacement curves due to forces on the cervical spine. *J Orthop Res*, 4(2):152–61, 1986. doi: 10.1002/jor.1100040203.
- [158] M M Panjabi, J Duranceau, V Goel, T Oxland, and K Takata. Cervical human vertebrae. quantitative three-dimensional anatomy of the middle and lower regions. *Spine (Phila Pa 1976)*, 16(8):861–9, Aug 1991.
- [159] M M Panjabi, J J Crisco, A Vasavada, T Oda, J Cholewicki, K Nibu, and E Shin. Mechanical properties of the human cervical spine as shown by three-dimensional load-displacement curves. *Spine (Phila Pa 1976)*, 26(24):2692–700, Dec 2001.
- [160] M M Panjabi, T Miura, P A Cripton, J L Wang, A S Nain, and C DuBois. Development of a system for in vitro neck muscle force replication in whole cervical spine experiments. *Spine (Phila Pa 1976)*, 26(20):2214–9, Oct 2001.

- [161] MM Panjabi, JS Duranceau, TR Oxland, and CE Bowen. Multidirectional instabilities of traumatic cervical spine injuries in a porcine model. *Spine*, 14 (10):1111, 1989.
- [162] W W Parke. Correlative anatomy of cervical spondylotic myelopathy. *Spine (Phila Pa 1976)*, 13(7):831–7, Jul 1988.
- [163] A G Patwardhan, R M Havey, A J Ghanayem, H Diener, K P Meade, B Dunlap, and S D Hodges. Load-carrying capacity of the human cervical spine in compression is increased under a follower load. *Spine (Phila Pa 1976)*, 25(12): 1548–54, Jun 2000.
- [164] L Penning. Nonpathologic and pathologic relationships between the lower cervical vertebrae. *Am J Roentgenol Radium Ther Nucl Med*, 91:1036–50, May 1964.
- [165] L Penning. Normal movements of the cervical spine. *AJR Am J Roentgenol*, 130(2):317–26, Feb 1978.
- [166] L. Penning. Differences in anatomy, motion, development and aging of the upper and lower cervical disk segments. *Clinical Biomechanics*, 3(1):37–47, 1988. ISSN 0268-0033.
- [167] J W Pepin, R B Bourne, and R J Hawkins. Odontoid fractures, with special reference to the elderly patient. *Clin Orthop Relat Res*, 193:178–83, Mar 1985.
- [168] D I Peterson and K Altman. Central cervical spinal cord syndrome due to minor hyperextension injury. *West J Med*, 150(6):691–4, Jun 1989.
- [169] Gwynedd E Pickett, Jeffrey P Rouleau, and Neil Duggal. Kinematic analysis of the cervical spine following implantation of an artificial cervical disc. *Spine (Phila Pa 1976)*, 30(17):1949–54, Sep 2005.
- [170] Gwynedd E Pickett, Mauricio Campos-Benitez, Jana L Keller, and Neil Duggal. Epidemiology of traumatic spinal cord injury in canada. *Spine (Phila Pa 1976)*, 31(7):799–805, Apr 2006. doi: 10.1097/01.brs.0000207258.80129.03.
- [171] F A Pintar, M B Schlick, N Yoganandan, and D J Maiman. Instrumented artificial spinal cord for human cervical pressure measurement. *Biomed Mater Eng*, 6(3):219–29, 1996.
- [172] Farhad Pirouzmand. Epidemiological trends of spine and spinal cord injuries in the largest canadian adult trauma center from 1986 to 2006. *J Neurosurg Spine*, 12(2):131–40, Feb 2010. doi: 10.3171/2009.9.SPINE0943.

- [173] J S Pooni, D W Hukins, P F Harris, R C Hilton, and K E Davies. Comparison of the structure of human intervertebral discs in the cervical, thoracic and lumbar regions of the spine. *Surg Radiol Anat*, 8(3):175–82, 1986.
- [174] Sirikonda Siva Prasad, Michael O’Malley, Mark Caplan, Ian M Shackelford, and Ravi K Pydisetty. Mri measurements of the cervical spine and their correlation to pavlov’s ratio. *Spine (Phila Pa 1976)*, 28(12):1263–8, Jun 2003. doi: 10.1097/01.BRS.0000065570.20888.AA.
- [175] S.C. Rao and M.G. Fehlings. The optimal radiologic method for assessing spinal canal compromise and cord compression in patients with cervical spinal cord injury: Part i: An evidence-based analysis of the published literature. *Spine*, 24(6):598, 1999. ISSN 0362-2436.
- [176] V S Regenbogen, L F Rogers, S W Atlas, and K S Kim. Cervical spinal cord injuries in patients with cervical spondylosis. *AJR Am J Roentgenol*, 146(2): 277–84, Feb 1986.
- [177] J D Reid. Effects of flexion-extension movements of the head and spine upon the spinal cord and nerve roots. *J Neurol Neurosurg Psychiatry*, 23:214–21, Aug 1960.
- [178] Charles A Reitman, John A Hipp, Lyndon Nguyen, and Stephen I Esses. Changes in segmental intervertebral motion adjacent to cervical arthrodesis: a prospective study. *Spine (Phila Pa 1976)*, 29(11):E221–6, Jun 2004.
- [179] Charles A Reitman, Kristin M Mauro, Lyndon Nguyen, James M Ziegler, and John A Hipp. Intervertebral motion between flexion and extension in asymptomatic individuals. *Spine (Phila Pa 1976)*, 29(24):2832–43, Dec 2004.
- [180] J.D. Richman, T.E. Daniel, D.D. Anderson, P.L. Miller, and R.A. Douglas. Biomechanical evaluation of cervical spine stabilization methods using a porcine model. *Spine*, 20(20):2192, 1995.
- [181] M Richter, H J Wilke, P Kluger, L Claes, and W Puhl. Load-displacement properties of the normal and injured lower cervical spine in vitro. *Eur Spine J*, 9(2):104–8, Apr 2000.
- [182] Antonius Rohlmann, Thomas Zander, Hendrik Schmidt, Hans-Joachim Wilke, and Georg Bergmann. Analysis of the influence of disc degeneration on the mechanical behaviour of a lumbar motion segment using the finite element method. *J Biomech*, 39(13):2484–90, 2006. doi: 10.1016/j.jbiomech.2005.07.026.

- [183] S Rossitti. Biomechanics of the pons-cord tract and its enveloping structures: an overview. *Acta Neurochir (Wien)*, 124(2-4):144–52, 1993.
- [184] Colin M Russell, Anthony M Choo, Wolfram Tetzlaff, Tae-Eun Chung, and Thomas R Oxland. Maximum principal strain correlates with spinal cord tissue damage in contusion and dislocation injuries in the rat cervical spine. *J Neurotrauma*, 29(8):1574–85, May 2012. doi: 10.1089/neu.2011.2225.
- [185] A Saari, E Itshayek, and P A Cripton. Cervical spinal cord deformation during simulated head-first impact injuries. *J Biomech*, 44(14):2565–71, Sep 2011. doi: 10.1016/j.jbiomech.2011.06.015.
- [186] Frank J Salvi, John C Jones, and Bonnie J Weigert. The assessment of cervical myelopathy. *Spine J*, 6(6 Suppl):182S–189S, 2006. doi: 10.1016/j.spinee.2006.05.006.
- [187] Y Saruhashi, S Hukuda, A Katsuura, S Asajima, and K Omura. Clinical outcomes of cervical spinal cord injuries without radiographic evidence of trauma. *Spinal Cord*, 36(8):567–73, Aug 1998.
- [188] A T Scher. Hyperextension trauma in the elderly: an easily overlooked spinal injury. *J Trauma*, 23(12):1066–8, Dec 1983.
- [189] René Schmidt, Marcus Richter, Lutz Claes, Wolfhart Puhl, and Hans-Joachim Wilke. Limitations of the cervical porcine spine in evaluating spinal implants in comparison with human cervical spinal segments: a biomechanical in vitro comparison of porcine and human cervical spine specimens with different instrumentation techniques. *Spine (Phila Pa 1976)*, 30(11):1275–82, Jun 2005.
- [190] L.H.S. Sekhon and M.G. Fehlings. Epidemiology, demographics, and pathophysiology of acute spinal cord injury. *Spine*, 26(24S):S2, 2001. ISSN 0362-2436.
- [191] Daniel Shedid and Edward C Benzel. Cervical spondylosis anatomy: pathophysiology and biomechanics. *Neurosurgery*, 60(1 Suppl 1):S7–13, Jan 2007. doi: 10.1227/01.NEU.0000215430.86569.C4.
- [192] Theo H Smit. The use of a quadruped as an in vivo model for the study of the spine - biomechanical considerations. *Eur Spine J*, 11(2):137–44, Apr 2002. doi: 10.1007/s005860100346.
- [193] S.R. Smith, T. Purzner, and M.G. Fehlings. The epidemiology of geriatric spinal cord injury. *Topics in Spinal Cord Injury Rehabilitation*, 15(3):54–64, 2010.

- [194] J M Spivak, M A Weiss, J M Cotler, and M Call. Cervical spine injuries in patients 65 and older. *Spine (Phila Pa 1976)*, 19(20):2302–6, Oct 1994.
- [195] Venkat Subramaniam, Robert H Chamberlain, Nicholas Theodore, Seungwon Baek, Sam Safavi-Abbasi, Mehmet Senoğlu, Volker K H Sonntag, and Neil R Crawford. Biomechanical effects of laminoplasty versus laminectomy: stenosis and stability. *Spine (Phila Pa 1976)*, 34(16):E573–8, Jul 2009. doi: 10.1097/BRS.0b013e3181aa0214.
- [196] N Tanaka, Y Fujimoto, H S An, Y Ikuta, and M Yasuda. The anatomic relation among the nerve roots, intervertebral foramina, and intervertebral discs of the cervical spine. *Spine (Phila Pa 1976)*, 25(3):286–91, Feb 2000.
- [197] A R Taylor. The mechanism of injury to the spinal cord in the neck without damage to vertebral column. *J Bone Joint Surg Br*, 33-B(4):543–7, Nov 1951.
- [198] A F Tencer, B L Allen, Jr, and R L Ferguson. A biomechanical study of thoracolumbar spinal fractures with bone in the canal. part i. the effect of laminectomy. *Spine (Phila Pa 1976)*, 10(6):580–5, 1985.
- [199] A F Tencer, B L Allen, Jr, and R L Ferguson. A biomechanical study of thoracolumbar spine fractures with bone in the canal. part iii. mechanical properties of the dura and its tethering ligaments. *Spine (Phila Pa 1976)*, 10(8):741–7, Oct 1985.
- [200] A F Tencer, R L Ferguson, and B L Allen, Jr. A biomechanical study of thoracolumbar spinal fractures with bone in the canal. part ii. the effect of flexion angulation, distraction, and shortening of the motion segment. *Spine (Phila Pa 1976)*, 10(6):586–9, 1985.
- [201] Manof K Tewari, Difender S Gifti, Paramjit Singh, Virender K Khosla, Suresh N Mathuriya, Sunil K Gupta, and Ashis Pathak. Diagnosis and prognostication of adult spinal cord injury without radiographic abnormality using magnetic resonance imaging: analysis of 40 patients. *Surg Neurol*, 63(3):204–9; discussion 209, Mar 2005. doi: 10.1016/j.surneu.2004.05.042.
- [202] Ryan T Tierney, Catherine Maldjian, Carl G Mattacola, Stephen J Straub, and Michael R Sitler. Cervical spine stenosis measures in normal subjects. *J Athl Train*, 37(2):190–193, Jun 2002.
- [203] J S Torg, R J Naranja, Jr, H Pavlov, B J Galinat, R Warren, and R A Stine. The relationship of developmental narrowing of the cervical spinal canal to reversible and irreversible injury of the cervical spinal cord in football players. *J Bone Joint Surg Am*, 78(9):1308–14, Sep 1996.

- [204] Jennifer A Tracy and J D Bartleson. Cervical spondylotic myelopathy. *Neurologist*, 16(3):176–87, May 2010. doi: 10.1097/NRL.0b013e3181da3a29.
- [205] K.H. Tsai, G.L. Chang, and R.M. Lin. Differences in mechanical response between fractured and non-fractured spines under high-speed impact. *Clinical Biomechanics*, 12(7-8):445–451, 1997.
- [206] M E L van den Berg, J M Castellote, I Mahillo-Fernandez, and J de Pedro-Cuesta. Incidence of spinal cord injury worldwide: a systematic review. *Neuroepidemiology*, 34(3):184–92; discussion 192, 2010. doi: 10.1159/000279335.
- [207] Marije van der Werf, Patrick Lezuo, Otto Maissen, Corrinus C van Donkelaar, and Keita Ito. Inhibition of vertebral endplate perfusion results in decreased intervertebral disc intranuclear diffusive transport. *J Anat*, 211(6):769–74, Dec 2007. doi: 10.1111/j.1469-7580.2007.00816.x.
- [208] H. Van Mameren, H. Sanches, J. Beurgens, and J. Drukker. Cervical spine motion in the sagittal plane ii: Position of segmental averaged instantaneous centers of rotation-a cineradiographic study. *Spine*, 17(5):467, 1992. ISSN 0362-2436.
- [209] C Weiler, M Schietzsch, T Kirchner, A G Nerlich, N Boos, and K Wuertz. Age-related changes in human cervical, thoracal and lumbar intervertebral disc exhibit a strong intra-individual correlation. *Eur Spine J*, Aug 2011. doi: 10.1007/s00586-011-1922-3.
- [210] A A White, 3rd and M M Panjabi. Biomechanical considerations in the surgical management of cervical spondylotic myelopathy. *Spine (Phila Pa 1976)*, 13(7): 856–60, Jul 1988.
- [211] A.A. White and M.M. Panjabi. *Clinical biomechanics of the spine*, volume 2. Lippincott Philadelphia, 1990.
- [212] H J Wilke, A Kettler, and L E Claes. Are sheep spines a valid biomechanical model for human spines? *Spine (Phila Pa 1976)*, 22(20):2365–74, Oct 1997.
- [213] H J Wilke, A Kettler, K H Wenger, and L E Claes. Anatomy of the sheep spine and its comparison to the human spine. *Anat Rec*, 247(4):542–55, Apr 1997.
- [214] H J Wilke, B Jungkunz, K Wenger, and L E Claes. Spinal segment range of motion as a function of in vitro test conditions: effects of exposure period, accumulated cycles, angular-deformation rate, and moisture condition. *Anat Rec*, 251(1):15–9, May 1998.

- [215] H J Wilke, K Wenger, and L Claes. Testing criteria for spinal implants: recommendations for the standardization of in vitro stability testing of spinal implants. *Eur Spine J*, 7(2):148–54, 1998.
- [216] H J Wilke, A Rohlmann, S Neller, M Schultheiss, G Bergmann, F Graichen, and L E Claes. Is it possible to simulate physiologic loading conditions by applying pure moments? a comparison of in vivo and in vitro load components in an internal fixator. *Spine (Phila Pa 1976)*, 26(6):636–42, Mar 2001.
- [217] King H Yang, Jingwen Hu, Nicholas A White, Albert I King, Clifford C Chou, and Priya Prasad. Development of numerical models for injury biomechanics research: a review of 50 years of publications in the stapp car crash conference. *Stapp Car Crash J*, 50:429–90, Nov 2006.
- [218] V R Yingling, J P Callaghan, and S M McGill. The porcine cervical spine as a model of the human lumbar spine: an anatomical, geometric, and functional comparison. *J Spinal Disord*, 12(5):415–23, Oct 1999.
- [219] V R Yingling, J P Callaghan, and S M McGill. The porcine cervical spine as a model of the human lumbar spine: an anatomical, geometric, and functional comparison. *J Spinal Disord*, 12(5):415–423, 1999. ISSN 0895-0385 (Print).
- [220] N Yoganandan, S Kumaresan, and F A Pintar. Biomechanics of the cervical spine part 2. cervical spine soft tissue responses and biomechanical modeling. *Clin Biomech (Bristol, Avon)*, 16(1):1–27, Jan 2001.
- [221] K Yone, T Sakou, M Yanase, and K Ijiri. Preoperative and postoperative magnetic resonance image evaluations of the spinal cord in cervical myelopathy. *Spine (Phila Pa 1976)*, 17(10 Suppl):S388–92, Oct 1992.
- [222] J W Youdas, T R Garrett, V J Suman, C L Bogard, H O Hallman, and J R Carey. Normal range of motion of the cervical spine: an initial goniometric study. *Phys Ther*, 72(11):770–80, Nov 1992.
- [223] Q Yuan, L Dougherty, and S S Margulies. In vivo human cervical spinal cord deformation and displacement in flexion. *Spine (Phila Pa 1976)*, 23(15):1677–83, Aug 1998.
- [224] W M Yue, S B Tan, M H Tan, D C Koh, and C T Tan. The torg–pavlov ratio in cervical spondylotic myelopathy: a comparative study between patients with cervical spondylotic myelopathy and a nonspondylotic, nonmyelopathic population. *Spine (Phila Pa 1976)*, 26(16):1760–4, Aug 2001.